DESALINATION USING AIR GAP MEMBRANE DISTILLATION

BY

DAHIRU UMAR LAWAL

A Thesis Presented to the

DEANSHIP OF GRADUATE STUDIES

KING FAHD UNIVERSITY OF PETROLEUM & MINERALS

DHAHRAN, SAUDI ARABIA

In Partial Fulfillment of the

Requirements for the Degree of

MASTER OF SCIENCE

In

MECHANICAL ENGINEERING

NOVEMBER 2014

KING FAHD UNIVERSITY OF PETROLEUM & MINERALS

DHAHRAN- 31261, SAUDI ARABIA

DEANSHIP OF GRADUATE STUDIES

This thesis, written by **DAHIRU UMAR LAWAL** under the direction his thesis advisor and approved by his thesis committee, has been presented and accepted by the Dean of Graduate Studies, in partial fulfillment of the requirements for the degree of **MASTER OF SCIENCE IN MECHANICAL ENGINEERING.**

A. Khalifa

Dr. ATIA E. KHALIFA
(Advisor)

Dr. Z. M. GASEM
Department Chairman

MAntar

Dr. MOHAMMED A. ANTAR
(Member)

Dr. Salam A. Zummo
Dean of Graduate Studies

Dr. TAHAR LAOUI
(Member)

1/1/15

Date

DEDICATION

This work is dedicated to my family

ACKNOWLEDGMENTS

I would like to thank King Fahd University of Petroleum and Minerals (KFUPM) for funding my research work and providing me the environment to achieve this level of study. I would like to express my gratitude and sincere thanks to my thesis advisor Dr. Atia Khalifa. He is not only helpful with deep vision and understanding but also most importantly a kind person. I sincerely thank him for his exemplary guidance and encouragement. My profound and special thanks goes to my thesis committee members in the person of Prof. (Dr.) Mohammed Antar and Prof. (Dr.) Tahar Laoui for their support, guidance and constructive advice which really help me to successfully complete my thesis.

Many thanks to Mr. Mohammed Karam for his technical support throughout this work. My appreciation goes to Mr. Ali Kamal who assisted in machining the MD modules. My thanks also goes to Mr. Ibrahim Bahaaeldin, Mr. Sayed Younus and Mr. Ahmed A. Rahman for their technical support.

My appreciation goes to Professor M. Khayet of Universidad Complutense de Madrid (UCM), Spain and his group for carrying out membrane characterization test. My gratitude goes to people of Mechanical Engineering Department. I would equally like to thank all my friends and colleagues for their encouragement.

I am very grateful to the entire Nigerian and African community at KFUPM for their moral support and encouragement. Lastly, I would like to thank my family, who taught me the value of hard working by their own example. They rendered me enormous support whenever I needed it the most.

TABLE OF CONTENTS

LIST OF TABLES

LIST OF FIGURES

LIST OF ABBREVIATIONS

Symbols

A	Cross sectional area [m^2]
b	Air gap thickness [m]
C_p	Specific heat capacity [kJ/kg.K]
d	Diameter [m]
d_h	Hydraulic diameter [m]
D_{wa}	Diffusion coefficient of water vapour in air [m^2/s]
g	Gravitational acceleration [m/s^2]
h	Heat transfer coefficient [$W/m^2.K$]
h_d	Condensate film heat transfer coefficient [$W/m^2.K$]
H_v	Heat of vaporisation [kJ/kg]
J	Permeate flux [$kg/m^2.s$]
K	Thermal conductivity [W/m.K]
B_w	Mass transfer coefficient [$kg/m^2 \cdot hr \cdot Pa$]
K_n	Knudsen number
l	Thickness of the cooling plate [m]
L	Height of the cooling plate [m]
M	Molecular weight [kg/mole]
Nu	Nusselt Number
P	Total pressure [Pa]
P_v	Vapour pressure [Pa]
P_a	Air pressure [Pa]

Pe	Peclet Number
Gr	Grashof Number
Pr	Prandtl Number
Q_s	Sensible heat transfer [W/m^2]
Q_v	Latent heat transfer [kW/m^2]
Q_c	Conduction heat transfer [W/m^2]
r	Pore radius [m]
R	Gas constant [J/K.mol]
Ra	Rayleigh number
Re	Reynolds number
T	Absolute temperature [K]
H	Total heat transfer coefficient [W/m^2]
u	Velocity [m/s]
M_w	Molecular weight of water [kg/mole]
Z	Distance [m]
C	Concentration [g/L]
CM_{NaCl}	Mole solute concentration [mole/L]

Subscripts and Superscripts

a	air
w	water
f	feed
m	membrane

b	bulk
mf	feed side of membrane
cd	coolant side of membrane
m	mean; average
c	coolant water
h	hot region

Greek Letters:

δ	Membrane thickness; film thickness [m]
Δ	Difference
ε	Porosity
τ	Tortuosity
μ	Viscosity [N.s/m^2]
λ	Mean free path [m]
σ	Surface tension [N/m]
ρ	Density [kg/m^3]
θ	Temperature polarization
η	Thermal efficiency

ABSTRACT

Full Name : Dahiru Umar Lawal

Thesis Title : Desalination Using Air Gap Membrane Distillation

Major Field : Mechanical Engineering

Date of Degree : November, 2014

Membrane distillation (MD) is a developing thermally driven membrane desalination technology that has been applied in four different basic configurations. In membrane distillation, a hot, saline feed stream is passed over a hydrophobic membrane. The temperature difference between the two sides of the membrane leads to a vapour pressure difference that causes water vapour to permeate through the membrane pores, and then condensed on the cold side of the membrane. The hydrophobicity of the membrane prevents the liquid from passing through the pores, while the water vapour is allowed to pass through. The technique offers the attractiveness of operation at atmospheric pressure and low temperature (40– 90^{o}C), and has the theoretical ability to achieve 100% salt rejection. Thus, low-grade energy like solar and waste energy can be used for desalination.

In this work, an experimental investigation of the performance of Air Gap Membrane Distillation (AGMD) system was performed for seawater and laboratory prepared salt feed water solutions. The influences of system operating parameters such as feed temperature, feed flow rate, coolant temperature, coolant flow rate and air gap width on permeate flux were studied. The effects of membrane pore size as well as the concentration of feed solution on permeate flux were also investigated. The performance of the AGMD unit was statistically optimized using design of experiment (DOE) and

Taguchi technique. Furthermore, theoretical model describing heat and mass transfer analysis in AGMD was developed and discussed in detail.

The permeate flux was found to increase with increasing feed temperature and feed flow rate. However, it decreased with increasing air gap width and coolant temperature. The system performance tends to increase marginally with increasing coolant flow rate. The system performance is mostly dominated by the effect of both feed temperature and air gap width. Feed flow rate and coolant temperature have relatively considerable effect on flux. Increasing the membrane pore size from PTFE 0.22μm to PTFE 0.45μm leads to about 10% increment in flux production. While increasing the feed concentration from 0.075g/L to 60g/L lead to about 11% drop in permeate flux. The tested double-stage AGMD design was capable of achieving a maximum permeate flux of 128.46kg/m^2hr, which is almost twice that of single stage unit, under the same experimental conditions.

In general, the theoretical model results were found to be in good agreement with the experimental data as the maximum deviation of model results was within 15%. The model was also used to predict thermal efficiency and temperature polarization of the AGMD system.

Regarding system optimization using Taguchi methodology, the developed model proved to be in good agreement with the experimental data with a maximum deviation of about 10%. According to Taguchi orthogonal arrays, the experimental and model optimum system performance was found to be 76.0457 kg/m^2h, and 74.5916 kg/m^2h respectively. The conditions for the optimum performance are 80^{o}C feed temperature, 5 L/min feed flow rate, air gap width of 3mm and coolant temperature of 20^{o}C.

ملخص الرسالة

الاسم الكامل: داهيرو عمر لاوال

عنوان الرسالة: تحلية المياه باستخدام غشاء التقطير ذو الفراغ الهوائي

التخصص: هندسه ميكانيكيه

تاريخ الدرجة العلمية: نوفمبر 2014

غشاء التقطير هو عبارة عن تقنية مطورة لتحلية المياه باستخدام الاغشية والتي تعمل بالطاقة الحرارية حيث أنه تم تجريبها على أربعة تصاميم مختلفة. طريقة عمل هذه التقنية هي كالتالي: نقوم بتسخين الماء المالح وتمريره على غشاء ذو سطح طارد للموائع, وبسبب اختلاف درجة الحرارة بين طرفي الغشاء فإن فرق ضغط البخار يتسبب فى تخلل البخار ومروره خلال الغشاء والتكثف على الجانب البارد من الغشاء. من أبرز ما يميز هذه التقنية أنها تعمل عند الضغط الجوي العادي ودرجة حرارة منخفضة تتراوح مابين 40 و 90 درجة مئوية, كما انها لا تحتاج الى كميات كبيرة من الطاقة حيث يمكن تشغيلها باستخدام الطاقة الشمسة أو الطاقة المهدرة من العمليات الصناعية.

فى هذا البحث تم عمل تجارب معملية لدراسة أداء غشاء التقطير ذو الفراغ الهوائى باستعمال مياه البحر و محاليل مياه مالحة تم تجهيزها فى المعمل. تم دراسة تأثير عوامل التشغيل المختلفة على الاداء و منها درجة حرارة مياه التغذية و معدل تصرفها و درجة حرارة مياه التبريد و معدل تصرفها بالاضافة الى تأثير عرض الفجوة الهوائية. كما تم دراسة تأثير حجم فتحات الغشاء و درجة تركيز الاملاح فى مياه التغذية على أداء المنظومة و تم عمل دراسة إحصائية للوصول الى شروط الاداء الأمثل للتشغيل عن طريق تصميم التجربة و إستخدام طريقة تاجوشى . كما يهدف هذا البحث ايضا الى تطوير و مناقشة النموذج النظري لحساب انتقال الحرارة والمادة في هذه التقنية.

من خلال التجارب وجدنا أن تدفق بخار الماء عبر الغشاء يزداد مع زيادة درجة الحرارة و معدل التدفق لمياه التغذية الداخل الى النظام, بينما يقل عند زيادة كل من عرض الفراغ الهوائي و درجة حرارة ماء التبريد. نستطيع أن نقول أن أغلب ما يؤثر على أداء النظام هو درجة حرارة الماء الداخل الى النظام وعرض الفراغ الهوائي بينما معدل تدفق المبرد له تأثير محدود على أداء النظام. معدل تدفق مياه التغذية و درجة حرارة مياه التبريد لهم أثر واضح نسبيا على أداء المنظومة. زيادة حجم فتحات الغشاء من 0.22 الى 0.45 ميكروميتر أدى الى زيادة 10%

فى انتاج المياه المقطرة بينما زيادة تركيز الاملاح لمياه التغذية من 0.075 الى 60 جرام لكل لتر ادى الى انخفاض 11% فى الناتج. وكذلك من التجارب وجدنا أن تصميم المرحلتين من نظام غشاء التقطير ذو الفراغ الهوائي تعطي نتائج مضاعفة مقارنة بالتصميم ذو المرحلة الواحدة من هذا النظام.

بشكل عام النتائج النظرية مطابقة إلى حد كبير للنتائج المعملية مع اختلاف يصل إلى 15%. وجد من الدراسة أن الأداء الأمثل معمليا هو 76.0457 كجم/م^2 ساعة و نظريا هو 74.5916 كجم/م^2 ساعة عند درجة حرارة 80 درجة مئوية وبمعدل تدفق 5 لتر/دقيقة لماء التغذية الداخل إلى النظام و 3 مم عرض الفراغ الهوائي و20 درجة مئوية لمياه التبريد.

CHAPTER 1

INTRODUCTION

The quest for more and better fresh water production has consistently put researchers in search for superior and most efficient potable water production technology. Water is a common chemical compound composing of hydrogen and oxygen atoms. It is an odourless and colourless compound available in abundance on the earth surface. Water exists in different form, namely: solid, liquid and gaseous form. The form in which it exists depends on its temperature. Water covers about 1.4x109 Km^3, which is roughly 70% of the earth surface. About 97.5% of this water has high amount of salt content. Eighty percent of the remaining water is found in ice, glacier, etc. The actual portion of potable fresh water, which is available and accessible for human needs, is only 0.5 percent [1].

1.1 Water Scarcity

Water scarcity is defined as the point at which the aggregate impact of all users impinges on the supply or quality of water under prevailing institutional arrangements to the extent that the demand by all sectors, including the environment, cannot be fully satisfied [2]. It is the in-ability of water resources to meet its demands. Water is crucial for all for maintaining healthy life. As population increases, the demand for water resources

intensifies, leading to tensions, conflicts among users. The increasing stress on freshwater resources is brought about by ever-rising demand and profligate use.

‘‘A major study revealed that 1.2 billion People live in areas of physical water scarcity, and 500 million people are approaching this situation [3]. Another 1.6 billion people, or almost one quarter of the world's population faces economic water shortage (where countries lack the necessary infrastructure to take water from rivers and aquifers)’’. Water scarcity is one of the main problems faced by the world population in 21st century. Below are some useful information on water scarcity obtained from [2];

- When annual water supplies drop below 1,000 m3 per person, the population faces water scarcity, and below 500 cubic metres "absolute scarcity".
- Around 700 million people in 43 countries suffer today from water scarcity.
- By 2025, 1.8 billion people will be living in countries or regions with absolute water scarcity, and two-thirds of the world's population could be living under water stressed conditions.
- With the existing climate change scenario, almost half the world's population will be living in areas of high water stress by 2030, including between 75 million to 250 million people in Africa. In addition, water scarcity in some arid and semi-arid places will displace between 24 million to 700 million people.
- Sub-Saharan Africa has the largest number of water-stressed countries of any region.

1.2 Human Consumption and Needs for Fresh Water

Potable (fresh) water is the water that is safe enough for human consumptions. Fresh water is needed by human in order to maintain human life on this planet. Water represents 60-75 percent of the human body. Our inability to consumed fresh water as required by our body system will leads to health related issues. Large portion of earth is actually covered by salt water and consuming this water in it natural form will leads to dehydration. Other health related problems are high blood pressure; high heart beat rate, physiological changes, excessive thirst, brain damage, loss of consciousness, kidney failure and eventually death. Since the only available portion of fresh water is not enough to sustained life on earth, then the need for salt water desalination and its technologies become necessity.

1.3 Desalination Role

Due to urbanization and population rise, the bridged between the demand and supply of potable water is ever increasing. In some arid and semi-arid area, desalination remains the alternative solution to water scarcity problem. The existing desalination technology has been developed to a point where it can serve as a reliable source of water at a competitive price with that of conventional water treatment technology. Desalination plants are usually situated close to a large water body such as sea or ground water reserves.

The market for water desalination is increasing in Gulf Cooperation Council (GCC) countries as the populations grow, drought conditions worsen, and water demand per capital increases [4]. The latest trend in desalination practice in the Gulf Cooperation Council countries is to adopt privatization after the successful introduction of independent power and/or water producers (IPP and IWPP) in some countries [4].

1.4 Seawater Properties

The physical properties of salt water depend on the relative proportions and the concentration of the salts it contains. The chemical composition of open sea is constant, nevertheless, the total dissolved solids (TDS) may change from one local to local condition due to the fact that the time needed to obtain complete mixing of seas and oceans is less than the time needed for complete filling or replenishment [1]. Seawater is composed of 96.5% pure water and 3.5% other material, such as dissolved gases, salts, undissolved particles and organic substances.

Table 1.1 Major components of seawater [6]

Ion	Concentration of seawater (g/kg)	
	Salinity (35g/kg)	Chlorinity (19g/kg)
Sodium	10.759	10.561
Magnesium	1.2940	1.2720
Calcium	0.4130	0.4000
Potassium	0.3870	0.3800
Strontium	0.0135	0.0130
Boron	0.0040	0.0040
Chlorine	19.354	18.980
Sulphate	2.7120	2.6480
Bromide	0.0670	0.0650
Fluoride	0.0013	0.0013
Bi-carbonate	0.1420	0.1390

Table 1.2 some of the physical properties of seawater [6]

Heat Capacity Of Seawater Concentration (kJ/kg-K)					
Temperature	Salinity (g/kg)				
(°C)	20	40	60	80	100
20	4.078	3.973	3.875	3.784	3.699
40	4.079	3.982	3.890	3.802	3.719
60	4.085	3.991	3.901	3.814	3.731
80	4.097	4.003	3.912	3.825	3.741
100	4.116	4.020	3.927	3.837	3.753
Thermal Conductivity Of Seawater Concentration (mW/m-K)					
Temperature	Salinity (g/kg)				
(°C)	20	40	60	80	100
20	601	599	596	593	590
40	628	627	625	623	621
60	650	649	648	647	646
80	666	666	666	666	666
100	677	678	679	680	681
Vapour Pressure Of Seawater Concentration (bar)					
Temperature	Salinity (g/kg)				
(°C)	20	40	60	80	100
20	0.0231	0.0229	0.0226	0.0222	0.0219
40	0.0730	0.0721	0.0712	0.0702	0.0690
60	0.1971	0.1947	0.1923	0.1895	0.1864
80	0.4687	0.4632	0.4571	0.4505	0.4433
100	1.0025	0.9907	0.9777	0.9635	0.9480
Dynamic Viscosity Of Seawater Concentration (Cp)					
Temperature	Salinity (g/kg)				
(°C)	10	35	50	70	90
20	1.019	1.070	1.105	1.158	1.218
40	0.666	0.702	0.727	0.764	0.804
60	0.476	0.504	0.523	0.551	0.581
80	0.363	0.385	0.400	0.422	0.446
100	0.289	0.308	0.320	0.338	0.357
Density Of Seawater Concentration (Kg/m^3)					
Temperature	Salinity (g/kg)				
(°C)	10	30	50	70	90
20	1005.8	1020.8	1035.9	1051.2	1066.7
40	999.20	1013.9	1028.8	1043.8	1059.0
60	990.20	1004.9	1019.6	1034.5	1049.4
80	979.00	993.70	1008.4	1023.2	1038.1
100	965.80	980.60	995.40	1010.3	1025.2

The presence of salts in seawater affect most of the physical properties of sea water, such as compressibility, density, temperature, freezing point, etc. Usually, salt water properties are computed at the standard pressure of 0.101325MPa and standard absolute salinity of 35.16504 ± 0.007g/kg [5]. The major component of seawater is presented in Table 1.1.

Table 1.2 depicted some of the physical properties of sea water. These properties affect the salinity and temperature of sea water.

The density and the dynamic viscosity of seawater increased with increasing salinity of seawater and decreased with increase in seawater temperature. The heat capacity, thermal conductivity and the vapour pressure of seawater concentration decreases with increasing seawater salinity and increases with decreasing seawater temperature.

1.5 Water-Energy Nexus

Energy and water are among the most demanded and most critical resources ever known by human. However, these two basic most wanted resource displays some mutual relation in one way or the other. In order to generate or produce energy, large volume of water is required. And in order to produce, transport, and treat water for human consumption and irrigation application, huge amount of energy is needed. Therefore Water-energy nexus described the inter-linked between energy and water.

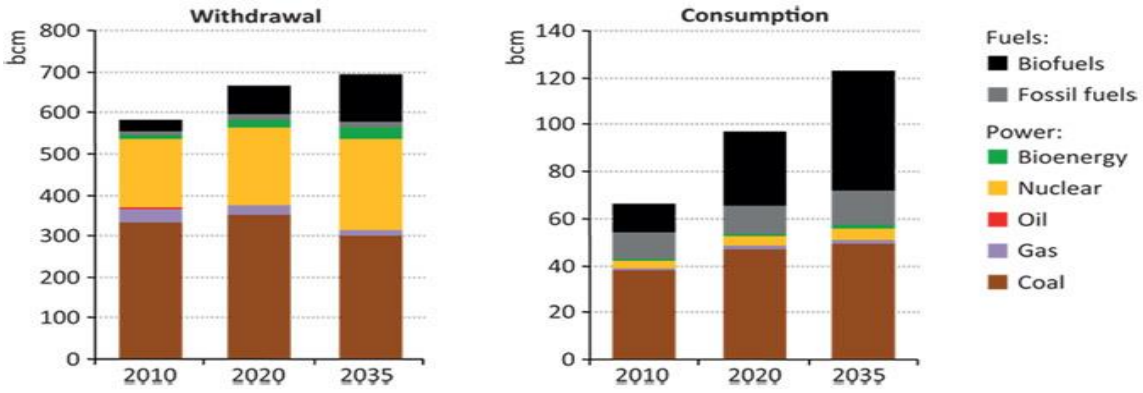

Figure 1.1 Global water uses for energy production [7].

Water can be found in almost every aspect of energy generation, which may include but not limited to hydro-power plant, steam power plant, and cooling towers for thermal power plants. Water is also utilized in large amount for refining and production of fuel. However, huge amount energy is used in water treatment plants like thermal desalination and its membrane desalination technology counterpart. Large amount of energy is also required to transport treated and raw water from one location to another. For household and industrial applications, energy is consumed especially for cooling and heating purposes. The use of energy for water can also be found in irrigation activities. Figure 1.1 represents some fact about water use for energy production fuel and power generation type.

1.6 Problems Facing Desalination

There is no doubt that in finding solution to the problem of fresh water scarcity and its high demand, desalination technology is the main solution. It is one of the cost effect and affordable way of providing solution to the problems of fresh water scarcity. Desalination

technologies however create other problems, which differ from one desalination plant to another. Some of these problems include; Desalination technology can kill marine life and the environment; ocean desalination plant costs more than any other option; desalination causes water pollution; desalination may fail to eliminate harmful dissolve and undissolved chemical substances from fresh water; desalination consumes more energy than any other option.

Desalination of sea water required more fuels than obtaining the equivalent quantity of fresh water from water bodies. One of the well-known problems associated with energy usage is the greenhouse gas emissions resulting from climate change caused by enormous amount of energy used in desalting seawater. This effect can intensify and aggravate draught conditions, which at the first place need the services of desalination. The other major problem of desalination is its impact on marine life. The highly concentrated brine water, which contains many other chemicals used during the process, is discharged back to the seawater body, which is at lower salt concentration; this may have certain impact on the marine life and its environment. The incoming seawater to the desalination plant may contain fish and other sea life, sometimes they are killed as they got trapped in the plant.

1.7 Current Desalination Techniques

The major categories of water treatment technologies employed for desalination are: thermal desalination and membrane based desalination technologies. In some case, both

membrane based desalination and thermal desalination technologies are combined to form one desalination plant.

1.7.1 Thermal Desalination

Evaporation and distillation processes are the concept upon which thermal desalination technology is based on. Thermal desalination processes are similar to the Earth's natural water cycle. The important stages involved in these processes include heating of salt water, evaporation and condensation. The output is the collection of produced clean water and brine. The example of thermal desalination technology includes Multi-Stage Flash desalination process (MSF), Multiple Effect Distillation (MED) and Vapour Compression (VC).

1. Multi-Stage Flash Desalination Process (MSF)

Multi-Stage Flash desalination process uses multiple (many) boiling chambers operating at different pressures. It is the mostly used thermal desalination processes in the world. In multi-stage flash desalination process, saltwater is admitted into MSF unit, the water is boiled and evaporated in each chamber, and the vapour is finally condensed. The results of this process is fresh water and concentrated brine water.

The salt water entering into MSF system is heated, the heated salt water is then passes via consecutive stages (effects) each at different pressure where the chamber pressure is lower. This causes the salt water to boil and flashes into steam in each chamber until the brine has reached its saturation temperature. The steam obtained from flashing is condensed into potable water after passing through demisters. The MSF process operates with maximum efficiency at temperatures of up to 115° C. The plant sizes of MSF is

usually large and the energy consumption is low because the process peak efficiency can occur at temperature up to 115^{o}C [8].

2. Multiple Effect Distillation (MED)

In Multiple Effect Distillation, saltwater is sprayed on series of stages (effects), which are equipped with heat exchanger (composed of pipes that are heated on the inside by condensed steam). The raw water get heated in the stages and part of it evaporates. The evaporated steam is used for next effect and it condensed on the inner surface of the pipe. The heat supplied to the MED system is only for the first stage. The subsequence stages get heat from the previous stage. The MED process works at low temperatures which leads to small to medium-sized plant sizes, reduced scaling risk, low thermal energy consumption, and reduced operating costs [9].

3. Vapour Compression (VC)

One of the most reliable and robust desalination technologies is the vapour compression. VC may be used as standalone plant and may be used in combination with Multi-effect Distillation unit. In Vapour Compression, vapour is used to change the raw water boiling point. The idea is that vapour is proportional to temperature at constant volume (ideal gas law), so the compression of vapour is used as source of heat for salt water. This process may contain many stages for bigger desalination plant and may contain single stage for small desalination plant. Some of the advantage of vapour compression desalination includes; low operating costs, smaller size equipment's in comparison with multi-stage flash or multi-effect flash distillation systems. The disadvantage of VC may include the following: compressors and heat exchangers is demands greater maintenance, high

capital cost, and high energy consumption in comparison with other thermal desalination processes. A single VC system has the capacity of 3000 m^3/day [10].

1.7.2 Membrane based Reverse Osmosis desalination (RO)

Membrane based reverse osmosis desalination technology involved forcing of saltwater through membrane sheets at high pressures. Membrane sheets are designed to prevent salt ions from penetrating through it. To understand the process of RO, the natural phenomena called osmosis must be understood first. Osmosis is a process that takes place in all living cell. In osmosis, two different fluids at different concentration is separated by semi-permeable membrane, the fluid with lower concentration diffuse via the membrane to the fluid with higher concentration in order to equalized solution strength. The height difference between the both fluids of different concentration is the osmotic pressure. When external pressure greater than the osmotic pressure is applied, the diffusion via the semi-permeable membrane is reversed which is the principle on which RO work. The RO Process produces clean water and brine. RO system is composed of the following basic components: High pressure pumping unit, Feed water supply unit, Permeate treatment and storage unit, Pre-treatment system, Cleaning unit, Instrumentation and control system, and Membrane element assembly unit. RO is a well-tested desalination technique for potable and industrial water production [8]. The operating pressures required in RO range from 250 to 400 psi for brackish water, and from 800 to 1 000 psi for desalination of seawater.

1.8 New Emerging Desalination Technologies

The need for new desalination technology arises as the demand for fresh water consumption increases and quest for lower energy consumption technology. Several new emerging desalination technologies had evolved in order to mitigate the problem facing fresh water scarcity. Some of the new emerging desalination technologies are briefly discuss below.

1.8.1 Forward Osmosis (FO)

Forward osmosis process used osmotic pressure (a pressure as a result of the height difference between the concentrations of both sides of the membrane) like RO [12]. In FO processes, the feed concentration diffuses through semi-permeable membrane to the ammonia salt solution. This happened because the salt water solution is at lower concentration than the highly concentrated ammonia solution. Heat will then be applied to the ammonia salt solution to evaporate ammonia salt leaving behind fresh water [13]. Forward osmosis process does not require higher pressure when compared to reverse osmosis.

1.8.2 Dew Evaporation

In this process, air is used as a carrier-gas which evaporates water from sea water. The vapour then condensed as potable condensate at constant atmospheric pressure. For dew evaporation process, the required heat for evaporation is obtained from the dew condensation on opposite sides of a heated wall. The heat supplied to the heated wall may be obtained from fuel combustion, solar collectors, or waste heat. The dew evaporation

technology belongs to the class of humidification-dehumidification technology but needs only one tower. This makes the process more energy efficient [14].

1.8.3 Membrane Distillation (MD)

Membrane distillation (MD) is a thermally-driven membrane desalination technology. Membrane distillation is composed of hot feed chamber and coolant chamber separated by a hydrophobic membrane sheet. In membrane distillation, hot feed salt solution is passed over a hydrophobic membrane sheet. The temperature difference between the two sides of the membrane leads to a vapour pressure difference that causes water to evaporate, diffuses via the membrane pores, and condenses on the opposite side of the membrane. Since MD has the theoretical ability to attained 100% salt rejection and can be operated at low temperatures (40^0C - 90^oC) and at atmosphere pressure, then low grade energy like solar and waste energy can be used for desalination [15].

1.8.4 Low Temperature Thermal Desalination (LTTD)

The idea for Low temperature thermal desalination process is based on the fact that water can evaporates at low temperatures at pressures [16]. In LTTD, vacuum pump is employed to produce low pressure environment (at low temperature) upon which water evaporates. The evaporated water is condensed using deep sea cooled water ranging from 7^0C to 15^oC. Low temperature thermal desalination process can be used for power plant and air conditioning application as well as potable water production.

1.8.5 Capacitive Deionization (CDI)

Capacitive deionization (CDI) is a controlled electrochemical method for removing salt from salt water solutions. In CDI, salt solution is deionized by applying potential difference between two carbon electrodes (anode and cathode). The negative charges are

separated from water and piles in positive polarized electrodes whereas the positive charges are stored in negative polarized electrode. In this way salt water is desalinated [17].

1.8.6 Solar Desalination

Solar desalination is a method for desalinating seawater by utilizing solar energy. In solar desalination, desalination can be achieved either by direct method or by indirect method [18]. Example of direct method is solar still. In this desalination method, seawater in glass tank is warmed by heat from the sun. Some portion of the seawater evaporates as a result of the heat, the vapours then condenses on the glass cover and collected through the gutter outlet.

1.8.7 Geothermal Desalination

For geothermal desalination method, geothermal energy (energy obtained from underground) is used to drive desalination plant (system). Geothermal plant generates large quantity of heat that can effectively be used for seawater system at low cost [19]. Geothermal energy can provide stable 24 hours heat a day and it is an environmental friendly technique.

1.8.8 Electro-Dialysis Reversal

It is an electrochemical separation method. Electro-dialysis uses membrane like reverse osmosis, but instead of applying external pressure to the feed salt water, electric charge is passes through the feed saline solution by direct current. The charges causes the negative ions (e.g. chlorine) to move across the membrane and towards the positively charged anode on one side, and the positive charge ions to migrate to negatively charge cathode.

The ions deposited at the cathode and the anode is removed leaving behind clean water. The process takes place in a special kind of configuration called electro-dialysis cell [20].

CHAPTER 2

LITERATURE REVIEW

2.1 Membrane Distillation

Membrane distillation (MD) is an emerging technology for desalination. It is a thermally driven separation process in which separation occurred due to phase change. Membrane distillation is based on the application of vapour pressure differential to permeate water through a hydrophobic membrane, while repudiating the non-volatile compound available in the feed solution. Findley [21] was the first to relate the separation techniques now known as membrane distillation. Membrane distillation MD differs from other membrane technology in the sense that the driving force for desalination is due to the vapour pressure difference, rather than the total pressure of water across the membrane. The membrane materials used for membrane distillation are hydrophobic in nature. In membrane distillation, evaporation occurs at the hot solution surface when the vapour pressure at the hot solution side of the membrane is greater than the vapour pressure at the cooler side of the membrane. The vapour then passes through the pores to the cooler side where it is condensed.

MD process is composed of hot and cold chambers containing hot water and cold water respectively. In between the two chambers is the membrane sheet. The elevated temperature of the hot side generates water vapour at the feed side. The vapour passes

through the membrane sheet, and then to the cold chamber. The vapour condenses on running cold water, in the case of DCMD; diffuses through stagnant air gap and condenses on a cooled surface in the case of AGMD; or swept away by an inert gas and condenses outside the module for SGMD; sucked by vacuum pump and condensed outside the module for the case of VMD.

MD process had been in existence since late 1960s but never get its due attention from the commercial market. Perhaps, the lack of membranes material suitable for MD process at that time, especially at reasonable prices may be the cause of its slow progress [22].

Some of the advantages of membrane distillation are [23, 24]:

- MD process consumes low energy
- Membrane fouling is less of a problem in comparison to pressure driven desalination processes like RO.
- Can work with low operating temperatures compared to temperature utilized in conventional distillation. The process can work at feed temperatures of considerably lower than the boiling point of water (i.e., temperatures as low as 30ºC have been used).
- Can achieve a very high salt rejection factors when feed containing no-volatile solutes (salts, colloids, etc.) is employed. This makes MD more attractive than other popular separation processes such as RO in the field of desalination as well as in nuclear desalination.
- Less demanding membrane mechanical properties.
- No Extensive pre-treatment is necessary as required in reverse osmosis.
- Lower operating hydrostatic pressures than the pressure-driven processes.

- Possibility to use equipment's made of plastic material. This mitigates the erosion problems.
- Possibility to use waste heat and renewable heat sources enabling MD technique to cooperate in conjunction with other processes in an industrial scale.

However, membrane distillation has the following disadvantages [23, 24]:

- Lack of membranes and modules designed specifically for MD.
- Permeate flux decay with time due to fouling, membrane deterioration, etc.
- Risk of membrane pore wetting.
- Uncertain and "high" energetic and economic costs. With respect to RO, higher energy consumption is needed to establish the thermal membrane operation.
- Low productivity (i.e. permeate flux).
- Commercial membrane modules are still expensive.

2.1.1 Membrane Distillation Configuration

Depending on the application of the membrane distillation, different configurations have been used. The MD configuration differs from one another from the way in which the module is designed. In all the configuration of MD, the feed solution is always kept in contact with the hydrophobic membrane surface. The different between the configurations lies on the coolant side of the module.

The four basic configurations mainly used in MD are the Vacuum Membrane Distillation (VMD), Direct Contact Membrane Distillation (DCMD), Sweeping Gas Membrane Distillation (SGMD) and Air Gap Membrane Distillation (AGMD).The main advantage, disadvantage, and applications of these MD configurations are summarized in table 2.1.

Table 2.1 Main advantages, disadvantages and application of MD [25]

MD configuration	Advantages	Disadvantages	Application area
DCMD	▪ High permeate flux ▪ Possible internal heat recovery	▪ High conductive heat losses ▪ High temperature polarization effect ▪ Risk of mass contamination of the permeate	▪ Desalination and water treatment ▪ Nuclear industry ▪ Food industry ▪ Textile industry ▪ Chemical and pharmaceutical industries
AGMD	▪ Low conductive heat losses ▪ Low temperature polarization effect ▪ Possible internal heat recovery	▪ Low permeate flux due to resistance to mass transfer	▪ Desalination and water treatment ▪ Food industry ▪ Chemical industry
SGMD	▪ Low conductive heat losses ▪ High permeate flux	▪ Complicated to handle the sweeping gas ▪ Difficult heat recovery	▪ Desalination and water treatment ▪ Chemical industry
VMD	▪ Low conductive heat losses ▪ High permeate flux	▪ Higher risk of pore wetting ▪ Difficult heat recovery	▪ Desalination and water treatment ▪ Food industry ▪ Textile industry ▪ Chemical industry

1. Direct Contact Membrane Distillation (DCMD)

In DCMD, both sides of the hydrophobic membrane sheet are directly exposed to hot feed saline solution on the feed side; and cooled permeate water on the permeate side. For DCMD, the temperature of the feed saline solution must be higher than that of the permeate water in order to create the vapour pressure difference between the both side of the membrane sheet. The condensation of the vapour passing through the membrane happens directly inside the liquid phase at the membrane boundary surface. Because of direct contact of permeate water with membrane material and poor conductivity of the polymeric material, heat losses through the membrane is the main problem associated with the configuration. The lost heat lowers the efficiency of the system because the heat is not used in the distillation process. The thermal efficiency of DCMD is relatively lower

than the other MD configuration [15]. However, DCMD is the most commonly used configuration because of its convenience to set up in laboratory [26]. Illustrated in figure 2.1 is the direct contact membrane distillation.

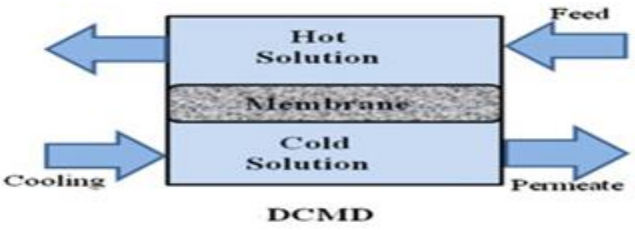

Figure 2.1 Direct Contact Membrane Distillation

2. Air-Gap Membrane Distillation (AGMD)

In air gap membrane distillation, the feed saline channel is similar to DCMD, but at the other side of the membrane, a stagnant air gap is staged between the membrane and a cooling surface. In AGMD configuration, the temperature difference between the sides of a membrane material creates partial pressure difference which encourages water molecules evaporated at the hot feed side to permeate the pores of the membrane. The vaporized water then diffuses through a stagnant air gap situated between the membrane and a condensation surface, and when comes in contact with the coolant plate, the vapour condenses to produce distilled water. The advantage of this configuration is that heat loss by conduction as found in DCMD is minimized through the provision of stagnant air gap. However, the introduction of air gap creates resistance to mass transport through it, thereby reducing the system performance. The other advantage of AGMD over DCMD is the fact that volatile substances with a low surface tension like alcohol can be separated from diluted solutions [27]. Depicted in figure 2.2 is the AGMD configuration.

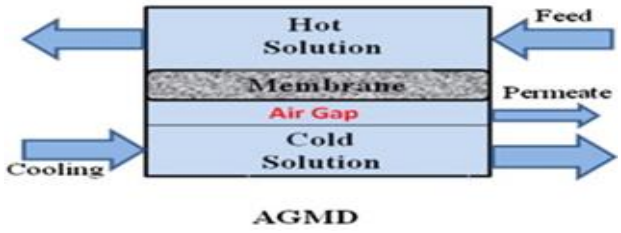

Figure 2.2 Air-Gap Membrane Distillations

3. Sweeping gas membrane distillation (SGMD)

Sweeping Gas Membrane Distillation otherwise known as air stripping, uses an empty gap on the permeate channel. In sweeping gas membrane distillation, a cold inert gas is used in permeate side for sweeping and carrying the vapour molecules to outside the membrane module where the condensation takes place. The SGMD configuration is similar to AGMD configuration in the sense that volatile substances with a low surface tension can be distilled using the process. The advantage of SGMD over AGMD is the resistance to mass transfer across the air gap barrier is reduced considerably by forced flow of the sweeping gas. However the setback for SGMD is caused by the gas component. This happened when using smaller gas mass flow rate as a result of self-heating by the gas at the hot membrane surface, thereby reducing the vapour pressure difference (driving force). Presented in figure 2.3 is the SGMD configuration. Due to the operational costs of the external condensation system, SGMD is the least used MD configuration.

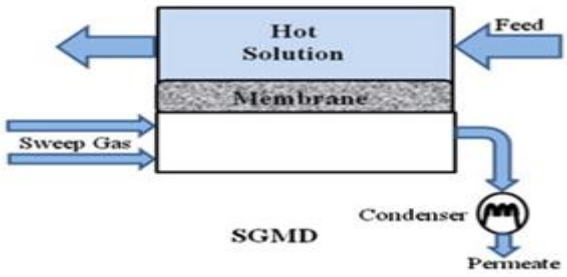

Figure 2.3 Sweeping Gas Membrane Distillations

4. Vacuum Membrane Distillation (VMD)

Illustrated in figure 2.4 is the vacuum membrane distillation configuration. Vacuum membrane distillation contains an air gap channel similar to AGMD configuration. The vacuum create at the permeate side enhance the driving force for the process. The vapour after permeating through the pores of the membrane is sucked out of the permeate channel and condenses outside the cell. One advantage of VMD is the sucking out the undissolved inert gasses blocking the membrane pores by the vacuum, thereby creating large effective membrane area for the system. The setback of VMD is the complex technical equipment required to produce the vacuum. The other problem associated with VMD is the higher demand for electrical energy in comparison with other MD configuration [26].

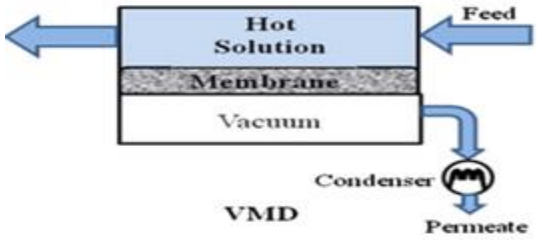

Figure 2.4 Vacuum Membrane Distillations

2.1.2 Membrane Materials

In membrane distillation process, variety membrane sheet made of polymeric and inorganic material that are hydrophobic nature have been used extensively. However, compared to other membrane materials commonly used in MD, polymeric membranes had drawn more attention [26]. The MD polymeric materials commonly employed are polytetrafluoroethylene (PTFE), polypropylene (PP) and poly-vinyl-di-fluoride (PVDF). Their lower value of surface tension is the reason behind their popularity in MD. Different preparation techniques like sintering, stretching, phase inversion or thermally induced phase separation depending on the properties of the materials can be used to produce hydrophobic porous membranes. The membrane porosity ranging from 0.60 to 0.95 is used in MD, the membrane pore size used in MD is in the range of 0.2 μm to 1.0μm, while thickness of the membranes used in MD ranges from 0.04mm to 0.25mm [28]. The value of surface tension used in some of the membrane materials are presented in table 2.2.

Table 2.2 Values of critical surface tension of some polymers [26]

POLYMERS	SURFACE TENSION (Dynes/cm)
Polytetrafluoroethylene (PTFE)	19
Polyvinylidenefluoride (PVDF)	25
Polypropylene (PP)	29
Polyethylene (PE)	31
Polypropylene (PP)	34
Polyvinyl alcohol (PVA)	37
Polysulfone (PS)	41
Polycarbonate (PC)	45
Polyurethane (PU)	45

The following qualities are requirement of material used in MD [15, 29]

- An adequate thickness, based on a compromise between increased membrane permeability (tend to increase flux) and decreased thermal resistance (tend to reduce heat efficiency or interface temperature difference) as the membrane becomes thinner;
- Reasonably large pore size and narrow pore size distribution, limited by the minimum Liquid Entry Pressure (LEP) of the membrane.
- Low surface energy: equivalent to high hydrophobicity. Material with higher hydrophobicity can be made into membranes with larger pore sizes, or membranes made from more hydrophobic material will be applicable under higher pressures for a given pore size;
- Low thermal conductivity: High thermal conductivities increases sensible heat transfer and reduce vapour flux due to reduced interface temperature difference; and
- High porosity: High porosity increases both the thermal resistance and the permeability of MD membranes, so both the heat efficiency and flux are increased. However, high porosity membranes have low mechanical strength and tend to crack or compress under mild pressure,
- Should not be wetted by the aqueous solution of salt with sufficiently high liquid entry pressure (LEP).
- Should not permit condensation to occur inside its pores
- Should not alter the vapour/liquid equilibrium interfaces formed at the entrances of membrane pores
- Long life with a stable MD performance, permeability and salt rejection.

2.1.3 Membrane Fouling and Wetting

Membrane fouling cause reduction in permeate flux and it is one of the major problem facing the application of membrane technologies [29]. The foulant, e.g. bio-film, precipitations of organic and inorganic matter, can reduce the permeability of a membrane by clogging the membrane surface and pores. Although membrane distillation is more resistant to fouling than conventional thermal processes, dosing of anti-scalants can be used to control scaling [30].

Membrane wetting is another problem encountered in membrane distillation. Membrane wetting takes place when water in it liquid state is able to pass through the hydrophobic membrane material that is designed to reject water (liquid) and allows only vapour to pass through it. Since the hydrophobic MD membrane is the barrier between the feed and permeate, membrane wetting will reduce the rejection of the non-volatiles.

Membrane wetting can occur under the following conditions [29]:

- The hydraulic pressure applied on the surface of the membrane is greater than the LEP;
- The foulant depositing on the membrane surface can effectively reduce the hydrophobicity of the membrane. This effect is usually found in a long-term operation or in treating high-concentration feeds such as for brine crystallization.
- In the presence of high organic content or surfactant in the feed, which can lower the surface tension of feed solution and/or reduce the hydrophobicity of the membrane via adsorption and lead to membrane wetting [29].
- Rapture from the membrane material.

2.1.4 Membrane Thickness

Membrane thickness plays an important role in the mass and heat transfer. Permeate flux is inversely proportional to the membrane thickness in MD. Mass and heat transfer resistance increase with thickness causing reduction in mass transfer and heat loss. Therefore, membrane must be as thin as possible to achieve high permeate flux. Mass transfer is desirable, while heat loss is undesirable. Thickness also plays an important role in the amount of conductive heat loss though the membrane. In order to reduce heat resistances, it should be as thick as possible leading to a conflict with the requirement of higher permeate flux. Hence membrane thickness should be optimized in order to obtain optimum permeate flux and heat efficiency [26]. The optimum thickness for MD has been estimated within the range of 30-60μm [31].

2.1.5 Membrane Porosity

Membrane porosity is determined as the ratio between the volume of the Pores and the total volume of the membrane. Evaporation surface area increases with the increasing porosity of the membrane this leads to higher permeate fluxes through the membrane. The membrane porosity also affects the amount of heat loss by conduction [26]. Membrane material with higher porosity indicates larger evaporation surface area [32]. The membrane porosity (ε) can be determined from Smolder's-Franken equation [33];

$$\varepsilon = 1 - \frac{\rho_{\mathrm{m}}}{\rho_{\mathrm{pol}}} \tag{2.1}$$

Where ρ_m and ρ_{pol} are the densities of membrane and polymer material, respectively.

2.1.6 Membrane Pore Tortuosity

Membrane tortuosity is the average length of the pores compared to membrane thickness. It is the deviation of the pore structure from the cylindrical shape. The membrane pores do not go straight across the membrane and the diffusing molecules must move along tortuous paths, leading a decrease in MD flux. Therefore, permeate flux increases with the decrease in tortuosity [32]. It must be mentioned that this value is frequently used as a correction factor for prediction of transmembrane flux due to the difficulties in measuring its real value for the membranes used. In general a value of 2 is frequently assumed for tortuosity factor [34]. The most successful correlation for calculating the membrane tortuosity (τ) is suggested by Macki-Meares [35],

$$\tau = \frac{(2-\varepsilon)^2}{\varepsilon} \tag{2.2}$$

Where ε is the membrane porosity.

2.1.7 Membrane Thermal Conductivity

The thermal conductivity of the membrane should be small in order to reduce the heat loss through the membrane from feed to the permeate side. The selection of a thicker membrane decreases both the flux production and permeability. Conductive heat loss is inversely proportional to the membrane thickness. Thermal conductivity of the membrane is a function of the thermal conductivity of both the membrane material and the gas inside the membrane (air usually). Thermal conductivity should be as low as possible to reduce the heat loss through the membrane. One promising approach may be the selection of a membrane with higher porosity since thermal conductivity of polymer membrane is significantly higher than thermal conductivity of water vapour in the membrane pores

[36].The thermal conductivities of polymers used in MD generally varies in the range of 0.15-0.45 W $m^{-1}K^{-1}$ depending upon temperature and the degree of crystallinity [22].

2.1.8 Mean Pore Size and Pore Distribution

Membrane pore size distribution affects the uniformity of vapour permeation mechanism. The optimum pore size of the membrane is a desirable property in the membrane distillation. Pore size should be large enough for high permeate flux, and small to avoid liquid penetration. In general, uniform pore size is preferable rather than distributed pore size [26]. Mean pore size is determined by 4 methods:

- Scanning Electron Microscopy
- Atomic Force Microscopy
- Bubble Point with Gas Permeation
- Permeability Method

2.1.9 Liquid Entry Pressure (LEP)

The hydrophobic nature of membranes used in membrane distillation prevents penetration of the aqueous solutions into the pores unless a critical penetration pressure is exceeded. Liquid Entry Pressure (LEP) is the minimum transmembrane hydrostatic pressure that must be applied before liquid solutions penetrate into the membrane pores. Since the membrane is hydrophobic, it will repel and prevent water from penetrating it in the liquid phase. However, water will pass through the membrane with the presence of the necessary pressure that exceeds the membrane entry pressure. LEP depends on the maximum pore size and the membrane hydrophobicity.

In MD, the hydrostatic pressure must be lower than LEP to avoid membrane wetting. This can be quantified by the Laplace (Cantor) Equation given as [32]:

$$\mathrm{LEP} = \Delta P = P_f - P_p = \frac{-2\beta\gamma_L \mathrm{Cos}\theta}{r_{max}} < P_{process} - P_{pore} \quad (2.3)$$

Where β is a geometric factor, γ_L is the surface tension of the solution, θ is the contact angle between the solution and the membrane surface which depends on the hydrophobicity of the membrane, r_{max} is the largest pore size, $P_{process}$ is the liquid pressure on either side of the membrane, and P_{pore} is the air pressure in the membrane pore.

LEP depends on membrane characteristics and knowing its value prevents wetting of the membrane pores during MD experiments. LEP increases with the decrease in maximum pore size at the surface and increase with increasing hydrophobicity (i.e., large water contact angle) of the membrane material. The presence of strong surfactants or organic solvents can greatly reduce the liquid surface tension therefore causing membrane wetting. Therefore, care must be taken to prevent contamination of process solutions with detergents or other surfacing agents [26].

2.1.10 Contact Angle

The contact angle is a common measurement of the hydrophobic or hydrophilic behaviour of a material. It is the angle at which liquid droplet interface coincide with solid surface. It enriches us with the information about the wettability of membranes. The contact angle is determined as the angle between the surface of the wetted solid and a line tangent to the curved surface of the drop at the point of three-phase contact. The equilibrium contact angle is specific for any given system and is determined by the

molecular interactions across the liquid and solid-liquid interfaces. With low affinity between liquid and solid, the value of contact angle is greater than 90°. For the case of high affinity, the contact angle between liquid and solid is less than 90°. When the contact angle is zero (0°), then wetting occurs. The wettability of a solid surface declines with the increasing contact angle. Generally, for hydrophobic surfaces, contact angle is less than 90°. But for polymers, the contact angle is more than 120° [15, 26].

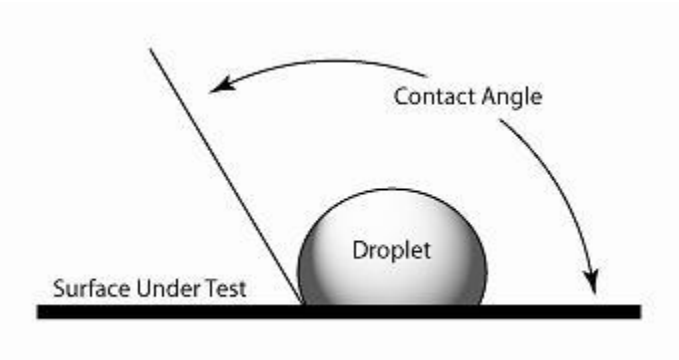

Figure 2.5 Contact angle

2.2 Literature Review

In this section, some of the past published research work are reviewed and presented in an attempt to provides more information about the world of membrane distillation for seawater desalination.

Smolders and Franken [37] compiled the nomenclatures which were defined at the "Round Table" at the "Workshop on Membrane Distillation" in Rome on May 5, 1986 into 'Terminology for Membrane Distillation'. Lawson, and Lloyd [38] presents the terminology and basic concepts associated with MD as well as the review of the past

research work in MD. Membrane properties, transport mechanism, and the design of the module were also analysed.

Jonsson et al. [21] developed simple theoretical expressions for heat and mass transfer in the air gap membrane distillation (AGMD). The developed expressions were used to calculate and studied the effect of membrane parameters on the rate of evaporation and heat loss. They found out that the air gap between the cooling surface and the membrane surface reduces the heat lost by conduction significantly but as for the rate of evaporation, air gap has little effect on it. The decrease in the heat loss when the temperature of the hot solution is increases causes an increase in the mass flux. In addition, the heat loss diminished when the membrane thickness reduces which results in increases in the mass flux.

Alklaibi and Lior [22] developed theoretical model for a two-dimensional problem in which a numerical solution of the momentum, energy and diffusion equations of the feed and cold solutions were carried out simultaneous for the air gap membrane distillation process. The model ere validated against the available experimental results. The results from the model give fundamental information about the nature of the process, and it usefulness for process optimization and improvement. The effect of air gap width, the inlet temperature of the hot solution, the coolant temperature, the feed water salt concentration, the velocity inlet of the hot and cold solution and the thermal conductivity of the membrane material on the water permeate flux and thermal efficiency of the module was studied and analysed.

Lawal and Khalifa [39] carried out theoretical analysis of heat and mass transfer in direct contact membrane distillation. Based on Kinetic theory of gas, the performance of different models of membrane permeability (coefficient) was investigated under different DCMD operating parameters including feed temperature, coolant temperature and feed flow rate. The transition type of flow model was found to give better prediction against the experimental data obtained from the literature. Knudsen diffusion model and molecular diffusion model tends to over predict the permeate flux.

De Andres et al. [40] investigated experimentally a combined membrane distillation module and a one stage multi-effect distiller. The hot brine rejected from the multi-effect distiller was used as the feed solution to the membrane module. Results revealed that permeate flux from this combine system is increased by about 7.5% and the gain output ration (GOR) of the system was increased by 10%. The temperature of about 85^0c was considered as the optimum operating condition for the feed at the evaporator inlet and a circulation flow of about 170kg/h.

Feng et al. [41] used Polyvinylidene fluoride nano fiber membrane in air gap membrane distillation to produce produced drinking water from feed saline water having NaCl concentration of 6 wt %. They were the first researcher to used electron spun nano fiber membrane in membrane distillation. After long time experiment under different conditions and different feed temperature, it was found that the membrane material was still intact and the result was comparable to commercial micro filtration membranes.

Memstill module on which almost ideal counter-current flow process is taking place was used by Meindersma et al. [42] to conduct experiment. It was found that there is

possibility of high recovery of evaporation heat when used this module. In addition, surface or waste water and salt water can be used as feed for the Memstill module. It was also found that by running the test with pre-treated surface water as feed solution for a period of about 6000 hrs, there was no penetration of micro-organisms. With waste heat as the source of energy, the Memstill process cost can be very low.

Matheswaran et al. [43] used nitric acid/water mixtures as feed solution in an air gap membrane distillation system experiment. Polytetrafluoroethylene (PTFE) hydrophobic porous membrane was used for the removal of water from the feed solution. Feed temperature, feed saline concentration, feed flow rate, and air gap width were the tested parameters. The impacts of these operating parameters on permeate flux and the selectivity of water was investigated. It was found that both permeate flux and the selectivity of water decreases with increasing feed concentration. However, increasing feed flow rate and feed temperature increases the permeate flux and decreases the selectivity of water. Furthermore, increasing the air gap width reduces the permeate flux.

Pangarkar and Sanean [44] experimentally investigated the performance of air gap membrane distillation (AGMD) for aqueous NaCl solution, natural ground water and seawater using a flat sheet PTFE membrane. The effect of operating parameters such as the feed flow rate, the feed temperature, the feed salt concentration, the coolant temperature and the air gap thickness on the membrane distillation (MD) permeation flux was also studied. In their study, the result shows that for over 90 hr continuous operation of the natural application of ground water and seawater, scale deposits was observed on the membrane surface and 23% reduction in permeate flux for ground water and 60% reduction in flux for seawater. The permeate flux increases with increases in feed

temperature and feed flow rate. It decreases with increases coolant temperature, and an air gap thickness. The optimum operating parameters of AGMD process was determined.

Singh and Sirkar [45] designed and fabricated two-hollow-fibre-sets based compact membrane device and it was investigated experimentally for air gap membrane distillation (AGMD) of hot brine. In their designed, a porous hydrophobic hollow fibre of either polypropylene (PP) or polyvinylidene fluoride (PVDF) was used for the first fibre set. The second set of hollow fibres is of solid polypropylene (PP). Cooling liquid was passed through the bore of each hollow fibre and water vapour condensation takes place on the outside surface of the hollow fibres. Different modules were considered in their study of hot brine containing 1% NaCl. The performances of such modules have been investigated for the ranges of feed brine temperatures, hot brine flow rate and the cooling liquid flow rate. Permeate flux of as high as 25kg/m^2 h was obtained from the modules at high brine temperature. Higher permeate flux were obtained as a results of higher brine flow rate and higher cooling flow rate which in turn reduces the thermal polarization and cooling side temperature resistance. It was concluded from their investigation that for a better performance of a module, it is very important to have efficient combination of the two different sets of hollow fibres.

Alkhudhiri et al. [32] investigate experimentally the impact of using a high concentration of NaCl, $MgCl_2$, Na_2CO_3, and Na_2SO_4 as feed solution in air gap membrane distillation. Different feed concentrations and membrane pore sizes are the conditions upon which the experiment was conducted. The flux declines as the concentration of salt increases, and increases as the pore size increases. Result shows that the permeate flux decreases with increasing feed concentration. It was also found that energy consumption at different

membrane pore size, and feed solution type and concentration is independent of feed solution concentration, feed solution type and membrane pore sizes.

Tian et al. [46] introduced a new design of AGMD with advanced improvement method, high efficient and low cost. The new module is capable of producing a maximum of 119kg/m^2h distil water when tap water was used as the feed solution. The maximum flux was obtained at the coolant and feed temperature of 12^0C and 77 ^{0}C respectively. The mechanistic rotational and tangent turbulent flow was used to reduce the concentration and temperature boundary layer thickness by washing the membrane surface and to speed up vapour diffusion and enhanced the heat and mass transfer efficiencies. The new design used the concept of membrane surface contact to reducing the additional resistance offered by the air gap thickness.

Khalifa [47] conducted an experiments to compare and contrast the performance of water gap membrane distillation (WGMD) and air gap membrane distillation (AGMD) designs under different operating and design variables. The effects of feed flow rate, feed temperature, gap width, coolant flow rate, and feed concentration, and the material of membrane supporting plate on the permeate flux are the tested variable. Results showed that the water gap design improved the permeate flux considerably. The water gap design recorded flux ranges between 80 to 140% greater than the air gap design. He also observed that the temperature inside the water gap is lower than that of the air gap under the same operating conditions. It was also noticed that the water gap is less sensitive to gap width compared to air gap.

Schofield et al. [48] developed equations for heat and mass transfer in membrane distillation (MD) and the equations was tested experimentally. The membrane mass transfer coefficient may was estimated from a combination of Knudsen and molecular diffusion theories. The important of Temperature polarisation was looked into and it's relevant to the discussion of experimental results. It was found that tubular and hollow fibre membranes manifest the least temperature polarisation. They discussed the role of temperature polarisation in the design and operation of large-scale MD cells. In their work it was found that hollow fibre and tubular type of module shows to be more effective compared to the other types.

Gryta and Tomaszewska [49] performed an experiment to investigation membrane distillation (MD) with a laminar flow of the streams in the MD module .The model equations describing the heat transfer in MD capillary modules were developed and verified with an experimental results. The equations were derived for the calculation of the feed and distillate temperature at a layer adjacent to the membrane. The physical model of the MD process was incorporated with the heat transfer correlations and the applicability of the model was validated with experimental result. The accuracy of the calculation of the interphase temperatures increases which results in the increase of MD model credibility. The Nusselt number correlation developed was said to be used for membrane distillation heat transfer in MD module.

Liu et al. [50] investigated both theoretically and experimentally the Air gap membrane distillation (AGMD). Theoretical model of heat and mass transfer associated with Air gap membrane distillation was developed and the developed model was validated against the experimental result. The developed model was in fair agreement with the experimental

results. The experimental investigations are carried out on AGMD of different aqueous solutions, namely: tap water, salted water, dyed solutions, alkali solutions and acid solutions simple relationships were obtained. The effects of solution concentration and the width of the air gap in AGMD module are analysed and discussed.

Martinez-Diez and Gonzalez [51] in a membrane distillation experiment investigated the transportation of water through a flat PTFE membrane material. Water and aqueous solutions of NaCl was used as feed. Evaluations on the effects of temperature and concentration polarization were made to the reduction of vapour pressure differences across the membrane. From the evaluation it was found that only temperature polarization becomes important while effect of concentration polarization was insignificant. A coefficient which measures this reduction was introduced. The introduction of the coefficient allows them to evaluate effective vapour pressure difference for the transport with regard to the imposed vapour pressure difference. This coefficient and the temperature polarization coefficient coincide when water is used as feed, but when salt concentration is been increased they are becomes different. The discussions on the measured permeate flux results and that of calculated polarization results were made for different temperatures, flow rates and solution concentrations. Polarization layers formed on either side of PTFE membrane reduce water passing through the membrane material. It was explain that the f values which mean an important reduction, between 40% and 65%, in the imposed force, depends on the experiment.

Khayet et al. [52] developed a theoretical model that describes sweeping gas membrane distillation processes in a counter flow plate-and-frame membrane module. The model was validated against an experiments carried out using two PTFE membrane materials

supported by a polypropylene net. Pure water was used as hot liquid feed and water saturated air as cold sweeping gas. They consider liquid feed and the sweeping gas to flow in an opposite direction (counter flow). The developed model explain the significance of the heat fluxes in the directions that is parallel and perpendicular to the membrane surface and the temperature profiles inside the fluid phases was obtained. The theoretical model for explicit expressions was obtained for the temperature profiles along the module for both the liquid feed and the sweeping gas. The important of some relevant parameters, like the inlet and outlet temperatures and the velocities of the fluids has been studied. The results from the experiment show that the temperature of the liquid feed and the circulation velocity of sweeping gas are important operative parameters.

Khayet et al. [53] used shell-and tube module and polypropylene (PP) to investigate theoretically and experimentally a desalination technique called sweeping gas membrane distillation. Humid air was used as the sweeping gas in the experiment. The operating parameters such as air flow rate, feed temperature, salt concentration, etc., were equally investigated. Theoretical models for heat and mass transfer as well as temperature and concentration polarization was developed and validated against the data from the experiment. This shows that mass flux depends on air flow rate and the feed temperature, the permeate flux decreases with salt concentration, they found that the results from the experiment and that from the theory are in good agreement. They also shows that at higher air flow rate, the experimental result was found to be lower than that of the predicted mass flux.

Dehesa-Carrasco et al. [54] experimentally and theoretically investigated air gap membrane distillation unit which was manufactured from an insulated material to

minimized heat losses. With the help of temperature and flow rate measurement, the enthalpy as well as diffusion coefficient of vapours in the gap width of different flows are evaluated. The experiments was conducted for different values of feed temperature and flow rate and one dimensional heat and mass transfer model with no free parameters was proposed. Model prediction and the experimental data show good match and the errors between measured and predicted temperatures was approximated to 5% accuracy. However, the trends of the model and the experimental data differ; as such the possible improvements to the model are discussed.

Alsaadi et al. [55] developed a one dimensional model based on theoretical equations governing the mechanism for mass and heat transfer process in air gap membrane distillation. The developed model is capable of modelling AGMD modules in counter-current and co-current flow regimes. An experiment was conducted at different operating factors and conditions. The model was validated against the experimental data. Comparison showed that the model flux predictions are strongly correlated with the experimental data, with model predictions being within +10% of the experimentally determined values. After model validation, the model was subsequently used to studied and analyse the thermal efficiency and the parameters that improved the AGMD unit.

Using fibre membranes and in a counter current flow configuration, C. M. Guijta et al. [56] developed a model for predicting flux in air gap membrane distillation. The permeate flux movement across the membrane material is described by the dusty-gas model of mechanism of mass transfer for Knudsen diffusion, molecular diffusion and viscous flow. Experiment was conducted to determine membrane mass transport properties. In the experiment, a single gas permeation experiment was used to determine

Knudsen diffusion and viscous flow membrane parameters whereas the molecular diffusion membrane parameter was achieved using binary gas diffusion experiments. It was however found that single gas permeation experiments in combination with a cylindrical pore membrane model are unfortunately, not enough to achieve a reliable membrane mass transfer properties for model calculations.

Guijta et al. [57] conducted an experiment for counter flow air gap membrane distillation and validate the results with the theoretical model calculations. Experimental data shows that earlier developed model exactly described the significant effect of temperature difference, temperature level, air gap total pressure, membrane type and feed flow rate. It was found that decreasing the total air gap pressure to the saturated water vapour pressure of the feed flow temperature of 65^0C increases the permeate flux by three folds. The energy efficiency of the system was equally analysed experimentally and theoretically and it was found that the thermal efficiency of the experiment slightly lower than that of the theoretical result as a result of heat loss.

Izquierdo-Gil et al. [58], present the results obtained from theoretical model and experiment conducted with air gap membrane distillation (AGMD). Sucrose aqueous solutions were used as the feed solution. The influence of important operating parameters such as feed temperature, flow rate, concentration, air gap width and membrane type were investigated. The theoretical models showed good agreement with the experimental data over the range of temperatures investigated. The result for diffusion coefficient of water vapour-air mixture and thermal diffusion coefficient were obtained and compared. It was found that the magnitude of diffusion coefficient of water vapour-air mixture was higher than thermal diffusion coefficient even though they are of the same magnitude.

Garcıa-Payo et al. [59] used air gap membrane distillation to study the aqueous solutions of alcohol ethanol, methanol and isopropanol experimentally. The experiment was conducted under different operating parameters such as feed temperature, flow rate, air gap width, feed solution type, etc. A theoretical model based on temperature polarization was as well developed. The equivalent film heat transfer coefficient and the overall membrane mass as well as alcohol and water membrane transfer coefficients we obtained from the experimental data and it was used to estimate the transmembrane composition and temperature. Subsequently, the temperature polarization model, and Sieder and Tate heat transfer correlation was used to investigate the influence of Reynolds number on the amount of distillate produced.

Geng et al. [60] developed a new AGMD module with internal heat recovery for water desalination to investigate the impact of AGMD operating parameters. The module consists of heat exchange and parallel hollow fibre membrane. Based on mass and energy balance, a theoretical model was developed to estimate the permeate flux and temperature drop along the membrane. Result reveals that higher permeate flux and temperature drop were observed at the upper part of the module when compared to that of lower part. Experimental results yield a maximum permeates flux of 5.30kg/m^2h and a GOR of 5.70. The experimental result also yields a minimum of 80% thermal efficiency.

Khalifa et al. [61] experimentally and theoretically studied the performance of air gap membrane distillation. The effect of feed temperature, coolant temperature, feed flow rate and air gap width on permeate flux was investigated in the study. The influence of feed solution on permeate flux was also investigated. The model prediction of permeate flux showed good agreements with experimental results. Results showed that the feed

temperature and the width of the air gap are very effective operating and design parameters to enhance the output flux.

While Traditional Design of Experiments focuses on how different design factors affect mean results, Taguchi's DOE put emphasis on variation rather than the mean. Additionally, the former treats noise as an extraneous factor, while the latter considers it as a central point of its analysis. Toraj and Safavi [62] applied Taguchi techniques in the optimizing the performance of vacuum membrane distillation system for water desalination. In the study, feed temperature in the range of 35°C to 55°C, feed flow rate of 15-60 mL/s, vacuum pressure of 30-130 mbar and feed concentration of 50-150 g/L were investigated. Application of ANOVA showed that all the operating parameters were significant, with each having different level of importance. The optimum permeate flux reported was 16.96 kg/m^{2}h at 55^{0}C feed temperature, 30 mL/s feed flow rate, 50 g/L feed concentration and 30 mbar vacuum pressure.

Khayet and Cojoucaru [63] modelled and optimized air gap membrane distillation system using response surface methodology. The specific performance index and performance index were predicted using developed regression model with the effect of energy consumption as function of different operating variables. Statistical analysis was performed using analysis of variance (ANOVA) to determine the significant level of each parameters. Using Monte Carlo simulation, an optimum variable combination for performance index were found to be 71°C feed inlet temperature, 13.9°C cooling inlet temperature and 183L/h feed flow rate. These variables combination gave an experimental permeate flux of 47.189 kg/m^{2}h. The optimum variables combination for specific performance index were found to be 59°C feed inlet temperature, 13.9°C cooling

inlet temperature and 205 L/h feed flow rate which resulted to an experimental output of 188.7kg/kWh.

Lawal and Khalifa [64] carried out statistical and theoretical analysis of DCMD using Taguchi design of experiment (DOE) approach. The statistical and the theoretical models were used to predict flux in DCMD system. Excellent agreement was reached between the both models results. Prior to the generation of the statistical model, the theoretical model was validated against an experimental work. Good agreement was reached between the theoretical and the used experimental data.

2.3 Research Objective

Due to numerous advantages associated with membrane distillation as compared to other desalination technology, a fundamental experimental and theoretical study on desalination using air gap membrane distillation module is carried out. The objective of this investigation is to theoretically and experimentally investigate the performance of air gap membrane distillation unit for water desalination under different experimental conditions and operating parameters. The other objective is to optimize the system performance.

The main objectives can be summarised as follow:

- Design and construct a lab scale AGMD desalination system.
- Investigate the influence of AGMD operating parameters on the distillate production.

- Conduct analytical modelling of heat and mass transfer in AGMD to predict the system flux.
- Validate the modelling results against the experimental findings.
- Optimized the system performance.
- Test the flux enhancement with double stages module.

2.4 Research Methodology

The above mentioned objectives are achieved through the following steps:

- A comprehensive literature review on membrane distillation (MD).
- Experimental design.
- A detailed design of AGMD module.
- Manufacturing of the designed AGMD module.
- Construction of set up.
- The AGMD module will be assembled and equipped with instrumentations and data acquisition systems (DAQ) for accurate measuring of temperature, pressure, flow rate, water conductivity (TDS), storing, monitoring, etc., of the experimental data.
- A comprehensive investigation on the performance of AGMD unit at different operating parameters and experimental conditions.

- Study of heat and mass transfer modes in AGMD to comes up with a theoretical model to predict the system flux.
- Comparison of the theoretical model result with the experimental data in order to ascertain the validity of the model.
- Optimization of the system using Taguchi method
- And double stage testing.

CHAPTER 3

HEAT AND MASS TRANSFER ANALYSIS IN AGMD

A schematic diagram of a typical AGMD is illustrated in Figure 3.1. The system consists of a micro porous hydrophobic membrane sheet situated between hot feed solution and the air gap. In between the air gap width and the cooling channel is a condensation surface. The theoretical modelling of air gap membrane distillation involves heat transfer and mass transfer concurrently. The process of heat and mass transfer may be split into the following analysis [21].

- Convective heat transfer from hot feed solution to the membrane surface.
- Evaporation formed at the membrane pores entrance (feed membrane interface).
- Movement of water vapour across the membrane pores
- Water vapour diffusion across the stagnant air gap.
- Vapour condensation over the cooling plate.
- Convective heat transfer between cold solution and the cooling surface.

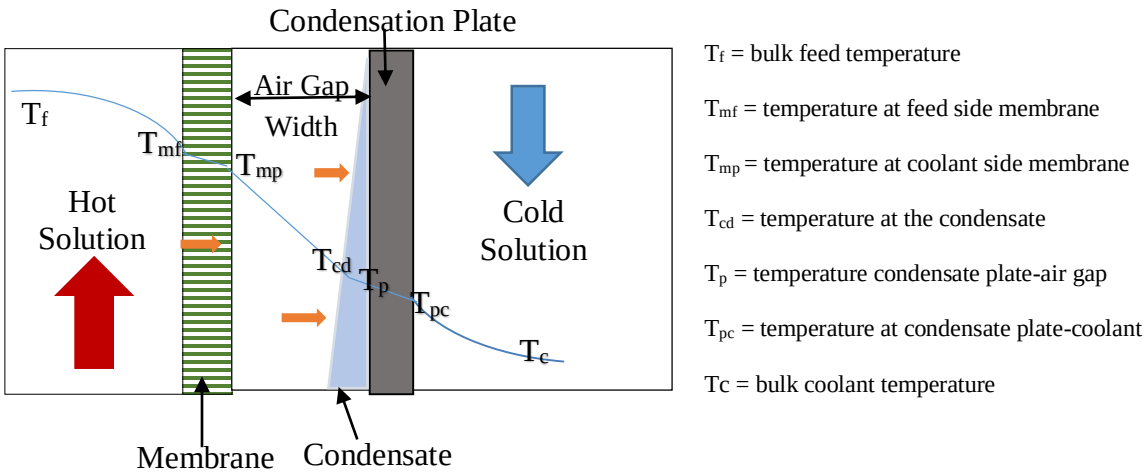

Figure 3.1 Model of heat and mass transfer in the AGMD

In modelling the AGMD, the following assumptions are considered,

- Steady state system
- Air within the membrane pore is considered to be stagnant
- No pressure drop inside the air gap, meaning constant pressure assumption is considered in the air gap
- Membrane material has no selectivity toward any species
- Liquid entrance pressure is greater than the pressure at the feed side of the membrane.
- Within the air gap, mass is transported by diffusion while heat is transfer by conduction
- No heat exchange between the system and the surrounding.
- Film-wise condensation is considered in the cooling plate

3.1 Mass Transfer

The mass transfer across the membrane material depends on the differences in vapour pressure between both sides of the membrane. The relationship between mass transfer and the vapour pressure differential across the membrane in MD is expressed as [15, 50].

$$J_W = B_w \, \Delta P \tag{3.1}$$

Where ΔP is the transmembrane vapour pressures differential (driving force) between the feed and coolant side of the membrane, J_w is mass transfer and B_w is the overall mass transfer coefficient.

Since condensation takes place on the plate surface (see fig. 3.1) in AGMD, the eq. (3.1) can be re-written as:

$$J_W = B_w \left(P_{mf} - P_{cd}\right) \tag{3.2}$$

Where P_{mf} is the vapour pressures at the feed side of the membrane while P_{cd} vapour pressures at the condensation surface.

In the vapour phase of a mixture of air and water vapour, the equations for a binary gas are used, since air can be considered as one component with water vapour in MD. The following equation can be used to evaluate the permeate flux of the water vapour across the membrane and the air gap [15, 56, 65, 66].

$$J_w = -cD_{wa}\frac{dy}{dz} + y(J_w + J_a) \tag{3.3}$$

Where y is the mole fraction of water vapour, z is the direction perpendicular to membrane surface, and c is the molar density, which is given by the equation below for the case of ideal gas law. It must be mentioned that the first and the second terms at the

left side of eq. (3.3) are the mass transfer by molecular diffusion, and the convective flux respectively.

$$c = \frac{P}{RT} \tag{3.4}$$

For negligible net flow of air, eq. (3.3) become

$$J_w = -cD_{wa}\frac{dy}{dz} + y(J_w) \tag{3.5}$$

$$J_w - y(J_w) = -cD_{wa}\frac{dy}{dz}$$

$$J_w(1-y) = -cD_{wa}\frac{dy}{dz}$$

$$J_w = \frac{-cD_{wa}}{(1-y)}\frac{dy}{dz} \tag{3.6}$$

At steady state, the mass transport across the air gap is constant. Therefore,

$$\frac{dJ_w}{dz} = 0 \tag{3.7}$$

The substitution of eq. (3.6) into (3.7) leads to:

$$\frac{-d}{dz}\left(\frac{-cD_{wa}}{(1-y)}\frac{dy}{dz}\right) = 0 \tag{3.8}$$

Integration of Eq. (3.8) with respect to the following boundary conditions at Z = 0, $Y = Y_{mf}$ and at Z = $\delta\tau + b = b'$, $Y = Y_{cd}$, and assuming $c\ and\ D_{wa}$ to be constant lead to:

$$\frac{1}{1-y}\frac{dy}{dz} = C_0 \tag{3.9}$$

where δ, τ, b are the membrane thickness, membrane tortuosity, and air gap width respectively.

$$\tfrac{1}{1-y}dy = C_0 dz$$

$$\int \tfrac{1}{1-y}dy = C_0 \int dz$$

$$-ln(1-y)\,|_{y_{mf}}^{y_{cd}} = C_0|_0^{b'}$$

$$-ln(1-y_{cd}) - (-ln(1-y_{mf})) = C_0(b')$$

$$ln(1-y_{mf}) - ln(1-y_{cd})) = b'C_0$$

$$ln\left(\frac{1-y_{mf}}{1-y_{cd}}\right) = b'C_0$$

$$C_0 = \frac{1}{b'} ln\left(\frac{1-y_{mf}}{1-y_{cd}}\right) \tag{3.10}$$

Substitute Eq. (3.10) into Eq. (3.9)

$$\frac{1}{1-y}\frac{dy}{dz} = \frac{1}{b'} ln\left(\frac{1-y_{mf}}{1-y_{cd}}\right) \tag{3.11}$$

Substitute for left hand side of Eq. (3.11) into Eq. (3.6)

$$J_w = \frac{-cD_{wa}}{b'} ln\left(\frac{1-y_{mf}}{1-y_{cd}}\right) \tag{3.12}$$

By incorporating the influence of membrane porosity into Eq. (3.12) leads to:

$$J_w = \frac{-\varepsilon cD_{wa}}{b'} ln\left(\frac{1-y_{mf}}{1-y_{cd}}\right) \tag{3.13}$$

Eq. (3.13) can be re-written as

$$J_w = \frac{\varepsilon cD_{wa}}{b' y_{aln}} (y_{mf} - y_{cd}) \tag{3.14}$$

Where

$$y_{aln} = \frac{(y_{amf} - y_{acd})}{ln\left(\frac{y_{amf}}{y_{acd}}\right)} \tag{3.15}$$

The vapour pressure is related to the mole fraction by [55]

$$\mathrm{y} = \frac{P_v}{\mathrm{P}} \tag{3.16}$$

Where P is the total pressure, P_v is the vapour pressure and y is the corresponding mole fraction. Thus, eq. (3.14) can be re-written in terms of pressure [15] as:

$$J_w = \frac{\varepsilon P D_{wa}}{R T_m b' |p_a|_{ln}} (p_{mf} - p_{cd}) \tag{3.17}$$

Where ε is the membrane porosity, R is the gas constant and is equivalent to 8.314472 J/mol.K, P is the total pressure, $D_{wa}$is the mass diffusivity between the air and water vapour, T_m is the mean temperature in kelvin (k) given by:

$$T_m = \frac{T_{mf} + T_{cd}}{2} \tag{3.18}$$

And $|p_a|$ is the air pressure in the pores of the membrane and it's given by:

$$|p_a|_{ln} = \frac{(p_{amf} - p_{acd})}{ln\left(\frac{p_{amf}}{p_{acd}}\right)} \tag{3.19}$$

The product of total pressure and the mass diffusivity of water into air in eq. (3.16) is given as[15, 67]:

$$P D_{wa} = 1.895 \times 10^{-5} T^{2.072} \tag{3.20}$$

Other similar equations that may be used instead of equation 3.20 are found in literature; see for example ref. [23] and [68].

To obtain the mass diffusivity (D_{wa}) in eq. (3.20), the following relation may be considered [66, 69]:

$$D_{wa} = D^0 \left[\frac{T_m}{298}\right]^{2.334} \tag{3.21}$$

Where D^0 is the mass diffusivity between the air and water vapour at standard condition.

The total pressure is equivalent to the summation of water vapour pressure and air pressure in the membrane pore. Therefore, air pressure inside the pore can be expressed as:

$$p_a = P - P_v \tag{3.22}$$

Where P_a is the air pressure, P is the total pressure and P_v vapour pressure.

With the air pressure in eq. (3.22), we can calculate the terms p_{amf} and p_{acd} in eq. (3.19). The corresponding $|p_a|_{ln}$ will be substituted in eq. (3.17) to estimate the flux.

The transmembrane vapour pressures $P_{mf}\ and\ P_{cd}$ in Eq. (3.17) can be evaluated from Antoine equation at transmembrane temperatures $T_{mf}\ and\ T_{cd}$ respectively. The respective Antoine equations are expressed as [15]:

$$P_{mf} = exp\left(23.328 - \frac{3841}{T_{mf}-41}\right) \tag{3.27}$$

$$P_{cd} = exp\left(23.328 - \frac{3841}{T_{cd} - 41}\right) \tag{3.24}$$

For feed solution containing dissolved salt, P_{mf} may be estimated using the Raoult's law expressed which may be given as [70]:

$$P_{mff} = (1 - CM_{NaCl})P_{mf} \tag{3.25}$$

Where CM = mole solute concentration and can be estimated from:

$$\mathrm{CM_{NaCl}} = \frac{\mathrm{NaCl\ concentration\ (g/L)}}{58.44\ \mathrm{(g/mol)}} \tag{3.26}$$

Where 58.44 (g/mol) is the molar mass of sodium chloride.

Replacing P_{mf} with P_{mff} in eq. 3.23 will take care of the salt concentration effect

3.2 Heat Transfer

In order to obtain the temperatures $T_{mf}\ and\ T_{cd}$ needed in Antoine equation, heat transfer analysis across the MD process is considered. For heat transfer analysis in AGMD

process, the following major steps arranged in a preceding order are of great important [15]:

- Heat transfer by convection from the hot feed solution to the membrane surface.
- Heat transport by conduction across the membrane material and mass transfer of vapour across the membrane sheet.
- The conduction heat transfer in the stagnant air gap and heat of condensation at the cold surface.
- Heat transfer by conduction through the cold plate and
- Heat transfer by convection between the cooling surface and the cooling water.

The steps involved in the analysis of heat transfer in AGMD are presented below.

The transfer of heat from the hot saline solution to the membrane feed surface at steady state can be expressed as [65, 71]:

$$Q_f = h_f(T_f - T_{mf}) + J_w C_f(T_f - T_{mf}) \tag{3.27}$$

$$Q_f = h_h(T_f - T_{mf}) \tag{3.28}$$

Where

$$h_h = h_f + J_w C_f \tag{3.29}$$

h_f and C_f are the heat transfer coefficient and the specific heat of the liquid feed respectively.

The convective term is dominant over the heat transfer associated with the mass transfer term in eq. (3.27). The convective term claims over 90% of the heat transfer in the feed chamber, while less than 10% of heat is associated with mass transfer.

The heat transfer from the hot membrane surface to the condensate liquid interface Q_{p1} takes place due to sensible heat flux, Q_s and the heat of vaporization at feed membrane surface. It can be expressed as:

$$Q_{p1} = Q_s + J_w H_w \tag{3.30}$$

$$Q_{p1} = h^*(T_{mf} - T_{cd}) + J_w H_w \tag{3.31}$$

H_w is the heat of vaporization in (kJ/kg) which may be calculated from [15]:

$$H_w = 1.753T + 2024.3 \tag{3.32}$$

and the heat transfer coefficient h* is expressed as [15, 65, 69],

$$h^* = h_y \left(\frac{\emptyset}{1 - e^{-\emptyset}} \right) \tag{3.33}$$

The heat transfer rate factor $\emptyset$ is given by $\emptyset = \frac{J_w C_{cd}}{h_y}$. The correction factor $\emptyset$ account for the influence of finite mass fluxes on the heat transfer coefficient h_y. For diminishing small mass transfer fluxes ($J_w \to 0$), the $\emptyset$ reduces to unity, resulting in linear temperature profile. The impact of this correction fact for on mass transfer in gas phase is minimal. The impact is close to unity for high mass flux in liquid phase [69].

C_{cd} is the gas phase specific heat capacity and h_y is the gas phase heat transfer coefficient given by $h_y = \frac{k}{b}$, where k and b are the thermal conductivity at the gas phase and air gap thickness respectively.

Upon substitution, Eq. (3.33) can be re-written as:

$$h^* = \left(\frac{J_w C_{cd}}{1 - e^{-\frac{J_w C_{cd}}{h_y}}} \right) \tag{3.34}$$

From the condensate surface to the cooling solution, the following mode of heat transfer takes place:

Heat transfer by convection via the condensate layer is given by [15]:

$$Q_c = h_d(T_{cd} - T_p) \tag{3.35}$$

Heat transfer by conduction through the cooling plate is given by [15]:

$$Q_c = \frac{k_c}{l}(T_p - T_{pc}) \tag{3.36}$$

Heat transfer by convection between cooling solution and the cooling plate is given as [15]:

$$Q_c = h_c(T_{pc} - T_c) \tag{3.37}$$

Heat transfer by convection from condensate layer to the cooling solution is given by [15]:

$$Q_c = h_p(T_{cd} - T_c) \tag{3.38}$$

From the condensation layer interface to the cooling liquid, the heat transfer at steady state can be written as [15],

$$Q_c = h_d(T_{cd} - T_p) = \frac{k_c}{l}(T_p - T_{pc}) = h_c(T_{pc} - T_c) = h_p(T_{cd} - T_c) \tag{3.39}$$

Where h_d is the heat transfer coefficient of the condensate, k_c is the condensate plate thermal conductivity, l is plate thickness, h_c is the heat transfer coefficient of coolant film and h_p is the overall heat transfer coefficient from vapour/condensate liquid interface to cooling solution and its expressed as.

$$h_p = \left(\frac{1}{h_d} + \frac{l}{k_c} + \frac{1}{h_c}\right)^{-1} \tag{3.40}$$

And by considering film-wise condensation as depicted in figure 6.2, h_d can be estimated from [15, 69]

$$h_d = \left(\frac{g\rho^2 H_w k_p^3}{L\mu_d(T_{cd} - T_p)}\right)^{\frac{1}{4}} \tag{3.41}$$

Where ρ, k_p and, μ_d are the fluid density, thermal conductivity and dynamic viscosity at the condensate film temperature respectively. L is the height of air gap (height of the cooling plate) and g is the acceleration due to gravity. The plate thickness and height is depicted in figure 3.2.

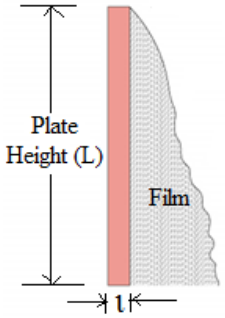

Figure 3.2 Film-wise Condensation on a vertical plate

Combination and manipulation of Eq. (3.27) to (3.41) leads to

$$T_{mf} = T_f - \frac{H}{h_f}\left((T_f - T_c) + \frac{J_w H_w}{h}\right) \tag{3.42}$$

And

$$T_{cd} = T_c + \frac{H}{h_f}\left((T_f - T_c) + \frac{J_w H_w}{h}\right) \tag{3.43}$$

Where

$$H = \left(\frac{1}{h_f} + \frac{1}{h} + \frac{1}{h_p}\right)^{-1} \tag{3.44}$$

The heat transfer coefficients (h_f and h_c) may be estimated from the empirical correlation of the dimensionless Nusselt numbers. For laminar channel flow, the following expression can be used [32, 72]:

$$Nu = 1.86 \left(Re\, Pr \frac{d}{L}\right)^{0.33} \tag{3.45}$$

Where Nu is the Nusselt number and it's given by $Nu = \frac{hd}{k}$

Pr is the Prandtl number expressed as $Pr = \frac{\mu C_P}{k}$, and Re is the Reynolds number given by $Re = \frac{\rho u d}{\mu}$.

Table 3.1 Correlations used to estimate heat transfer coefficient [32]

EQUATIONS	TYPES OF FLOW	REFERENCES
$\mathrm{Nu} = 0.027\ \mathrm{Re}^{\frac{4}{5}}\ \mathrm{Pr}^{\mathrm{n}} \left(\frac{\mu}{\mu_s}\right)^{0.14}$ $\mathrm{n} = 0.4$ for heating and $\mathrm{n} = 0.3$ for cooling	Turbulent flow	[73]
$\mathrm{Nu} = 0.023\ \mathrm{Re}^{0.8}\ \mathrm{Pr}^{\mathrm{n}}$ $\mathrm{n} = 0.4$ for heating and $\mathrm{n} = 0.3$ for cooling	Turbulent flow	[35]
$\mathrm{Nu} = 0.023\ \mathrm{Re}^{0.8}\ \mathrm{Pr}^{0.33} \left(\frac{\mu}{\mu_s}\right)^{0.14}$	Turbulent flow	[38]
$\mathrm{Nu} = 0.023 \left(1 + \frac{6\mathrm{d}}{\mathrm{L}}\right)\ \mathrm{Re}^{0.8}\ \mathrm{Pr}^{\frac{1}{3}}$	Suitable for Turbulent flow	[72, 74, 75]
$\mathrm{Nu} = 1.86 \left(\mathrm{Re}\,\mathrm{Pr} \frac{\mathrm{d}}{\mathrm{L}}\right)^{0.33}$	Laminar flow	[35, 51]
$\mathrm{Nu} = 1.86 \left(\mathrm{Re}\,\mathrm{Pr} \frac{\mathrm{d}}{\mathrm{L}}\right)^{0.33} \left(\frac{\mu}{\mu_s}\right)^{\frac{1}{7}}$	Laminar flow	[76, 77]
$\mathrm{Nu} = 1.86\ \mathrm{Re}^{0.33} \mathrm{Pr}^{0.33} \left(\frac{\mathrm{d}}{\mathrm{L}}\right)^{\frac{1}{3}}$	Laminar flow	[78]
$\mathrm{Nu} = 1.62 \left(\mathrm{Re}\,\mathrm{Pr} \frac{\mathrm{d}}{\mathrm{L}}\right)^{0.33}$	Laminar flow	[38]
$\mathrm{Nu} = 0.298\ \mathrm{Re}^{0.646} \mathrm{Pr}^{0.316}$	Laminar flow	[79]
$\mathrm{Nu} = 0.74 \mathrm{Re}^{0.2} (\mathrm{Gr}\,\mathrm{Pr})^{0.1} \mathrm{Pr}^{0.2}$	Laminar flow	[51]
$\mathrm{Nu} = 0.036\ \mathrm{Re}^{0.8}\ \mathrm{Pr}^{0.33} \left(\frac{\mathrm{d}}{\mathrm{L}}\right)^{0.055}$	Turbulent flow	[80]
$\mathrm{Nu} = 0.036\ \mathrm{Re}^{0.96}\ \mathrm{Pr}^{0.33} \left(\frac{\mathrm{d}}{\mathrm{L}}\right)^{0.055}$	Turbulent flow	[78]
$\mathrm{Nu} = 1 + 1.44 \left(1 - \frac{1708}{\mathrm{Re}}\right) + \left[\left(\frac{\mathrm{Re}}{5830}\right)^{\frac{1}{3}} - 1\right]$	Not mention	[81]

But d is the channel hydraulic diameter, k is the thermal conductivity, μ is the fluid viscosity and C_P is the specific heat capacity. It is worth mentioning that the considered flow condition is within the laminar flow range since the maximum calculated Re is about 450 (at feed flow rate of 5L/min). For channel flow, Re<500 (Laminar flow), while Re>2000 (Turbulent flow). Thus, eq. (3.45 is used in estimating heat transfer coefficient.

3.3 Temperature Polarization

Temperature polarization denoted by (θ) is considered as one of the setback of membrane distillation. The temperature polarization coefficient is used as the baseline for the energy efficiency. It is commonly used to measure the extent of the resistance of boundary layer over the resistance of total heat transfer. Temperature polarization is the ratio of differences in temperature between the liquid-vapour interface and the bulk temperature. It can be expressed as [15]:

$$\theta = \frac{T_{mf} - T_{cd}}{T_f - T_c} \tag{3.46}$$

The value of temperature polarization (θ) is expected to be one in ideal case. However, θ is always lower than one because the bulk temperatures are always greater than the difference in temperature between the interfaces of liquid-vapour. The value of temperature polarization (θ) determines whether MD module is designed properly or awfully designed. MD module is awfully design if θ is lower than 0.2, but MD module is considered to be well designed if θ is more than 0.6 [15].

3.4 Thermal Efficiency

Out of total heat supplied to MD process, large portion of it is used for as heat of vaporization while the remaining heat supplied is wasted in the form of conduction heat transfer. This conduction heat loss leads to reduction in MD thermal efficiency.

Thus, the thermal efficiency of MD system can be expressed as [15]:

$$\eta(\%) = \frac{Q_v}{Q_v + Q_c} \times 100\% \tag{3.47}$$

Where Q_v is the latent heat of the vapourized liquid which is expressed as $Q_v = J_w H_w$, and Q_c is the heat transfer by conduction via the membrane and the air gap. The conduction heat lost from the feed to the permeate in AGMD may be expressed as:

$$Q_c = \frac{(T_{mf} - T_{cd})}{\frac{\delta}{K_m} + \frac{b}{K_g}} \tag{3.48}$$

Where δ is the membrane thickness, $K_m$is the effective thermal conductivity of the membrane material and the gas filling it. K_m can be estimated from the expression [15]:

$$K_m = \varepsilon K_g + (1 - \varepsilon) K_p \tag{3.49}$$

Using the isostress model [15, 67]:

$$K_m = \left[\frac{\varepsilon}{K_g} + \frac{(1 - \varepsilon)}{K_p}\right]^{-1} \tag{3.50}$$

Where K_g and K_p are the thermal conductivity of the gas filling the membrane pores and membrane material respectively. The thermal conductivities of polymers (K_p) for example, PTFE range between 0.25 to 0.27 W $m^{-1}K^{-1}$ at 296 K and 0.29 W $m^{-1}K^{-1}$ at 348 K [15], and the thermal conductivity of air filling the pores at 298 K is 0.024 W $m^{-1}K^{-1}$.

Therefore, the thermal efficiency of the MD system is given by [15];

$$\eta(\%) = \frac{J_w H_w}{J_w H_w + \frac{(T_{mf} - T_{cd})}{\frac{\delta}{K_m} + \frac{b}{K_g}}} \times 100\% \quad (3.51)$$

3.5 Gain Output Ratio (GOR)

Another possible measure of the performance of MD system is gain output ratio. GOR is defined as

$$\text{GOR} = \frac{J_w H_w}{Q_{in}} \times \text{Effective membrane Area} \quad (3.52)$$

Where Q_{in} is the total heat supply to the system and it can be expressed as

$$Q_{in} = \dot{m} C_p (T_{f,in} - T_{f,out}) \quad (3.53)$$

Where $\dot{m}$ is the mass flow rate of the feed solution, C_p is the specific heat capacity of the feed solution, while $T_{f,in}$ and $T_{f,out}$ are the bulk feed inlet and outlet temperature respectively.

GOR represent the ratio between the energy used for evaporation to the energy consumed by the system.

3.6 Procedure for Flux Prediction (J_W)

For flux prediction, an iterative method was adopted. Guessed values were assumed for membrane surface temperatures (T_{mf} and T_{cd}) as initial guess, the guessed values were then utilized to estimates the Antoine equation and permeate flux (J_W) as given in Eqs.

(3.17, 3.23, and 3.24). The current flux (J_W) value is then utilized to estimate heat transfer coefficient given in eq. (3.29 to 3.37) with the help of eq. (3.45) or any other correlation from table 3.1. Eqs. ((3.42) and (3.43)) is then used to estimate the initial assumed temperatures, the obtained temperature results is compared with the initial assumed (guessed) values of temperatures. The above procedures are repeated until the difference between assumed temperatures and calculated temperatures is less than 0.1% (until the assumed values for $T_{mf}\ and\ T_{cd}$ concurred with the calculated ones with the relative error of less than 0.1%).

The water properties used in the code are obtained from different sources given by [82, 83].

CHAPTER 4

EXPERIMENTAL SET-UP AND PROCEDURE

4.1 Experimental Set-up

In this chapter, we presents the description of the AGMD set-up, materials used in the experiments, the components and instrumentations of the set-up, module design, selection of component and instrumentation, calibration of sensor, assembling of the module, and the assembling of the set up component. Furthermore, the experimental plan will be outline as well.

4.2 Description of set up

The layout of AGMD set up is illustrated in figure 4.1. The system consists of two water closed cycles, hot and cold, connected to the MD module. The main components of the experimental setup consists of a 0.5 hp centrifugal pump responsible for pumping hot feed saline water from feed bath to the module at selected flow rates; a thermostat water bath COLE-PARMER BT-15 (heater) responsible for supplying the hot feed solution; a refrigerated water circulating bath HAAKE D8-G (chiller) for providing cooling water; and the MD module (nucleus of the set up) where salt water separation takes place. The complete working setup is shown in figure 4.2.

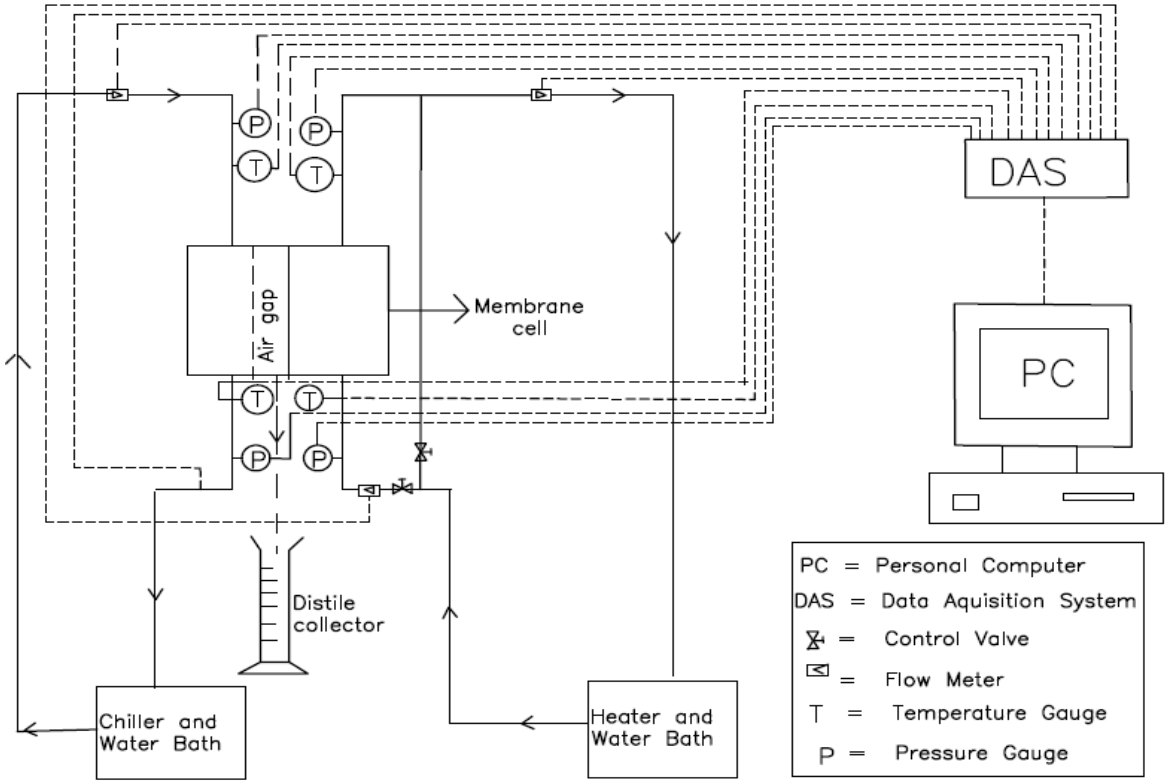

Figure 4.1 Schematic diagram of the experimental setup

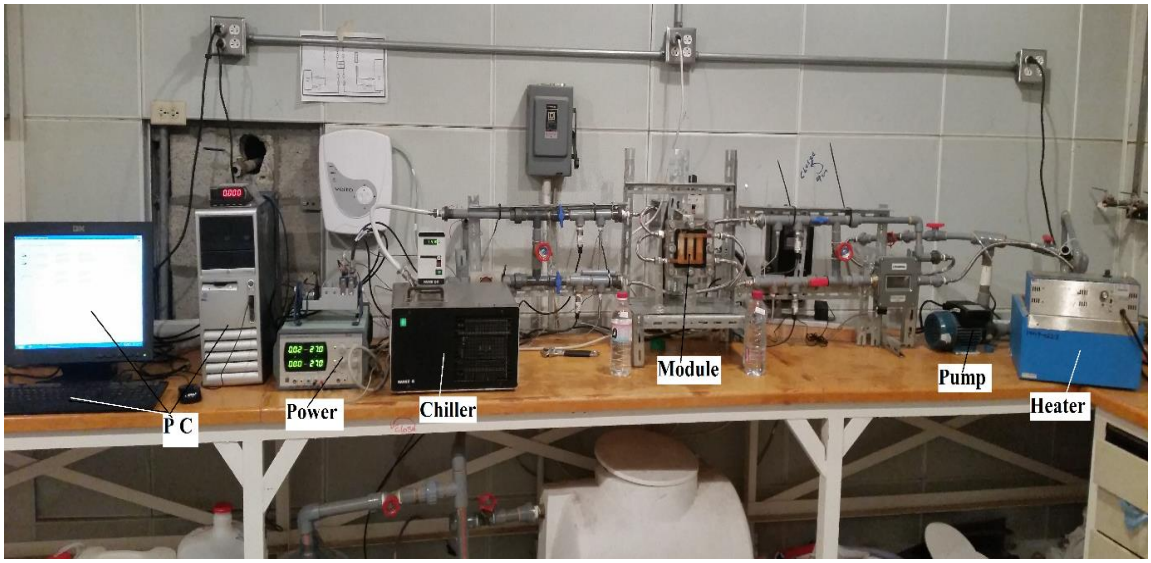

Figure 4.2 Schematic diagram of the experimental setup

The feed saline water from the hot water bath is pumped by the 0.5 hp centrifugal pump to the inlet of the MD module feed chamber. The feed saline water passes through the feed chamber and then returns to the feed water bath for reheating and recirculation. For the coolant cycle, cold water from the chiller is pumped through the coolant chamber to cool down the condensation plate located between the air gap and the coolant water. The coolant exits the cooling chamber and returns to the chiller for re-cooling and recirculation. Vapour pressure difference (the driving force) is created as a result of temperature difference between the feed chamber and cooling chamber. The water vapour created at the feed chamber diffuses through the membrane pores and then migrate through the stagnant air staged between the membrane sheet and coolant plate. The vapour eventually come in contact with the condensation plate and condensed to form a distillate which is collected and directed to outside the module. The sample time of each experiment is recorded. The permeate flux is then estimated by dividing the mass of distillate collected by the product of membrane effective area and sample time.

4.2.1 Membrane Characterization

The membrane material used in this study is polytetrafluoroethylene of 0.22 µm and 0.45 µm pore size acquired from TISH SCIENTIFIC. It is a composite membrane that is composed of an active layer and support layer. The properties of the membrane material are measured in Universidad Complutense de Madrid (UCM), Spain and are tabulated in Table 4.1.

Table 4.1 Membrane properties

Properties	PTFE 0.22 µm	PTFE 0.45 µm
$\delta_{full\ membrane}$ (µm)	159.5 ± 18.0	153.9 ± 13.6
δ_{teflon} (µm)	7.9 ± 1.8	6.9 ± 2.0
$\delta_{support}$ (µm)	143.3 ± 15.6	141.4 ± 15.8
d_p (nm)	236 ± 6	379 ± 8
ε (%)	75.9 ± 5.4	79.7 ± 8.7
θ (º) active layer	138.3 ± 2.4	139.0 ± 2.8
θ (º) support layer	121.4 ± 3.4	119.3 ± 1.0

4.2.2 Module Design

The idea for the used AGMD module was conceived and sketched. The actual design was implemented using the solidworks software. The solidworks design of the MD cell is presented in figure 4.3. It consists of two chambers: a feed chamber and a cooling chamber, with three flow channels in each chamber. A condensation plate which provides necessary surface area for the condensation of vaporized water is situated at the cooling side. In-between every components within the module is a rubber gasket to prevent leakage prevention and in some case to control the air gap width. The module flow channels were machined from Plexiglas material using CNC machine located at the main ME workshop. Presented in figure 4.4 are the module detail design and its dimensions.

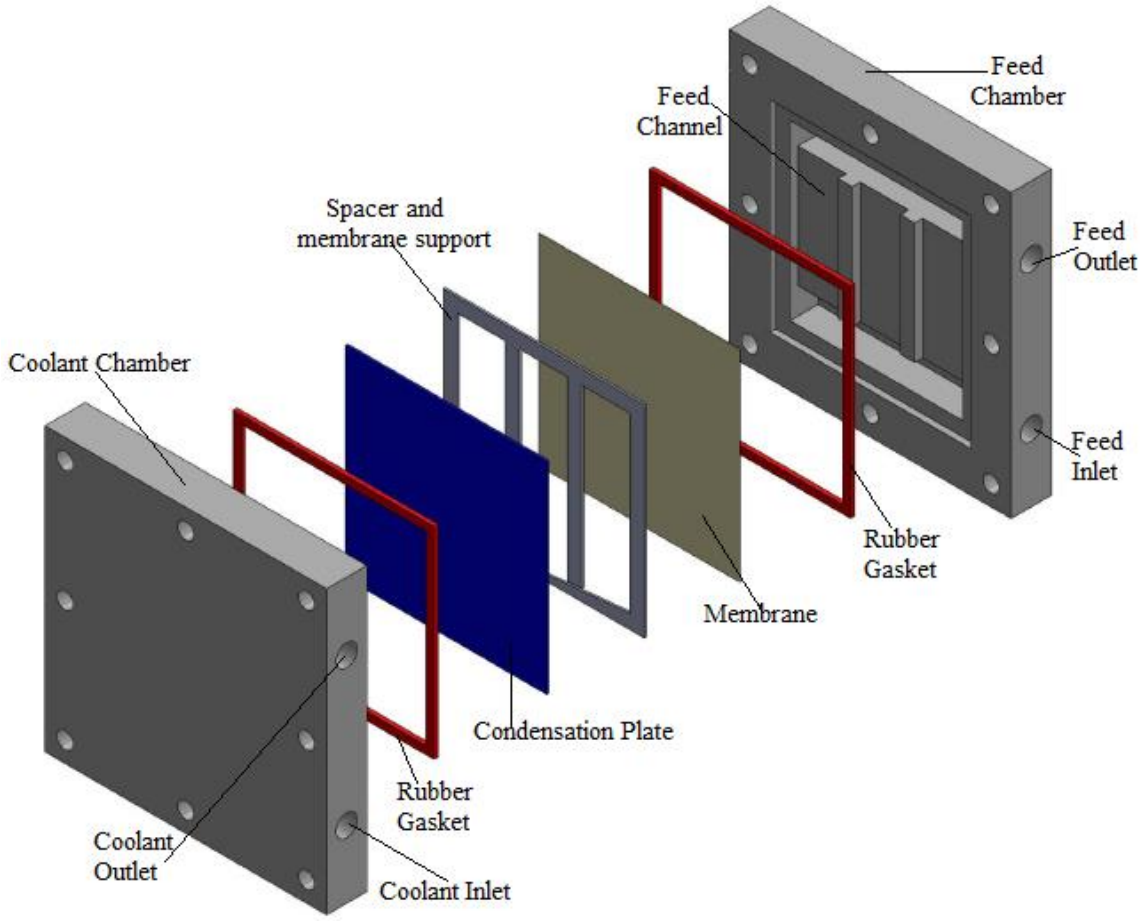

Figure 4.3 An exploded view of the AGMD

The feed chamber and cooling chamber are identical with the following channels dimensions: The dimensions of the feed chamber are 66 mm width, 4mm depth, and length of 66 mm. The cooling channel dimensions are 66 mm width, 6mm depth, and length of 66 mm. The effective membrane area at the feed chamber is $5.676\times10^{-4}m^2$ with wetted perimeter and hydraulic diameter of 0.144m and 0.011m respectively. The condensation surface is made of 1.5 mm-thick brass material of $100cm^2$ square area.

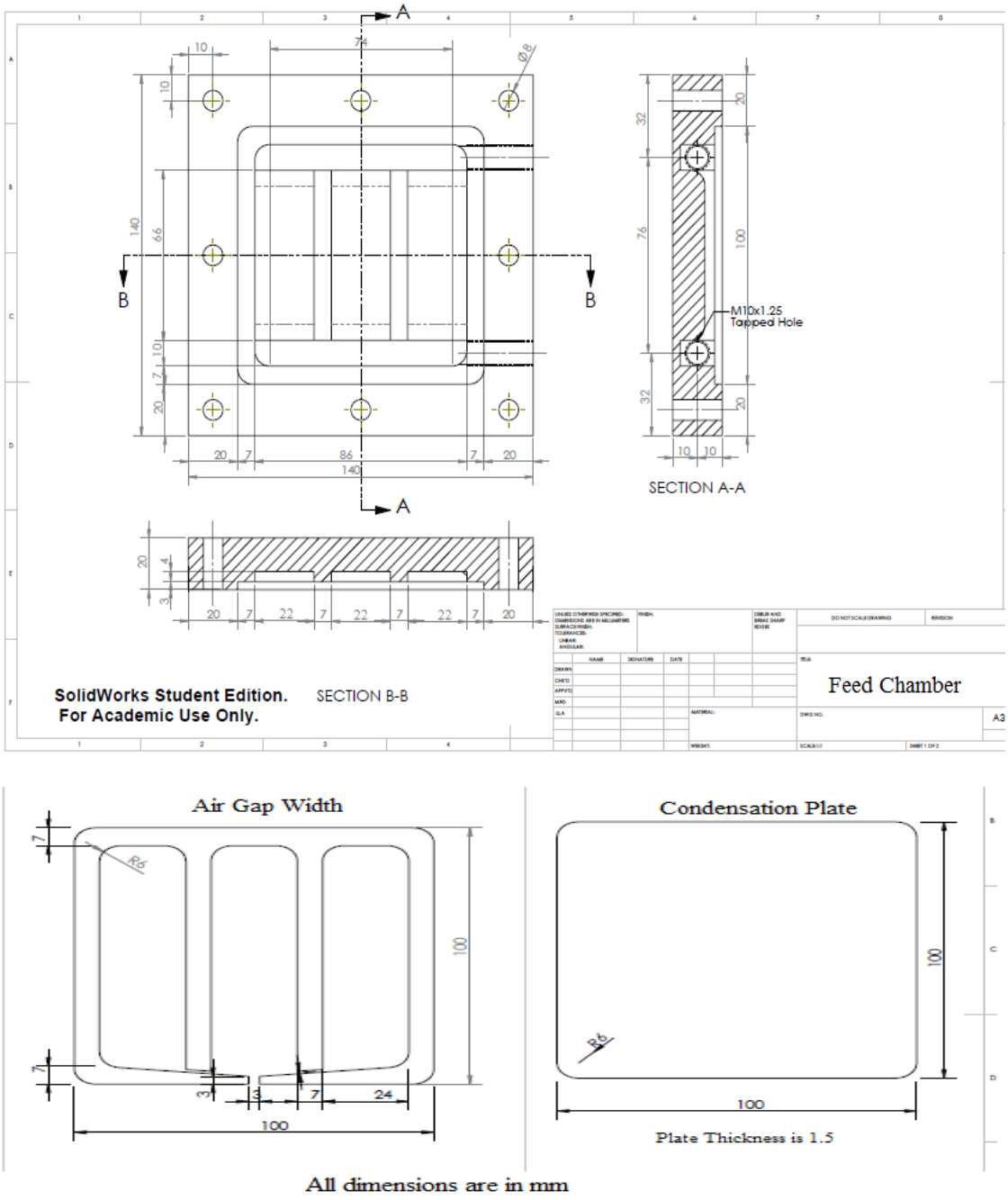

Figure 4.4 Module Detailed Design and Dimensions

4.2.3 Selection of set-up components and instrumentation

The selection of appropriate component needed for the experimental setup is of paramount important. Table 4.2 presents serial number, model number, short description, manufacturers and the quantities of some of the components and instrumentation used in the experiment.

Table 4.2 Set-up component and instrumentation

S/N	Items	Model	Description	Manufacturers	Quantity.
1	CDAQ Module	NI 9234	4-Channel, ±5V, 51.2 kS/s per Channel, 24-Bit IEPE	National Instruments	2
2	CDAQ Module	NI 9211	4-Channel, 14 S/s 24-Bit, ±80 mV Thermocouple Input Module	National Instruments	2
3	NI CDAQ, 1-slot Chassis	NI USB-9162	NI Compact DAQ 1-Slot USB Chassis with USB cable	National Instruments	1
4	Flow meter	FLR6302 D	0.2 to 2.0 GPM, ½ NPT	Omega	2
5	Pressure Transducer	PX309-005G5V	(0 to 0.34 bar) 5 psi gage pressure range, cable connection	Omega	2
6	Pressure Transducer	PX309-015G5V	(0 to 1 bar) 15 psi gage pressure range, cable connection	Omega	2
7	Thermocouple Probe with ¼ NPT Fitting	TC-K-NPT-U-72	Type K Ungrounded Pipe Plug Probe	Omega	4

4.3 Calibration of Pressure Transducer

In order to ensure accurate readings of the purchased sensors, Pressure transducers were taken to the fluid mechanics lab for calibration. A Dead Weight Tester for calibrating pressure transducers was used for this purpose. A photo and some of the calibration results are presented in figures 4.5 - 4.7.

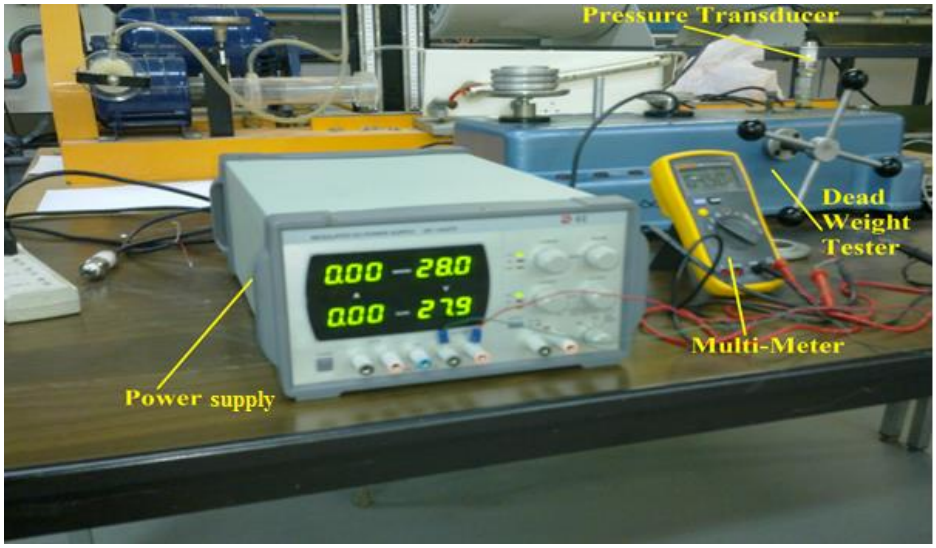

Figure 4.5 Calibration of Pressure transducer

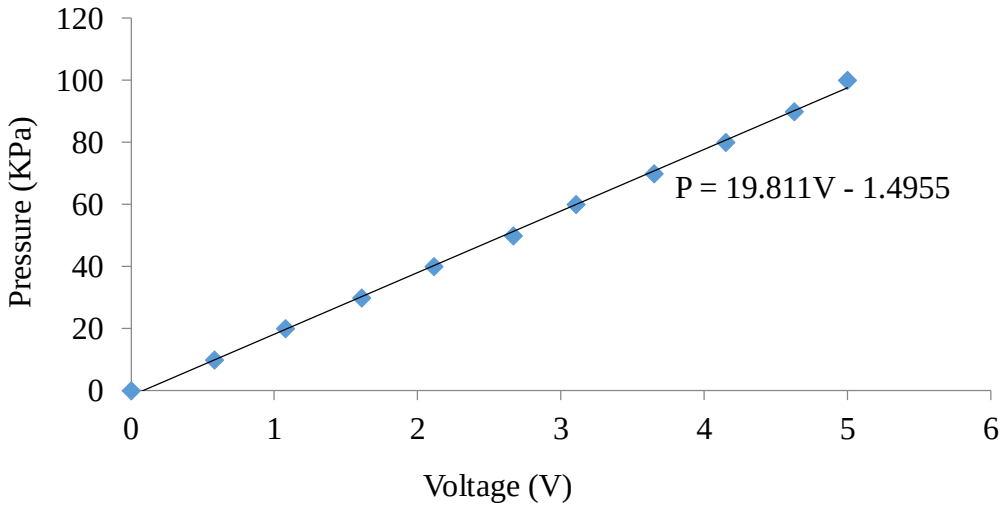

Figure 4.6 Calibration result for PX 309-015G5V

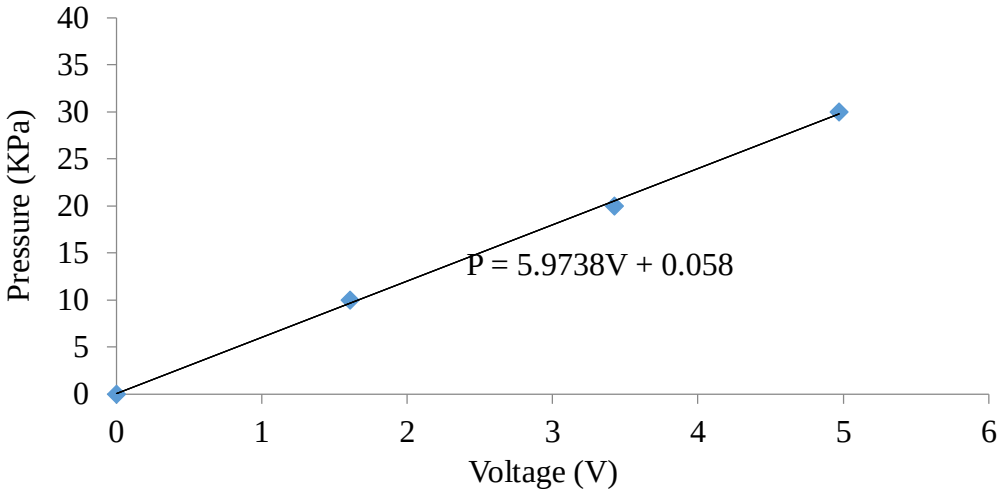

Figure 4.7 Calibration result for PX 309-005G5V

4.4 Main components and sensors

The components of the used AGMD system are depicted in figures 4.4, 4.7 - 4.13. The components include but not limited to: Digital linear power supply for powering pressure transducers (see figure 4.5); multi meter for measuring voltage output of the sensors (figure 4.5); a 0.5 hp centrifugal pump for pumping feed solution at higher flow rate (figure 4.8); a data acquisition slot Chassis for hosting the modules (figure 4.9); CDAQ modules which assist in measuring temperatures, pressure and flow rate of the working fluid(figure 4.9); HAAKE refrigerated water bath for providing coolant water at the desired temperature (figure 4.10); COLE-PARMER water heating bath for providing hot feed solution (figure 4.11); a complete computer system for monitoring and storing data (Figure 4.12); flow meter for measuring the flow rate of the working fluid (Figure 4.13) and thermocouple probes, and pressure transducer for measuring temperatures and pressures of the working fluid respectively (Figure 4.14).

Figure 4.8 Centrifugal Pump

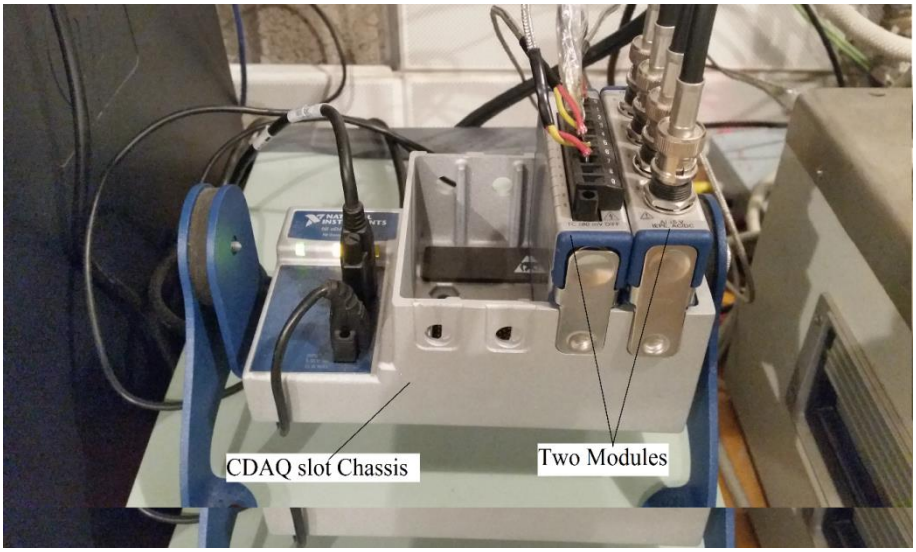

Figure 4.9 CDAQ slot Chassis and two Modules

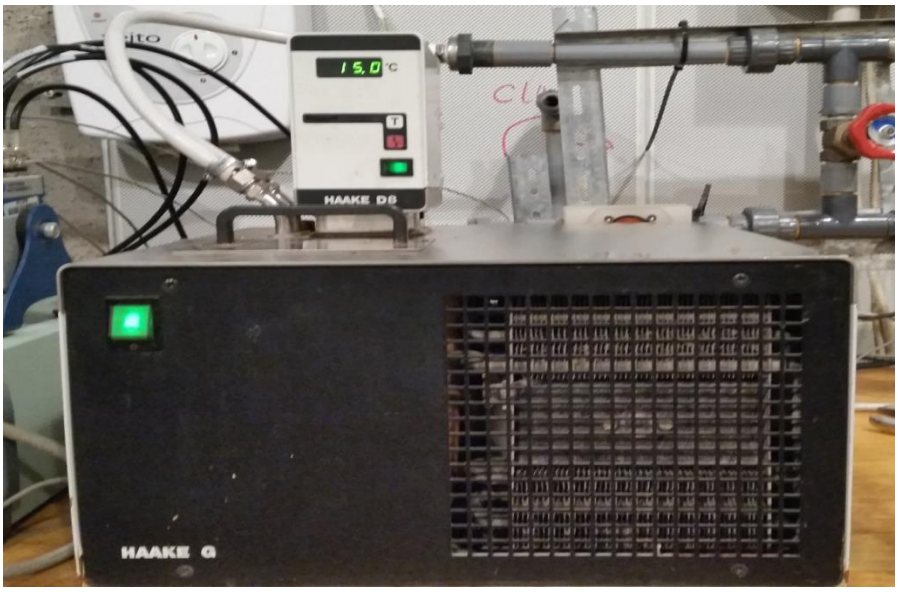

Figure 4.10 HAAKE D8-G refrigerated water circulation bath (Chiller)

Figure 4.11 COLE-PARMER thermostat water bath (Heater)

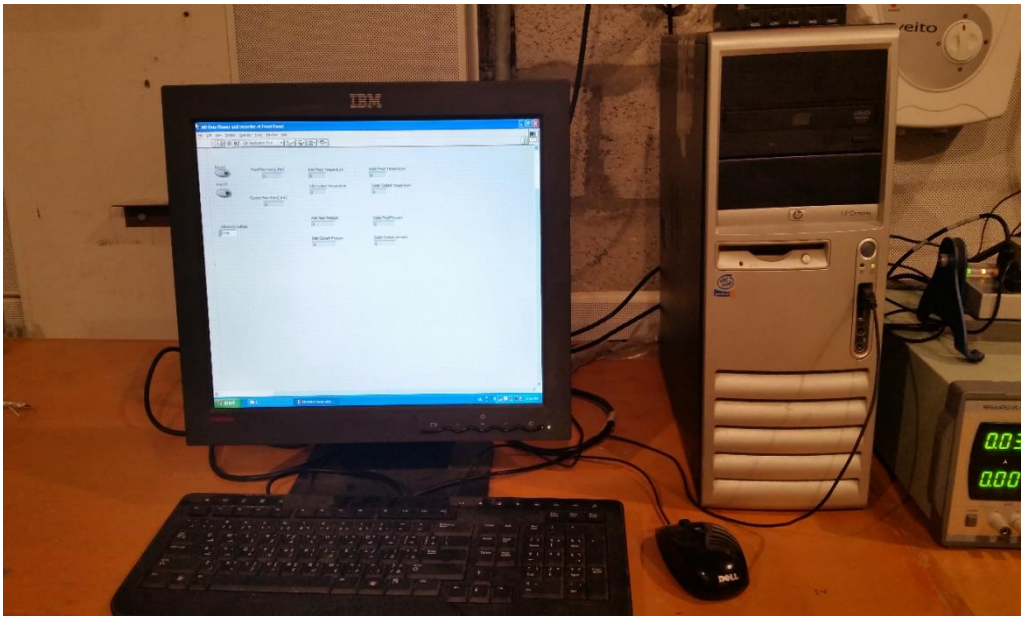

Figure 4.12 Computer system for monitoring and recording data

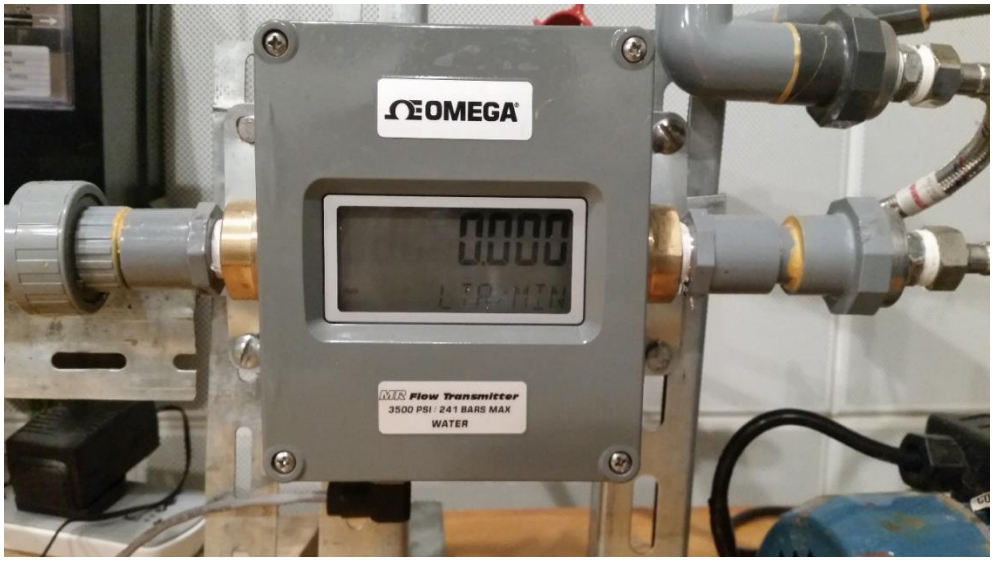

Figure 4.13 Flow Meter

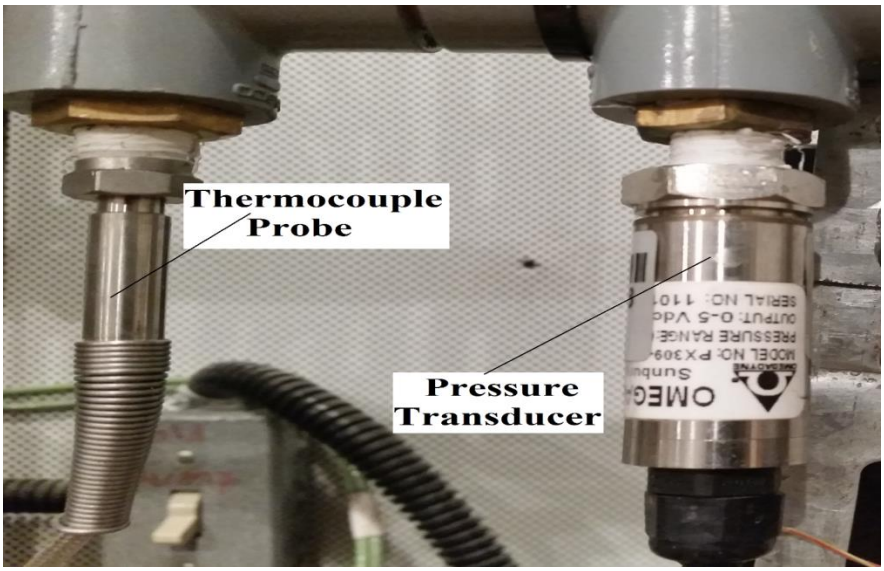

Figure 4.14 Thermocouple Probe and pressure Transducer

4.5 Assemble of the Module

Different parts of the used module are assembled as demonstrated in figures 4.15(a)-4.15(g). Figure 4.15 (a) presents the feed side channels, while Figure 4.15 (b) displays the positioning of rubber gasket over the feed chamber. Figure 4.15 (c) shows the placement of membrane sheet over the rubber gasket and Figure 4.15 (d) display the positioning of another rubber gasket which controls the air gap thickness. Figure 4.15 (e) depicted the positioning of condensation plate over the air gap thickness, while Figure 4.15 (f) shows placing of another rubber gasket to prevent leakage. Figure 4.15 (g) displays the positioning of coolant chamber over the other module components to complete the module assembling process while figure 4.16 presents the connection of assembled module to the AGMD set up.

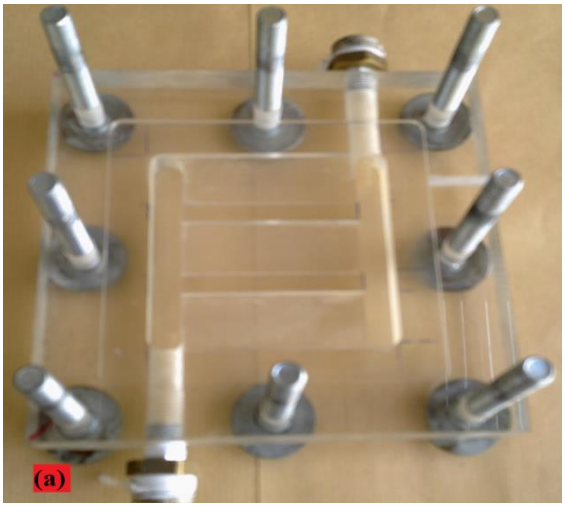
(a)

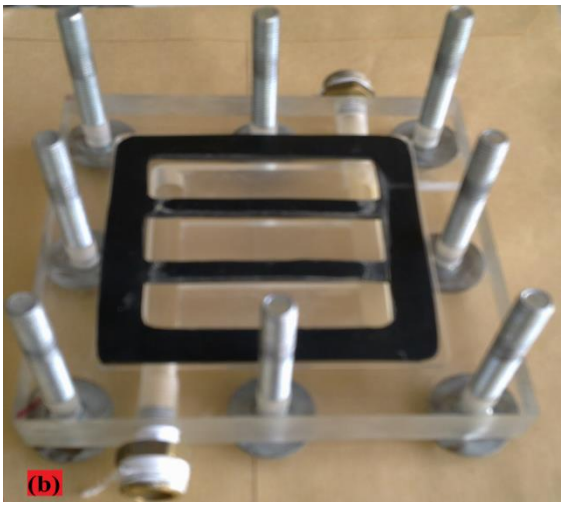
(b)

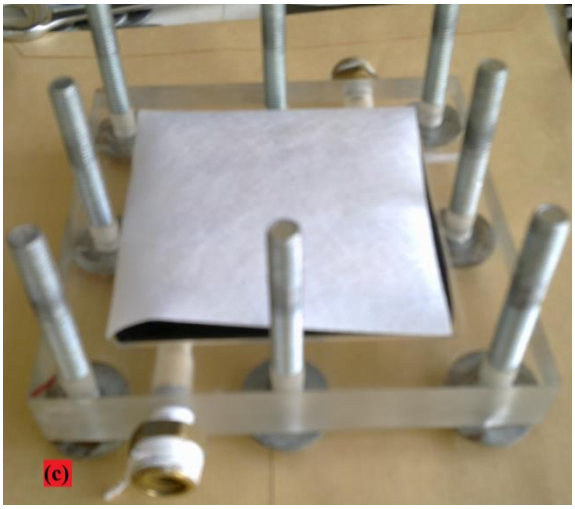
(c)

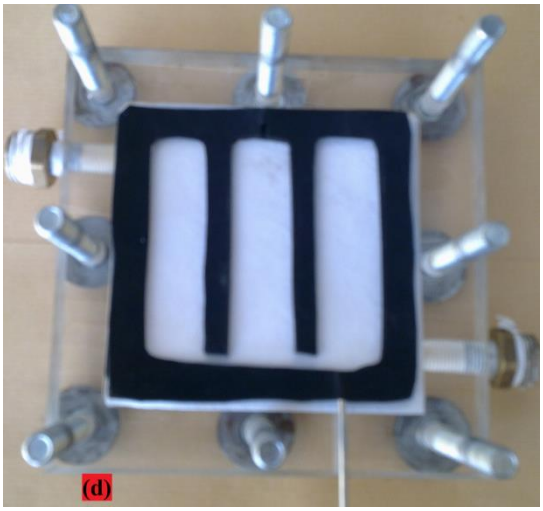
(d)

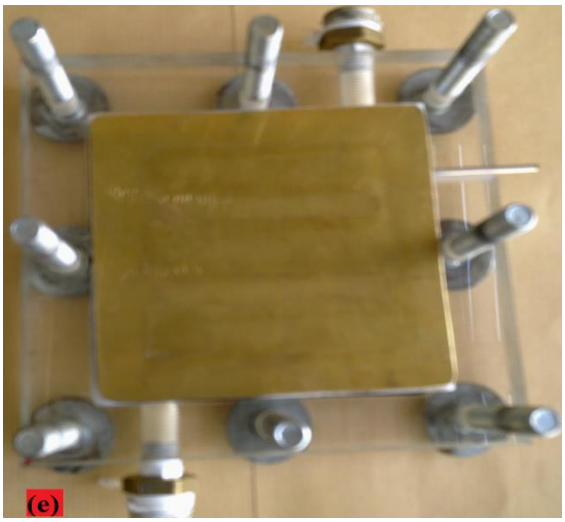
(e)

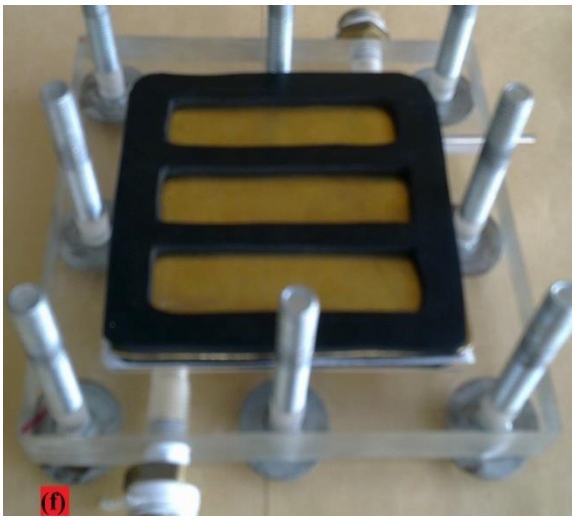
(f)

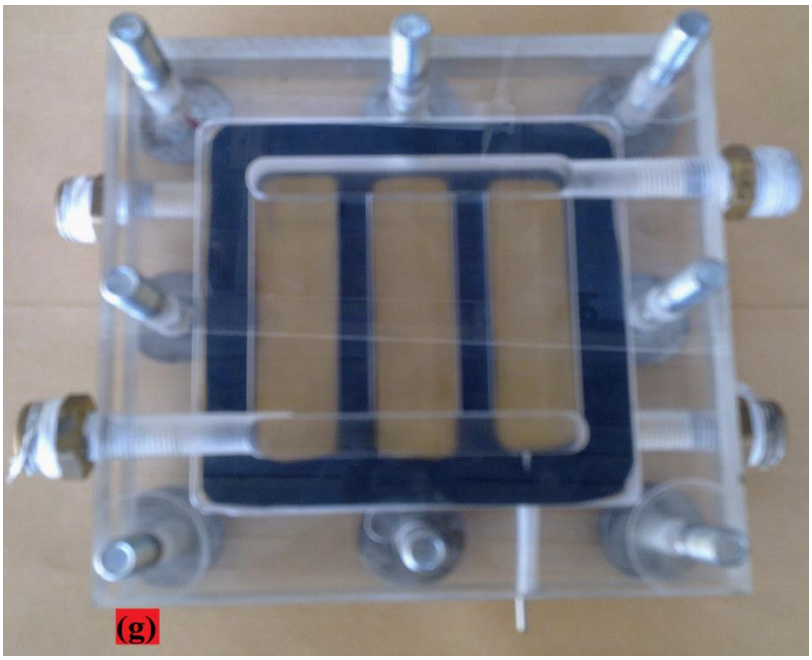

Figure 4.15 (a - g) AGMD module assembling

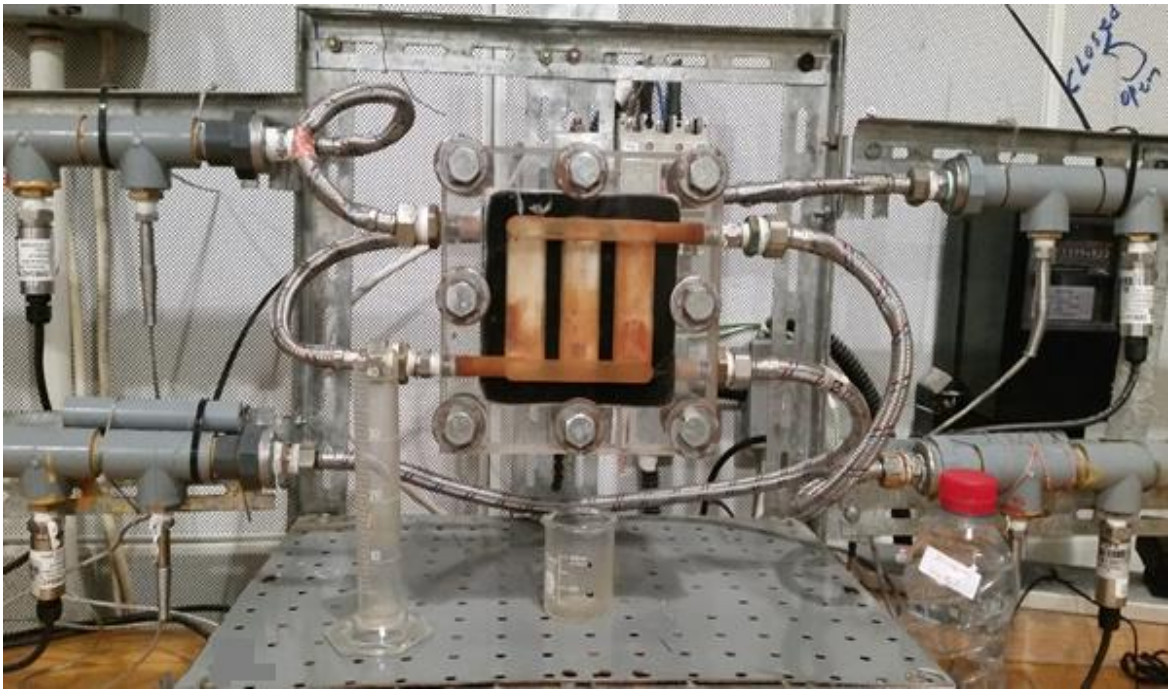

Figure 4.16 AGMD module connected to the setup

Figure 4.17 revealed the exploded view of double stage module design in solidworks, while figure 4.18 illustrate the flow diagram of the multi-stage design, and the actual module used for multi stage testing is depicted in figure 4.19.

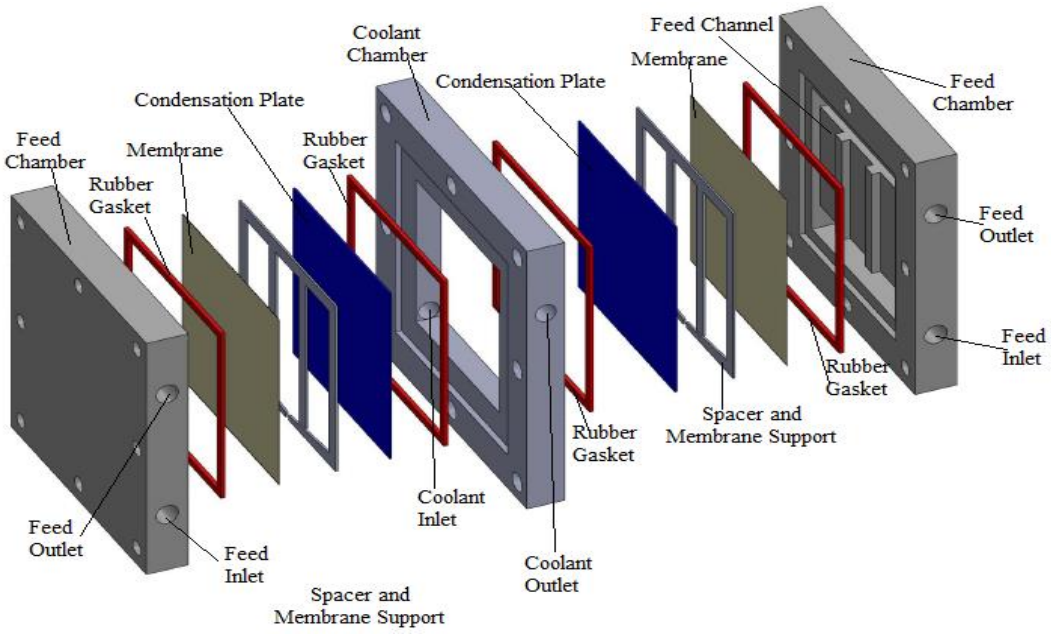

Figure 4.17 An exploded view of double-stage AGMD

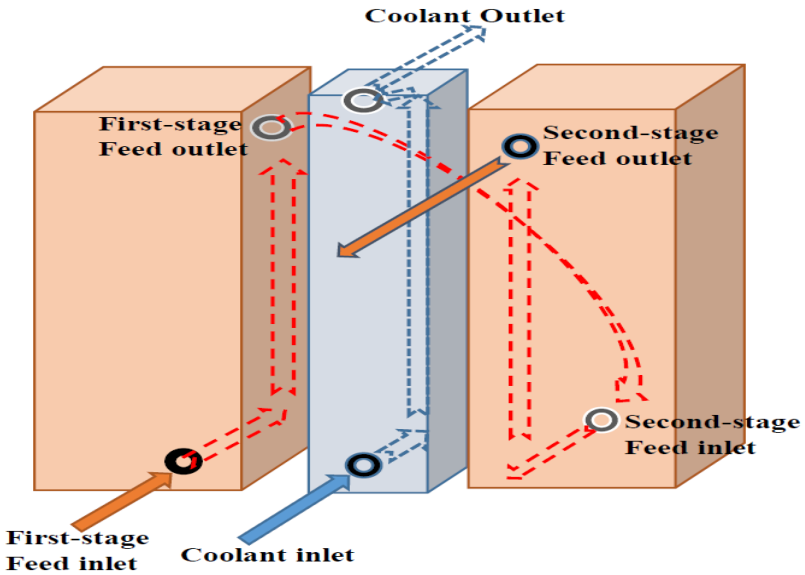

Figure 4.18 A flow diagram of double-stage AGMD

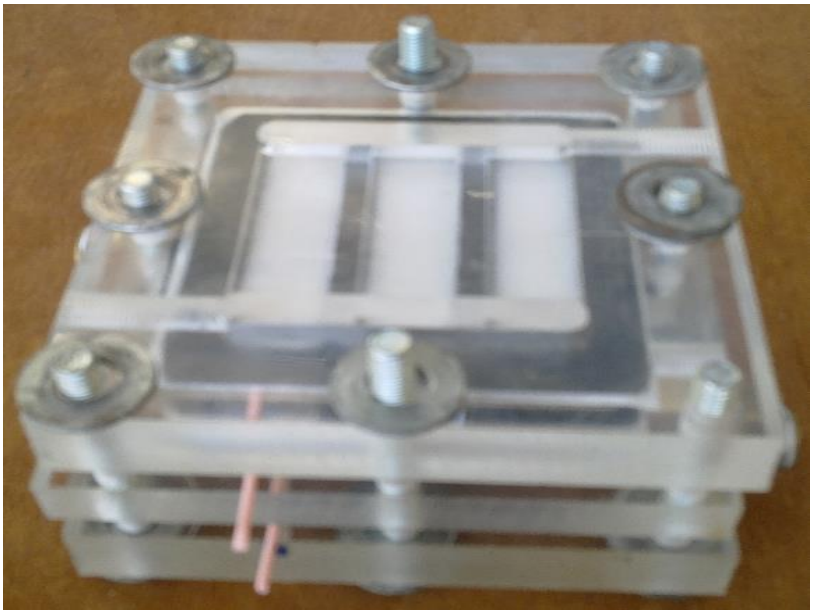

Figure 4.19 A photo of actual double stage module

4.6 Experimental work plan

A parametric study on different operating and design parameters is carried out to study the effect of these parameters on the permeate flux. This is done by varying one operating parameter while keeping the others constant. The investigation of feed solution concentration and membrane pore size on permeate flux is also carried out.

The investigated operating parameters are the feed temperature, feed flow rate, coolant temperature, coolant flow rate and air gap width, while the design parameter is the multi-staging. The table 4.3 below summarized the experimental condition. It must be mentioned here that the experimental data will be presented in combined effects to reduce the number of plots.

Table 4.3 Experimental plan

	Variable	Range	Comments
1	Feed Temperature	40-80^{0}C	The interval is 10^{0}C
2	Coolant Temperature	15-30^{0}C	The interval is 5^{0}C
3	Feed Flow rate	1-5L/min	The interval is 1L/min
4	Coolant Flow rate	1-3.5L/min	The interval is 1L/min
5	Air Gap Width	3-7mm	The interval is 2mm
6	Feed solution conc.	0.075-60g/L	The interval is 10g/L
7	Membrane Pore size	0.22µm and 0.45µm	PTFE membrane material will be used
8	Multi staging	1 and 2 stages	Only a two-stages design is tested

Three type of feed solution were used in this study are: The laboratory prepared feed saline solutions ranging from 4 g/L to 50g/L, distilled water acquired from chemistry department at KFUPM and row seawater having salt concentration of about 60 g/L which is obtained from the Arabian gulf, the city of Khobar, Saudi Arabia.

CHAPTER 5

RESULTS AND DISCUSSION

The impact of AGMD operating parameters were investigated and depicted in figures 5.1 to 5.7. The investigation was conducted using PTFE 0.45µm membrane. The influences of feed temperature on the amount of permeate flux produced at different coolant temperature, feed flow rate, coolant flow rate and air gap width are illustrated in Figures 5.1 - 5.4.

5.1 Effect of Feed Temperature on permeate flux

Figure 5.1 illustrated the effect of feed temperature on the permeate flux at different coolant temperature. The variable conditions are: feed temperature which was varied from 40 - 80 ^{0}C and the coolant temperature changes from 15-30^{0}C. The fixed test conditions: Feed flow rate of 3 L/min, coolant flow rate of 3 L/min, feed Concentration of 75.5 mg/L and air gap thickness of 3mm. It can be noticed that permeate flux increases with increasing feed temperature and decreases with increasing coolant temperature. Increasing the feed temperature leads to exponential rise in the permeate flux. This is due to a reason best explained by Antoine equation (Eqs. 3.22 and 3.23). According to the Antoine equation, the effect of temperature on vapour pressure is considerable low at lower feed temperature, and becomes very significant at higher temperature.

Furthermore, vapour pressure depends on temperature exponentially and a small rise in temperature can lead to greater rise in vapour pressure. This indicates that the higher the vapour pressure (the driving force) as a result of feed temperature increase, the higher the flux and the better the performance of the AGMD system.

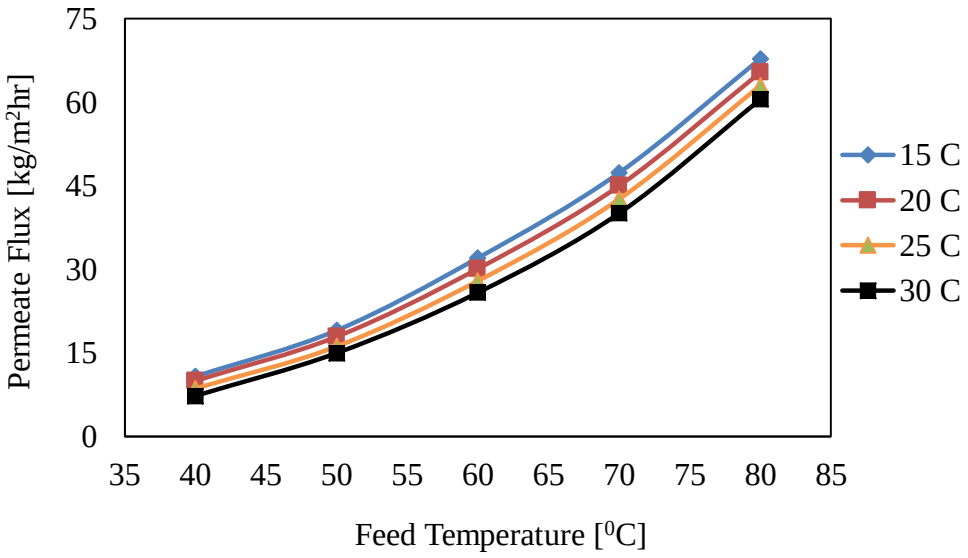

Figure 5.1 Effect of Feed Temperature on flux at different Coolant Temperature

Test conditions: Feed Flow rate of 3 L/min, Coolant flow rate of 3 L/min, Feed Concentration of 75.5 mg/L and Air gap thickness of 3mm, and using 0.45µm PTFE membrane material

The observed reduction in permeate flux due to increasing coolant temperature is best attributed to the reduction in transmembrane driving force responsible for permeation. Careful observation of figure 5.1 revealed that the maximum recorded percentage increment in flux produced is about 730% when feed temperature increases from 40^0C to 80^0C. An average percentage reduction in permeate flux of about 25.89% was observed when the coolant temperature increases from 15^0C to 30^0C.

Illustrated in figure 5.2 is the effect of increasing feed inlet temperature on flux at different feed flow rates. The variable conditions are: feed temperature which was varied from 40 - 80 ^{0}C and the feed flow rate ranging from 1-5L/min. while the fixed test conditions: Coolant temperature of 20^{0}C, coolant flow rate of 3 L/min, feed concentration of 75.5 mg/L and air gap thickness of 3mm. It can be noticed that the flux increases with increasing feed flow rate and feed temperature. The observed rise in permeate flux as a result of increasing feed flow rate is due to reduction in temperature and concentration polarization effects. Increasing the feed flow rate encourages turbulence level in the flow and increases heat transfer coefficient of the feed boundary layer.

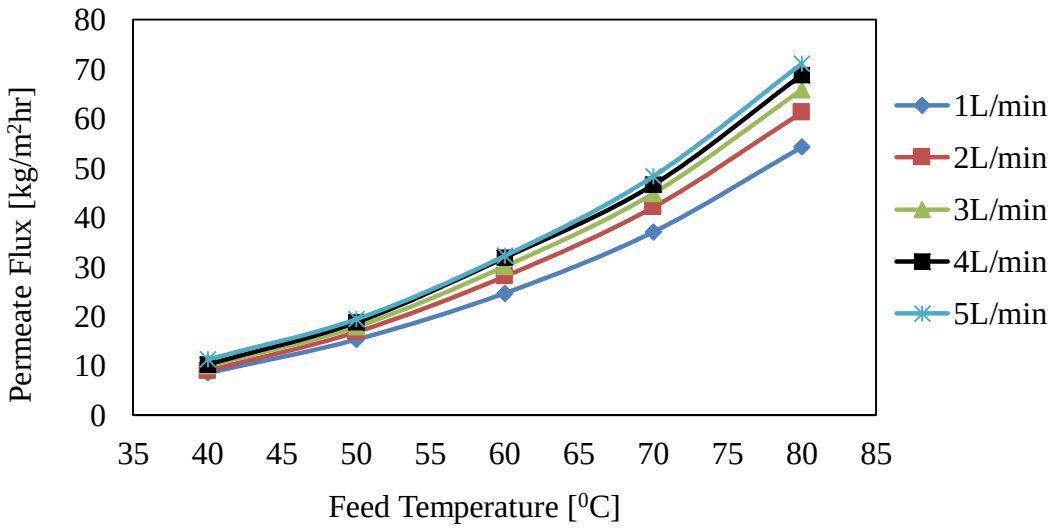

Figure 5.2 Effect of Feed Temperature on flux at different Feed flow rate

Test conditions: Coolant Temperature of 20 ^{0}C, Coolant flow rate of 3 L/min, Feed Concentration of 75.5 mg/L and Air gap thickness of 3mm, and using 0.45µm PTFE membrane material

Besides, increasing the feed flow rate also reduce water resistance time in the feed channels and make the feed bulk temperature in the feed channels closer to the feed inlet temperature. The average percentage increment in the permeate flux when the feed flow

rate increases from 1L/min to 5L/min is about 32%. As explained earlier in figure 5.1 and as observed in this figure, increasing feed temperature leads to exponential rise in permeate flux.

Figure 5.3 depicted the impact of feed temperature on flux at different coolant flow rate. The variable conditions are: feed temperature ranging from 40 - 80 ^{0}C and the coolant flow rate ranging from 1-3.5L/min. The fixed test conditions are: Coolant temperature of 20^{0}C, feed flow rate of 3 L/min, feed concentration of 75.5 mg/L and air gap thickness of 3mm. It can be seen that flux increases with increasing feed temperature. However, little or no effect were observed in flux when we increase the coolant flow rate from 1 L/min to 3.5 L/min, as we could only record about 2% rise in flux. We must understand that increasing cooling water flow rate mean increasing the cooling water heat transfer coefficient of the cooling surface.

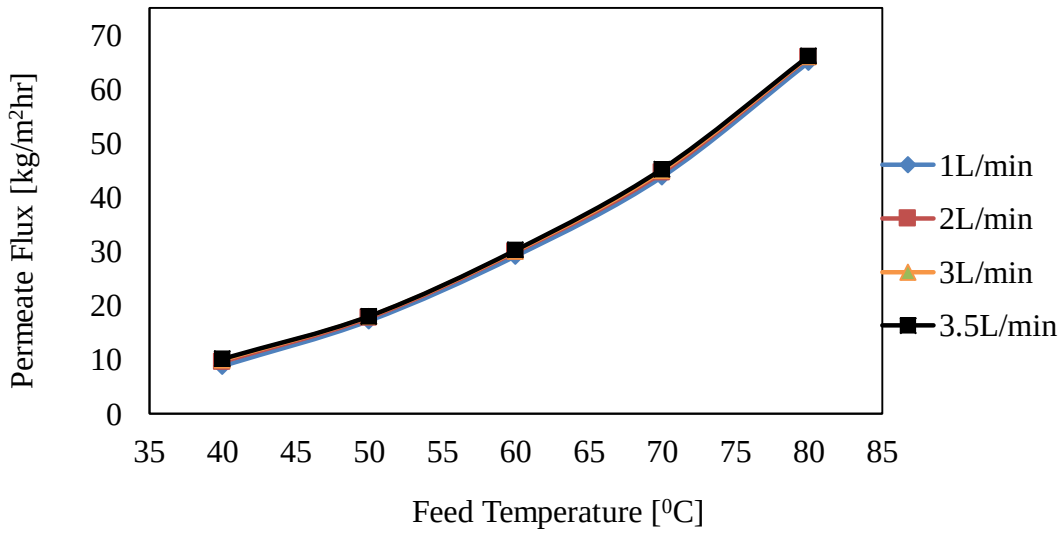

Figure 5.3 Effect of Feed Temperature on flux at different Coolant flow rate

Test conditions: Coolant Temperature of 20 ^{0}C, Feed Flow rate of 3 L/min, Feed Concentration of 75.5 mg/L and Air gap thickness of 3mm, and using 0.45µm PTFE membrane material

It is obvious from figure 5.3 that coolant flow rate has negligible effect on flux. The effect of coolant flow rate is meaningless as far as we have minimum flow to conduct the heat from the condensate surface. It can also be observed that feed temperature dominate the flux with average 601.26% rise in flux when it is increased from 40 to 80^0C.

Another important operating parameter dominating the performance of AGMD is the air gap width. The influence of air gap thickness at different feed temperatures is presented in figure 5.4. The investigation is conducted using different air gap width of 3, 5, and 7mm at different feed temperature ranging from 40 to 80^0C. The results shown in figure 5.4 are obtained at coolant temperature of 20^0C, feed flow rate of 3 L/min, coolant flow rate 3 L/min, and feed concentration (TDS) of 75mg/L.

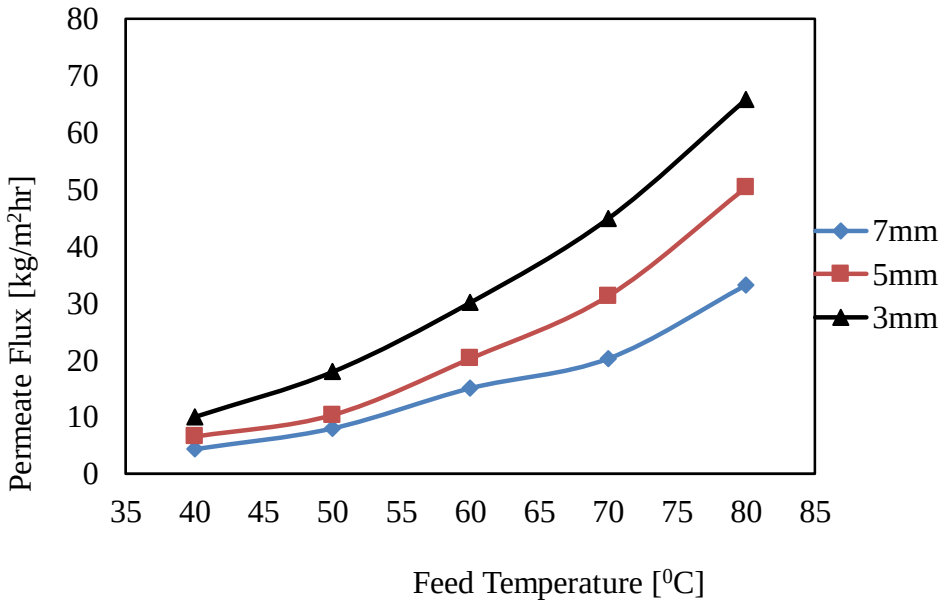

Figure 5.4 Effect of Air Gap Width on flux at different Feed Temperature

Test conditions: Feed Temperature of 70 0C, Coolant Temperature of 20 0C, Feed flow rate of 3 L/min, Coolant flow rate of 3 L/min and Feed Concentration of 75.5 mg/L, and using 0.45µm PTFE membrane material.

It can be noticed that decreasing the air gap width from 7mm to 3mm at different feed inlet temperature resulted in tremendous increment in permeate flux especially at higher temperature. Reducing the air gap from 7mm to 3mm leads to about 131.23% rise in system performance at 40^0C feed temperature.

Decreasing the air gap width means reducing the vapour diffusion path length within the air gap compartment. This in turn reduces the time taken by the vapour to travel within the air gap compartment thereby enhancing the flux production. Increasing the air gap width also means increasing the resistance to mass transfer within the vapour compartment, this lead to drops in permeate flux. An average drop of 115.9% drop in flux was recorded when the air gap width was increased from 3mm to 7mm gap.

5.2 Effect of Feed flow rate on permeate flux

The impact of feed flow rate on permeate flux at different coolant flow rate is presented in figure 5.5. The variable conditions are: Feed flow rate ranging from 1-5L/min and the coolant flow rate which changes from 1-3.5L/min. The fixed test conditions: Feed temperature of 80^0C coolant temperature of 20^0C, feed concentration of 75.5 mg/L and air gap thickness of 3mm. An average rise in permeate flux of about 30.42% was noticed when feed flow rate increases from 1 L/min to 5 L/min. Flux was however observed to increase by a maximum of 1.34% when coolant flow rate increases from 1 L/min to 3.5 L/min. This observation also indicated that the coolant flow rate is not a significant parameter affecting the performance of air gap membrane distillation.

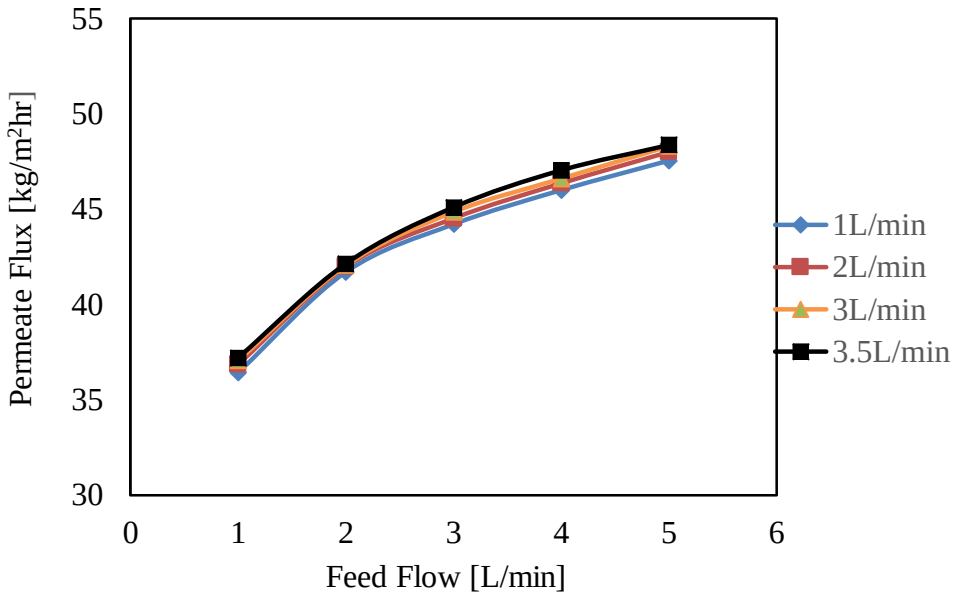

Figure 5.5 Effect of Feed Flow rate on flux at different Coolant flow rate

Test conditions: Coolant Temperature of 20 0C, Feed Temperature of 70 0C, Feed Concentration of 75.5 mg/L and Air gap thickness of 3mm, and using 0.45µm PTFE membrane material.

Figure 5.6 illustrates the influence of feed flow rate at different coolant temperature. The variable conditions are: feed flow rate ranging from 1-5L/min and the coolant temperature changing from 15-30^{0}C. The fixed test conditions: Feed temperature of 70^{0}C, coolant flow rate of 3 L/min, feed concentration of 75.5 mg/L and air gap thickness of 3mm. It can be seen that both feed flow rate and coolant temperature have some influence on the system performance. The effect of increasing feed flow rate on flux is positive while that of increasing coolant temperature on flux is negative. Furthermore, it can be observed that the impact of feed flow rate on flux is greater than that of coolant temperature. According to Figure 5.6, the observed average percentage rise in permeate flux was found to be 31.08% when feed flow rate increases from 1 L/min to a maximum flow rate of 5 L/min. Whereas the average percentage drops in the distillate production was 10.69% when coolant temperature increases from 15^{0}C to 30^{0}C.

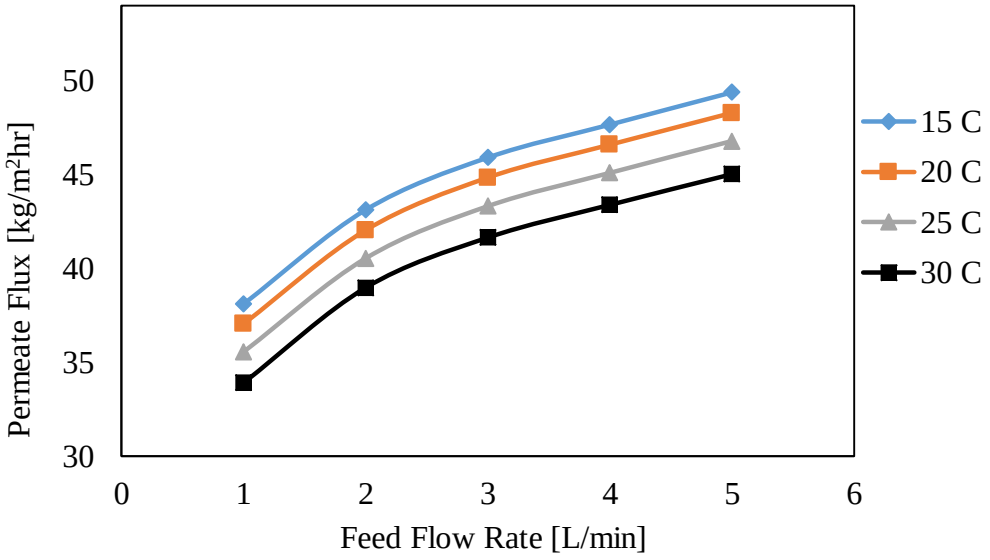

Figure 5.6 Effect of Feed Flow rate on flux at different Coolant Temperature

Test conditions: Feed Temperature of 70 0C, Coolant flow rate of 3 L/min, Feed Concentration of 75.5 mg/L and Air gap thickness of 3mm, and using 0.45µm PTFE membrane material.

5.3 Effect of Coolant temperature on permeate flux

Presented in figure 5.7 is the effect of coolant temperature on flux at different coolant flow rate. The variable conditions are the coolant temperature changing from 15-30^{0}C and the coolant flow rate ranging from 1-3.5L/min. The fixed test conditions are: Feed temperature of 70 ^{0}C, feed flow rate of 3 L/min, feed concentration of 75.5 mg/L and air gap thickness of 3mm. An average of about 9.51% percentage drops in permeate flux was observed when coolant temperature increases from 15^{0}C to 30^{0}C. The role of coolant temperature on flux in this case proves less significant when compared to the likes of feed temperature and air gap width, since we could only record less than 10% rise in flux when we decrease coolant temperature from 30^{0}C to 15^{0}C. As such, using cooling water at atmospheric condition is advisable in this context if the feed temperature is high

enough. This will lower the cost of energy input for maintaining the cooling temperature below the room temperature. Hence it is advisable to locate the MD plant near a water body where cooling water at atmospheric condition can be obtained. It can also be noticed in figure 5.7 that a maximum of 1.45% rise in flux was recorded when the coolant flow rate increases from 1L/min to 3.5L/min. This result is consistent with previously discussed results in figures 5.3 and 5.5. Thus this investigation shows that the effect of coolant flow rate on permeate flux is marginal.

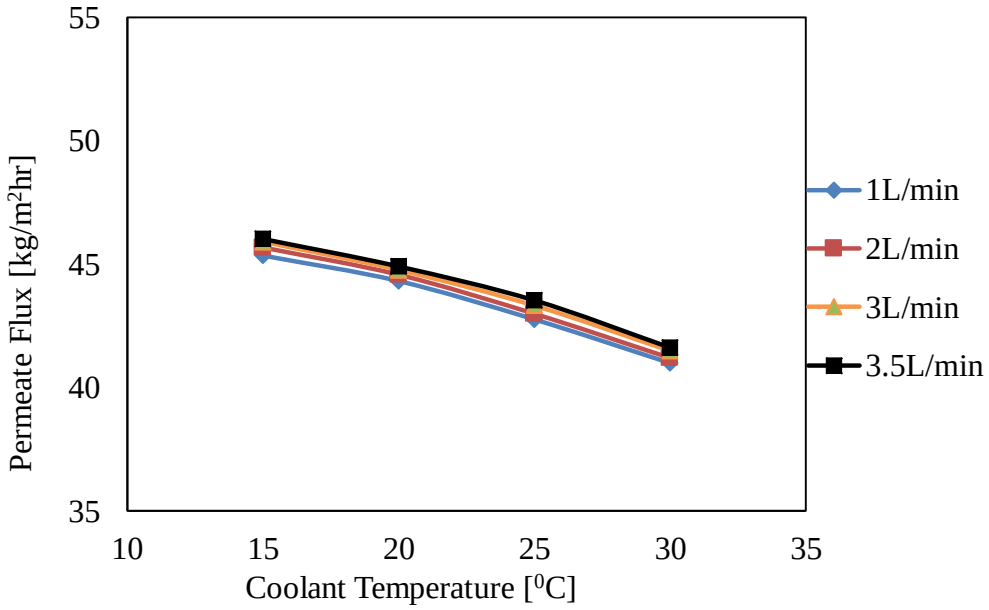

Figure 5.7 Effect of Coolant Temperature on flux at different Coolant flow rate

Test conditions: Feed Temperature of 70 0C, Feed Flow rate of 3 L/min, Feed Concentration of 75.5 mg/L and Air gap thickness of 3mm, and using 0.45µm PTFE membrane material.

From the foregoing analysis, it can be seen that the distillate production increases with increasing feed temperature and feed flow rate. However, it decreases with increasing air gap width and coolant temperature. But increasing coolant flow rate pretends to increases

the system performance. Furthermore, the system performance is significantly affected by both feed temperature and air gap width. Feed flow rate have reasonable effect on flux. Coolant temperature has relatively lower influence on distillate production while coolant flow rate is observed to have a marginal or negligible effect on system performance. It must be mentioned that apart from the investigation of membrane pore size on flux, all other investigation throughout this work were conducted using PTFE 0.45µm membrane.

5.4 Effect of Membrane Pore Size on Permeate Flux

The role of membrane pore size on permeate flux was investigated and presented in figures 5.8 to 5.10. Illustrated in figure 5.8 are the results for the influence of membrane pore on flux at different feed temperatures and feed flow rate. Two different membranes with two different pore sizes (PTFE 0.45µm and PTFE 0.22µm) were used in the investigation. The variable conditions are: feed temperature ranging from 40-80^{0}C, feed flow rate changing from 1-5L/min. the fixed experimental conditions are: coolant temperature of 20^{0}C, coolant flow rate of 3 L/min, feed concentration of 75.5 mg/L and air gap thickness of 3mm. It can be noticed that membrane pore size has an influence on permeate flux. Flux obtained by using PTFE 0.45µm is slightly higher than that obtained using PTFE 0.22µm at different feed temperature and feed flow rate. This is indications that permeate flux increases with increasing membrane pore size. The quality of permeate flux obtained using PTFE 0.45µm membrane material was expected to be lower than that obtained using PTFE 0.22µm membrane material due to its larger pore size. But that was not the case in this investigation as we could not established any clear difference between

the qualities of flux obtained using the two membrane material. PTFE 0.45µm recorded an average of 10.97% rise in permeate flux over PTFE 0.22µm when the feed temperature and feed flow rate was increased from 40 to 80^{0}C, and 1 to 5L/min respectively.

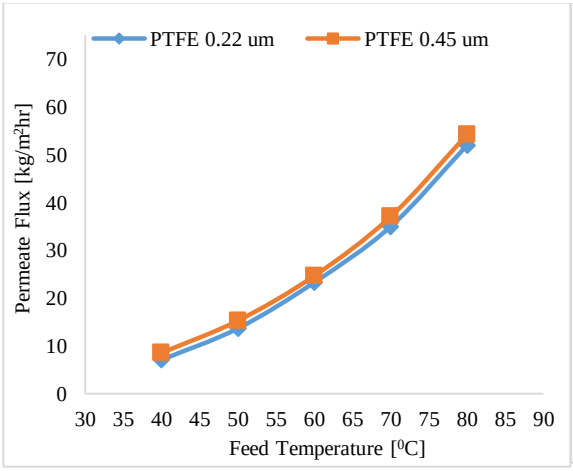

(a) At 1L/min

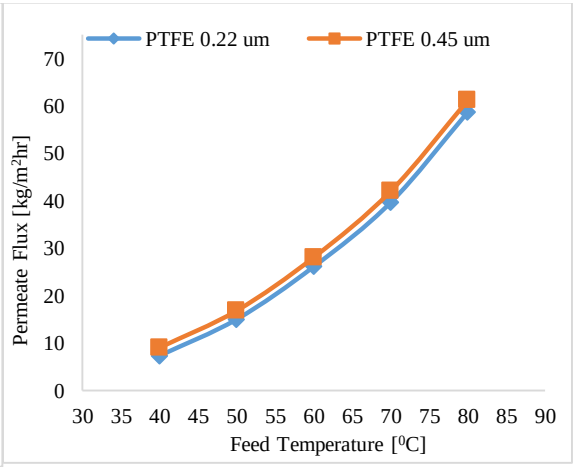

(b) At 2L/min

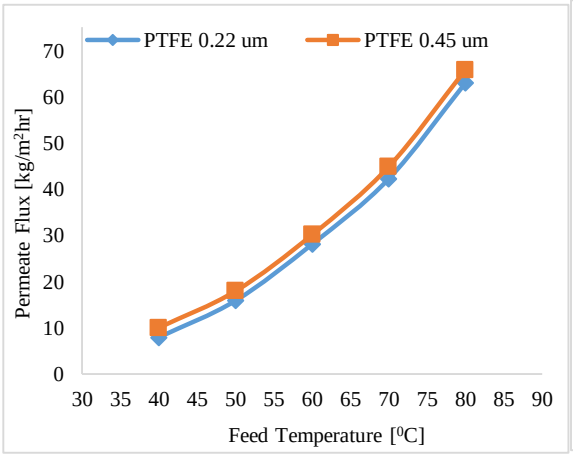

(c) At 3L/min

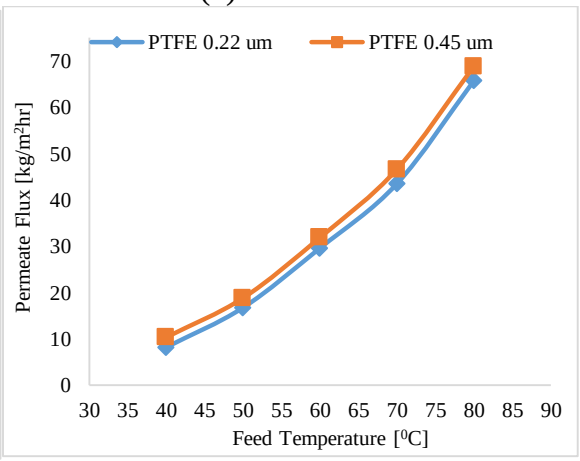

(d) At 4L/min

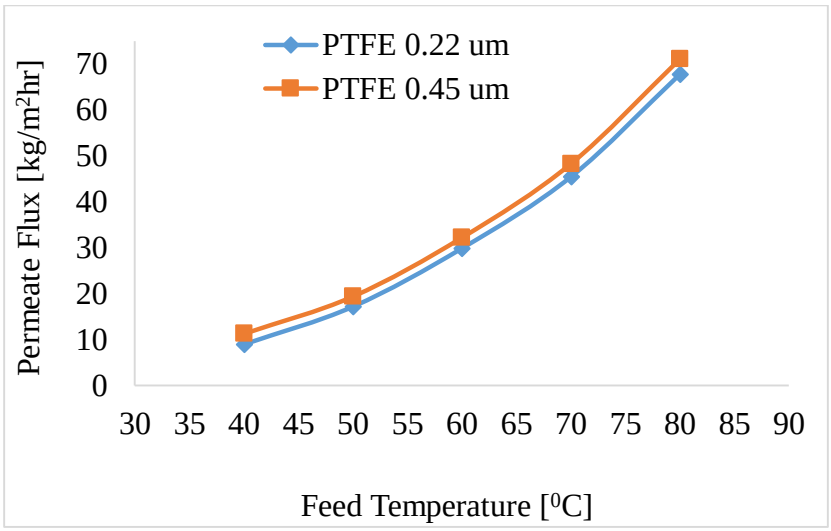

(e) At 5L/min

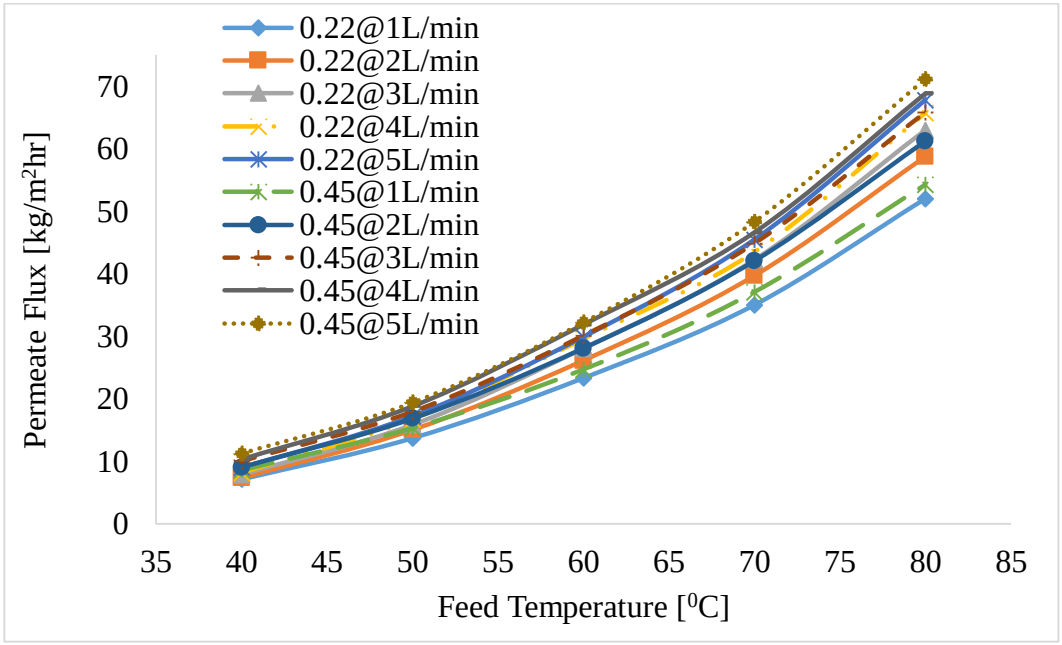

(f) At 1, 2, 3, 4, & 5L/min

Figure 5.8 Effect of membrane pore size on flux at different feed temperature and feed flow rate

Test Conditions: Coolant Temperature of 20 0C, Coolant flow rate of 3 L/min, Feed Concentration of 75.5 mg/L and Air gap thickness of 3mm

Figure 5.9 depicted the effect of membrane pore size on flux at different feed flow rate and coolant temperature. The variable conditions are: feed flow rate changing from

1L/min-5L/min and coolant temperature ranging from 15-30^{0}C. The fixed experimental conditions are: Feed Temperature of 70 ^{0}C, coolant flow rate of 3 L/min, feed concentration of 75.5 mg/L and Air gap thickness of 3mm. It can be observed that system performance is affected by membrane pore size. PTFE 0.22µm produced lower flux in comparison to PTFE 0.45µm. The membrane material PTFE 0.45µm recorded an average of 6.51% rise in flux over PTFE 0.22µm when feed flow rate is increase from 1L/min to 5L/min and coolant temperature increases from 15 to 30^{0}C.

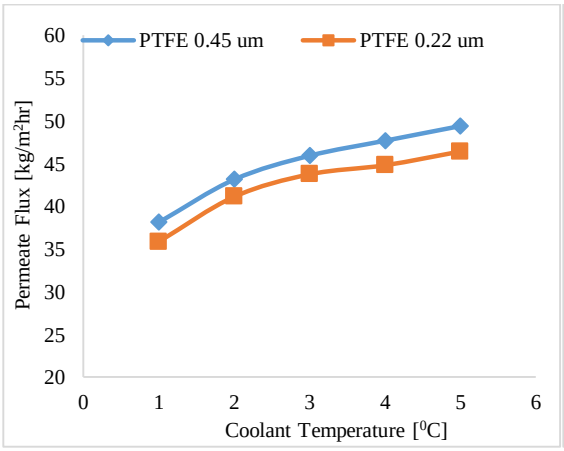

(a) At 1L/min

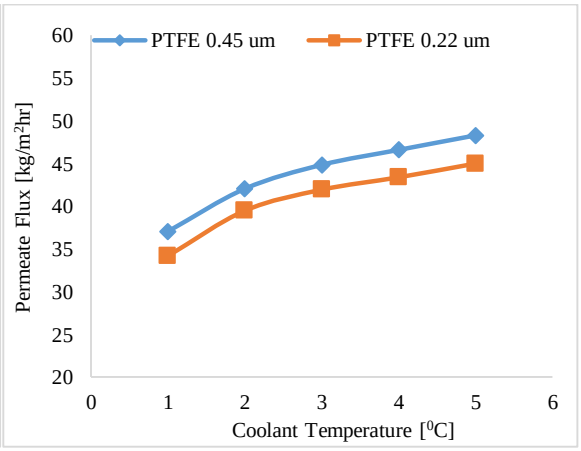

(b) At 2L/min

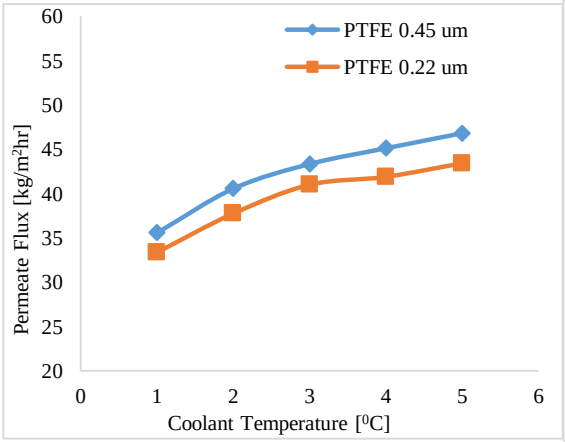

(c) At 3L/min

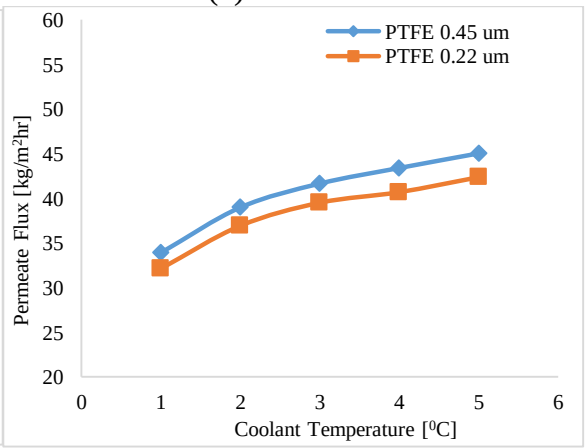

(d) At 3.5L/min

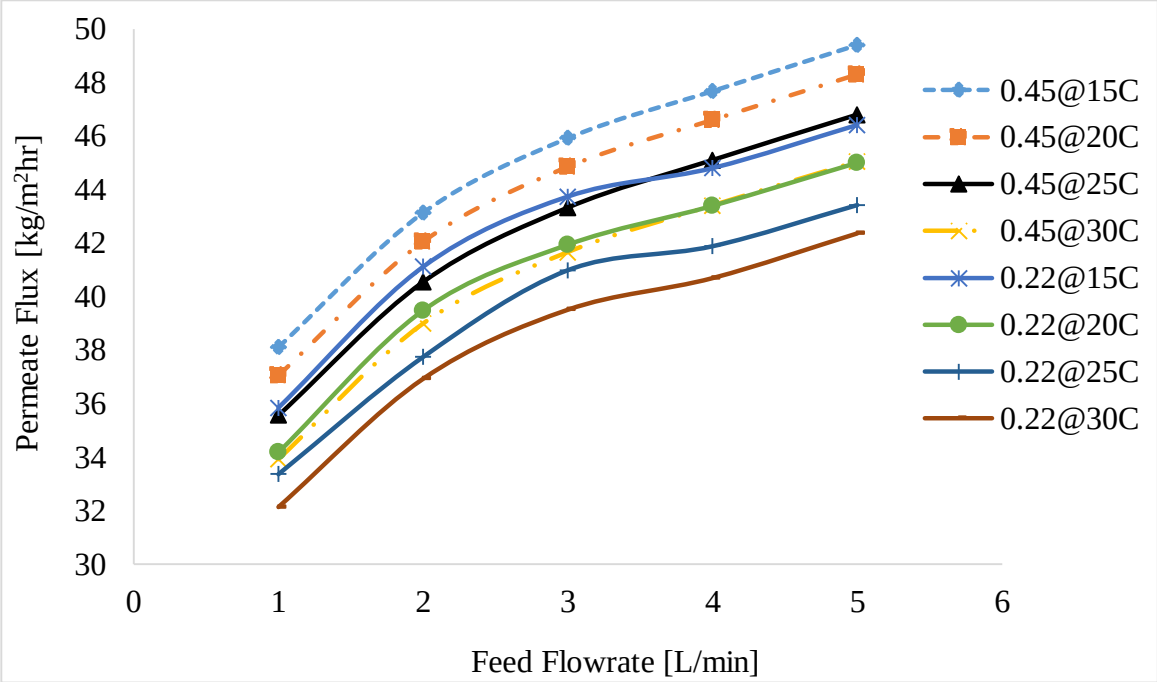

(e) At 1, 2, 3, & 3.5L/min

Figure 5.9 Effect of membrane pore size on flux at different feed flow rate and coolant temperature

Test Conditions: Feed Temperature of 70 0C, Coolant flow rate of 3 L/min, Feed Concentration of 75.5 mg/L and Air gap thickness of 3mm.

The effect of membrane pore size on the permeate flux at different feed temperature and coolant temperature was investigated and presented in figure 5.10. The variable conditions are: are feed temperature from 40^0C-80^0C and coolant temperature ranging from 15-30^0C. The fixed test conditions are: feed flow rate of 3L/min, coolant flow rate of 3 L/min, feed concentration of 75.5 mg/L and air gap thickness of 3mm. It is obvious from the figure that the permeate flux increases with increasing membrane pore size.

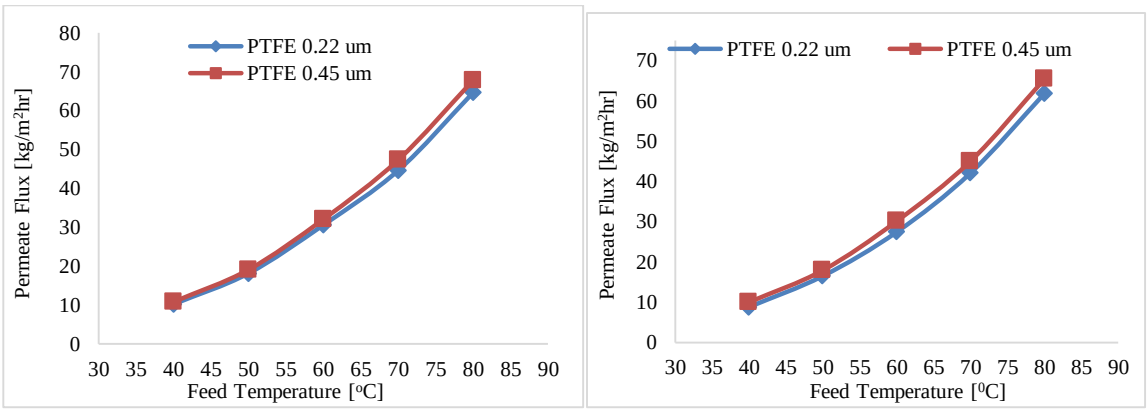

(a) At 15°C

(b) At 20°C

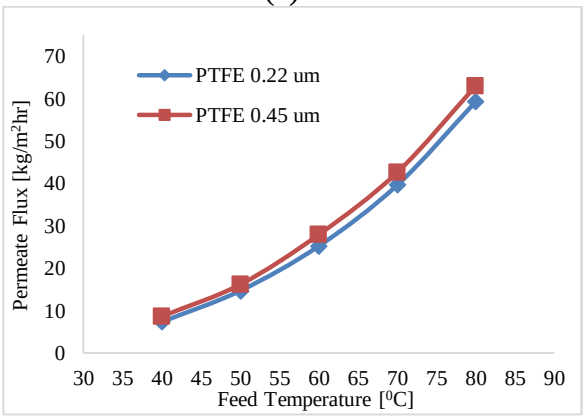

(c) At 25°C

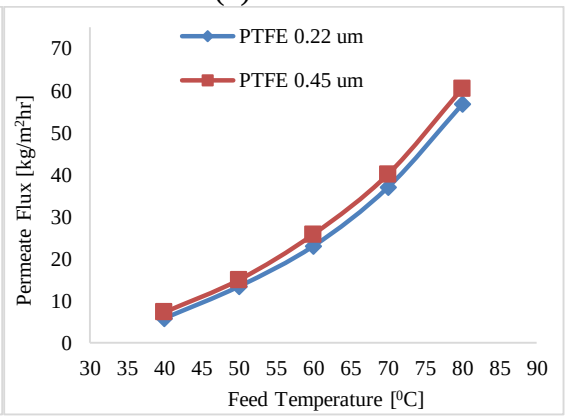

(d) At 30°C

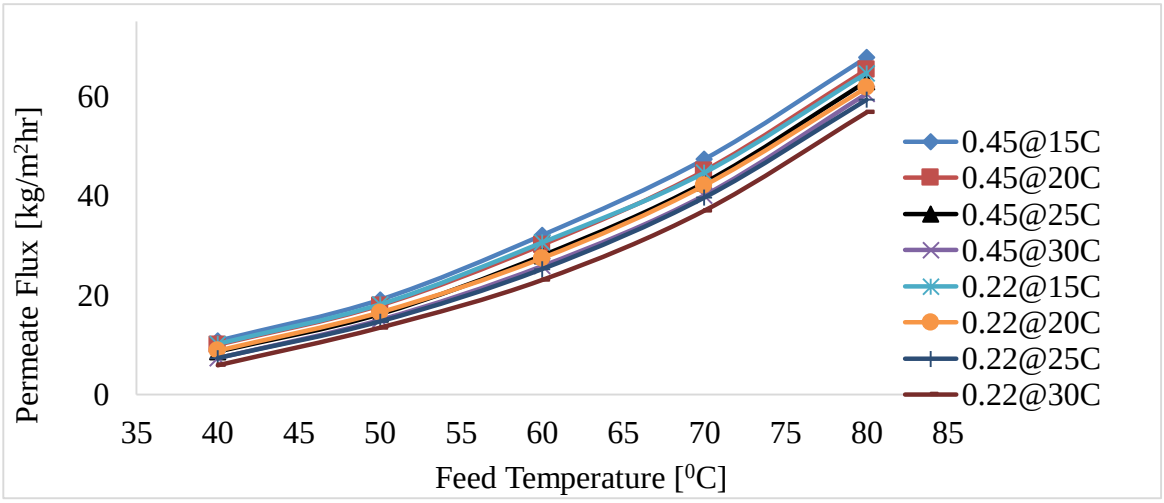

(e) At 15, 20, 25, & 30°C

Figure 5.10 Effect of membrane pore size on flux at different feed temperature and coolant temperature

Test Conditions: Feed flow rate of 3 L/min, Coolant flow rate of 3 L/min and Feed Concentration of 75.5 mg/L and Air gap thickness of 3mm.

It is worth mentioning that the average measured and recorded salt rejection factor of the permeate flux for both PTFE 0.45µm and PTFE 0.22µm throughout the investigation of membrane pore size are 99.9869% and 99.9899% respectively. Both membrane materials exhibit a very high rejection factor. However, PTFE 0.22µm salt rejection factor appears to be slightly greater than that of PTFE 0.45µm. This is perhaps due to its lower pore size which may also be the reason for it lower permeates flux.

5.5 Effect of Feed Solution Concentration on Permeate Flux

The effect of feed concentration on permeate flux was investigated at different of feed temperature, feed flow rate, and coolant temperature. The tested feed solutions are the distilled water (TDS of 0.075g/L), the laboratory prepared feed solutions ranging from 4 g/L to 50g/L, and row seawater (TDS of about 60 g/L). The obtained experimental results are presented in figures 5.11 to 5.13.

Depicted in 5.11 is the impact of feed concentration on flux at different feed temperature. Each feed solution ranging from distilled water to raw seawater was tested at different feed temperature ranging from 40-80^{0}C. The fixed experimental condition are the coolant temperature of 20^{0}C, feed flow rate of 3L/min, coolant flow rate of 3 L/min and air gap thickness of 3mm. It can be observed from figure 5.11 that the permeate flux tends to gradually decrease with increasing feed concentration. The average, and the maximum percentage reduction in permeate flux when feed concentration was increases from 0.075 g/L to 60g/L was about 9%, and 5% respectively. The gradual reduction in system performance with increasing feed concentration is as a result of increasing effect of

concentration polarization, which resulted in reduction of water vapour pressure. Thermal efficiency and temperature polarization effects may be the other reasons for the decline in permeate flux [84]. In general, the impact of feed concentration on the flux can be said to be insignificant when compared to other membrane desalination technology like reverse osmosis where higher feed concentration seriously affect the performance of the system. It was observed that the effect of increasing feed saline concentration on flux tends to decreases with increasing feed temperature. The measured salt rejection factor was found to be 99.98% in most cases of the studied.

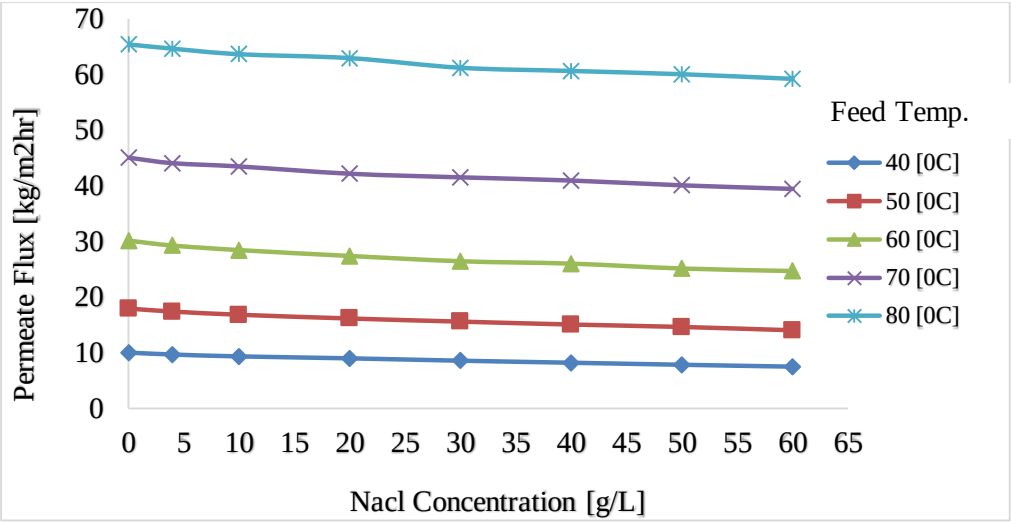

Figure 5.11 Effect of Feed Concentration on Flux at Different Feed Temperature

Test Conditions: Coolant Temperature of 20 ^{0}C, Feed flow rate of 3 L/min, Coolant flow rate of 3 L/min and Air gap thickness of 3mm

The investigation of the effect of feed saline concentration on flux at different feed flow rate is presented in figures 5.12. Each feed solution was tested at different fee flow rate ranging from 1-5L/min. The constant test conditions are the feed temperature of 70^{0}C, coolant temperature of 20^{0}C, coolant flow rate of 3 L/min and air gap thickness of 3mm.

It can be noticed that the system production rate gradually decrease with increasing feed concentration. The maximum and average percentage reduction in permeate flux when feed concentration was increased from 75mg/L to 60g/L are about 11% and 5% at 5L/min feed flow rate respectively. The Feed concentration was found to have lesser impact at higher feed flow rate than at lower flow rate. This is because turbulent flow at higher flow rate decreases the effect of concentration polarization and as a result reduces the effect of feed concentration.

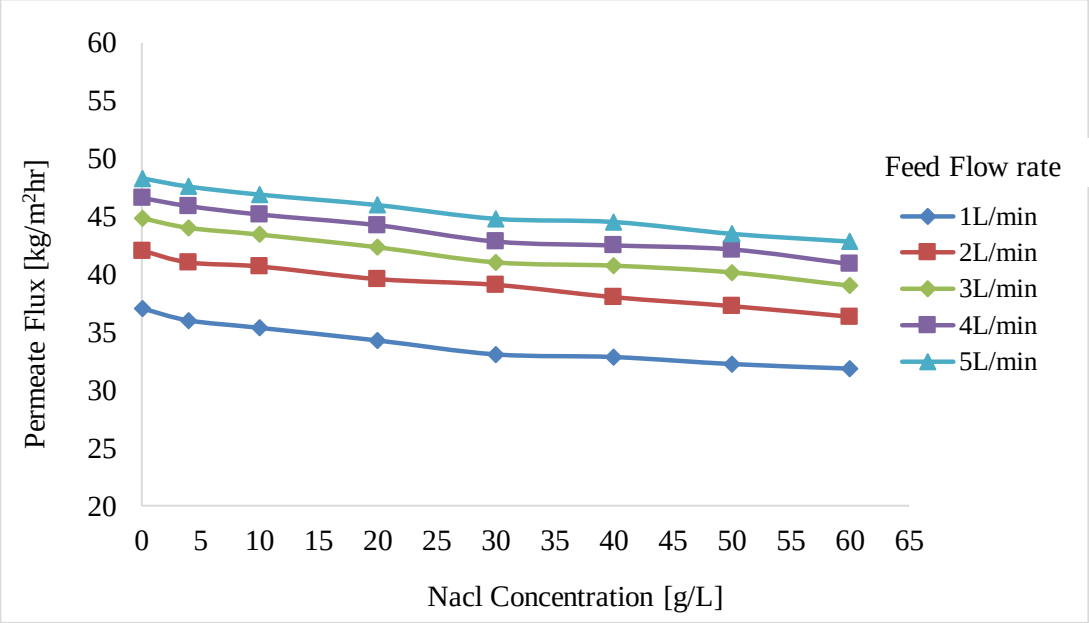

Figure 5.12 Effect of Feed Concentration on Flux at Different Feed Flow rate

Test Conditions: Feed Temperature of 70 ^{0}C, Coolant Temperature of 20 ^{0}C, Coolant flow rate of 3 L/min and Air gap thickness of 3mm

The effect feed concentration on permeate flux was also investigated at different coolant temperature. The effect of each feed solutions are tested at different coolant temperature ranging from 15^{0}C - 30^{0}C and the achieved results are presented in figure 5.13. The fixed

experiment conditions are the feed temperature of 70^0C, feed flow rate of 3L/min, coolant flow rate of 3 L/min and air gap thickness of 3mm. Again, it can be observed that permeate flux slightly decreases with increasing feed concentration. The maximum, and the mean percentage drop in permeate flux when the feed concentration increase from 0.075g/L to 60g/L at different coolant temperature are about 11% and 6% respectively.

Generally, the system performance slightly decreases with increasing feed concentration. However, the impact is observed to be marginal when compared to other membrane desalination technology such as reverse osmosis. Hence, AGMD system can be used for desalination of seawater. This investigation also shows that pre-treatment of feed solution are not essential in AGMD since membrane fouling is not much a problem.

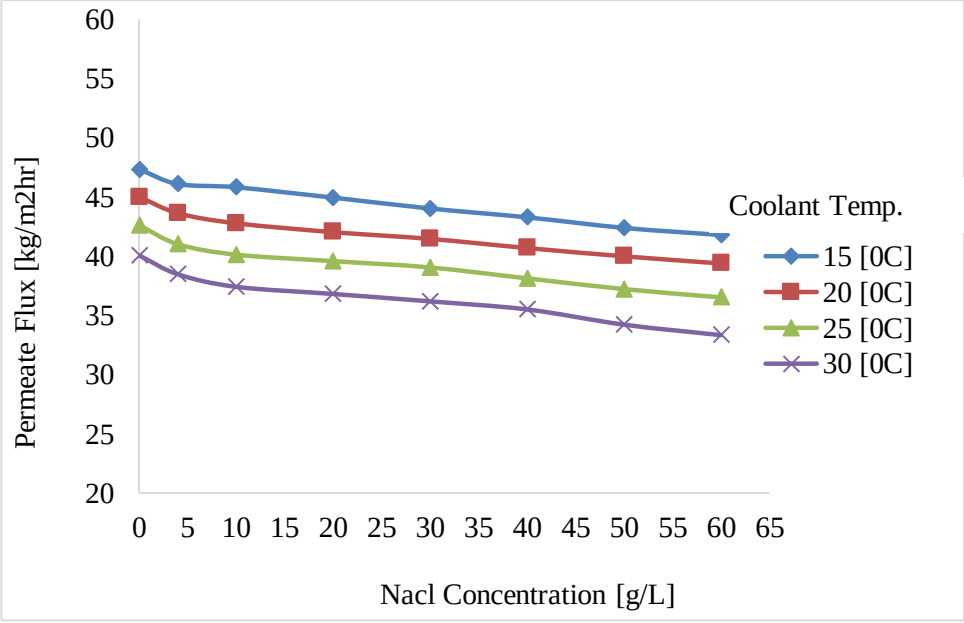

Figure 5.13 Effect of Feed Concentration on Flux at different Coolant Temperature

Conditions: Feed Temperature of 70 ^{0}C, Feed flow rate of 3L/min, Coolant flow rate of 3 L/min and Air gap thickness of 3mm

5.6 Membrane Degradation Test (Long Term Experiment)

Long-time experiment was conducted to investigate the effect of membrane continuous operation on membrane degradation and the corresponding effect on system flux. A single membrane material (PTFE 0.45µm) was used in the investigation. We run the experiment continuously without interruption for the total duration of 38 hours. The experimental conditions are: feed temperature of 70 ^{0}C, coolant temperature of 20 ^{0}C, feed flow rate of 3 L/min, coolant flow rate of 3 L/min and air gap thickness of 3mm. Row seawater obtained from Arabian Gulf was used as the feed solution. It is worth mentioning that the used seawater was neither filtered nor was it pre-treated.

Illustrated in figures 5.14 and 5.15 are the achieved results from the experiment and figure 5.16 presents the percentage reduction in flux over the experimental duration. The effect of experimental time on flux was presented in figure 5.14. It can be noticed that for the first twelve hours of the experimental time, the system production rate appear to be fairly constant. After this period, the flux begins to drop gradually with time (with little fluctuations) till the end of the experiment (38 hours). The declines in permeate flux may be attributed to membrane fouling. Running the system at constant feed flow rate for long period could leads to deposition of salts over membrane surface. This could result in increased concentration polarization effect that could lead to reduction in the permeate flux. Over the time, the feed pump is corroded because of salt water left over inside the pump when the pump is not in use. The corroded part of the pump react with the fresh feed solution and increases the number of species in the feed solution, leading to more concentrated and contaminated feed solution. This may just be another reason for the

observed drop in permeate flux. The quality of permeate flux against the experimental time is depicted in figure 5.15. Drops in salt rejection factor were observed over the time. Since we are using closed loop system, the concentration of the feed solution is expected to increase over time. This increase in feed concentration over time is the reason behind the observed reduction in quality of the system output. Pump corrosion problem may be other reason behind the drop in flux quality. Figure 5.16 displayed percentage reduction in permeate flux against the experimental time. The maximum percentage reduction in flux over the whole experiment (38 hours) was found to be about 27%. The average recorded percentage reduction in flux was about 9%.

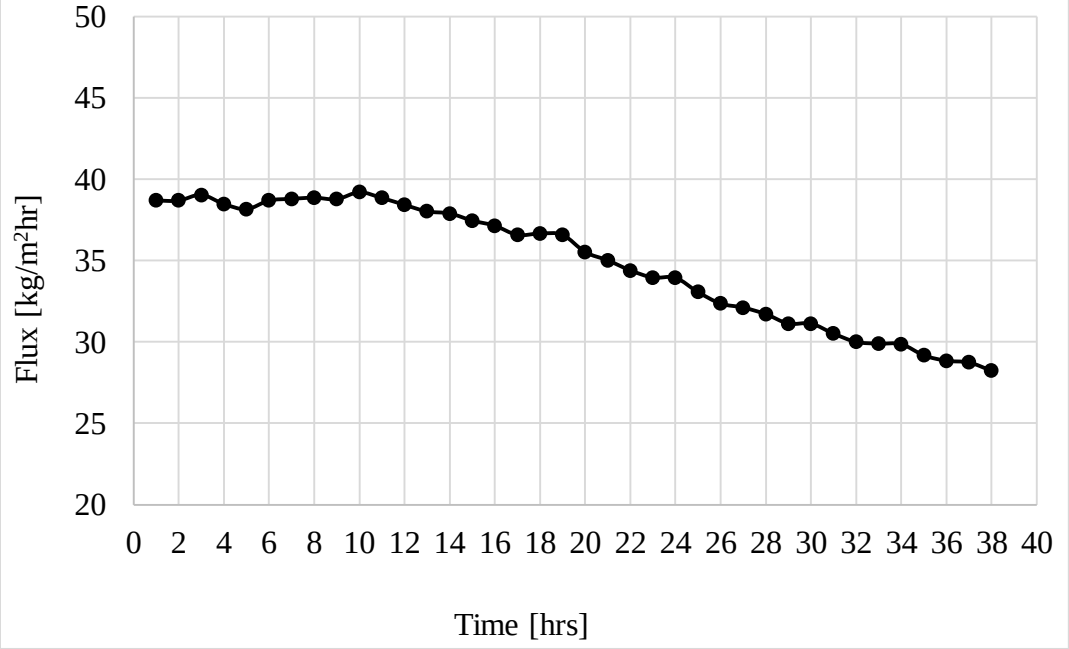

Figure 5.14 Impact of membrane operating time on flux

Test Conditions: Feed Temperature of 70 ^{0}C, Coolant Temperature of 20 ^{0}C, Feed Flow rate of 3 L/min, Coolant flow rate of 3 L/min and Air gap thickness of 3mm.

One of the setbacks of MD process is lack of membrane material specifically designed for membrane distillation. Moreover, most of the required characteristics of membrane material are not met by the most commercially available membrane material [15]. So the used membrane material in this investigation may not be an exception.

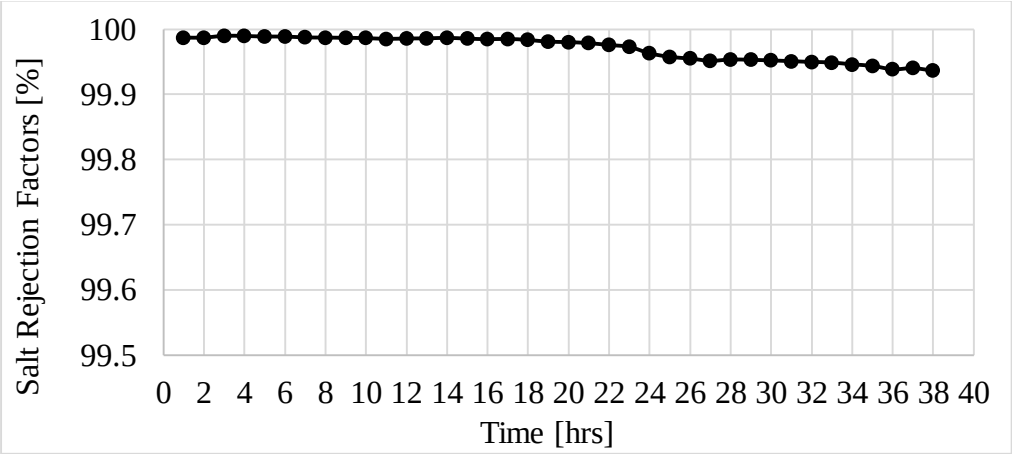

Figure 5.15 Impact of membrane operating time on salt rejection factor

Test Conditions: Feed Temperature of 70 ^{0}C, Coolant Temperature of 20 ^{0}C, Feed Flow rate of 3 L/min, Coolant flow rate of 3 L/min and Air gap thickness of 3mm.

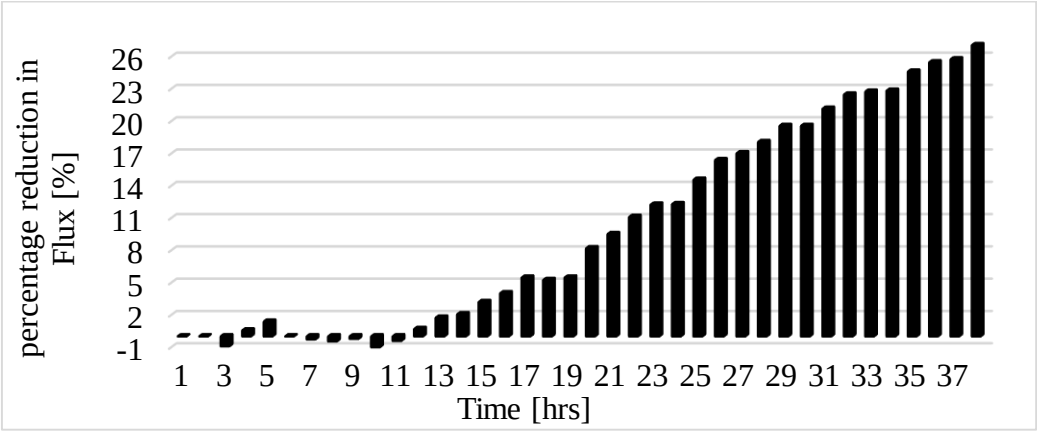

Figure 5.16 Impact of membrane operating time on Percentage drop in flux

Conditions: Feed Temperature of 70 ^{0}C, Coolant Temperature of 20 ^{0}C, Feed Flow rate of 3 L/min, Coolant flow rate of 3 L/min and Air gap thickness of 3mm.

5.7 Multi-Stage Testing

In order to enhance the performance of air gap membrane distillation at lower energy input, double stage module was designed, built and tested. The test was conducted at AGMD operating parameters and the achieved results are presented and discussed below.

5.7.1 Effect of Feed Temperature on Flux

The roles of feed inlet temperature on the amount of permeate flux produced for single and double stages are illustrated in Figure 5.17. Feed temperature was varied from 40 to 80^0C. The data are collected at coolant temperature of 20 ^{0}C, feed flow rate of 3 L/min, coolant flow rate of 3 L/min, feed concentration of 4.06g/L and air gap thickness of 3mm. It can be observed that increasing the feed temperature leads to exponential rise in the permeate flux. This may be due to a reason best explained by Antoine equation. According to the Antoine equation, the effect of temperature on vapour pressure is marginally low at lower temperature, but becomes very significant at higher temperature. As noticed from figure 5, the permeate flux production from the first stage is slightly higher than that of second stage by about 1.2 times. This is attributed to the temperature drops (about 2^0C) between the first stage and the second stage as a result of conduction heat loss to the membrane material and the surrounding. The maximum recorded permeate flux from double stage unit is about 128.47kg/m^{2}hr. This result is about twice that of single stage which has a maximum permeate flux of 65.81 kg/m^{2}hr. Using double stage unit leads to almost 100% rise in distil water production. Although, the energy input required by the double stage system is expected to be greater than that of single stage unit since its membrane area is twice that of single stage unit. However, comparing the energy

input with system production, one will ascertain that double staging the MD is essential for efficient energy usage.

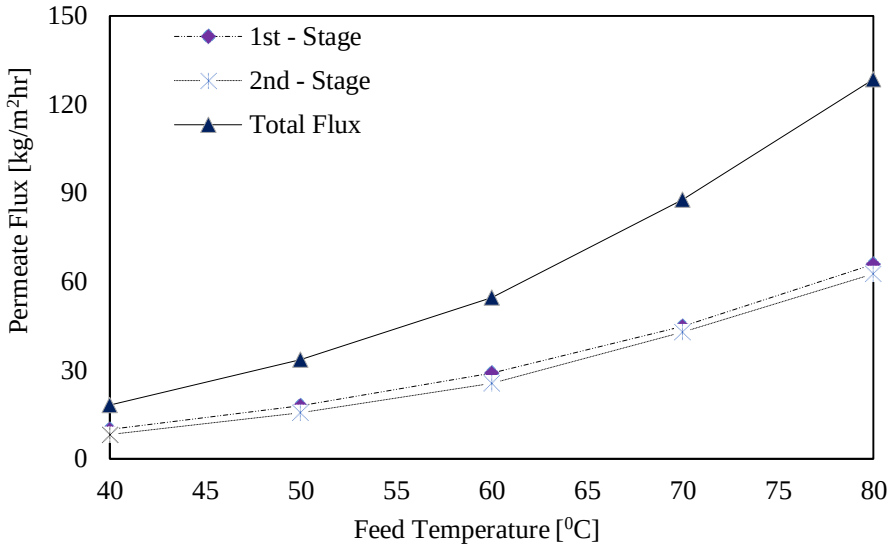

Figure 5.17 Effect of feed temperature on permeate flux

5.7.2 Effect of Coolant Temperature on Flux

Coolant temperature is another operating parameter whose impact cannot be ignored because; operating the AGMD system at inappropriate coolant temperature will definitely affect the production rate of the AGMD system. Hence, the need for appropriate range of coolant temperature at which maximum possible permeates flux can be achieved thereby arises. In order to investigate the influence of coolant temperature on system performance, coolant temperature was varied from 15 to 30^0C, at feed inlet temperature of 70^0C, feed flow rate of 3 L/min, coolant flow rate of 3 L/min, feed concentration of 4.06g/L and air gap thickness of 3mm. The obtained result is illustrated in figure 5.18. In general, drops in permeate flux was observed when coolant temperature was increases

from 15 to 30^{0}C. By increasing the coolant temperature from 15^{0}C to 30^{0}C, there is about 10% drops in permeate flux production. This is due to reduction in transmembrane driving force responsible for producing permeating flux. In a nutshell, increasing coolant temperature leads to reduction in temperature difference between the feed and coolant chambers, which decline the driving force, hence the observed drops in permeate flux. Using cooling water at atmospheric condition is advisable in this context since the system performance could only drop by a maximum of 10% when the coolant temperature is reduced from 30 to 15^{0}C. This will lower the cost of energy input for maintaining the cooling temperature below the room temperature.

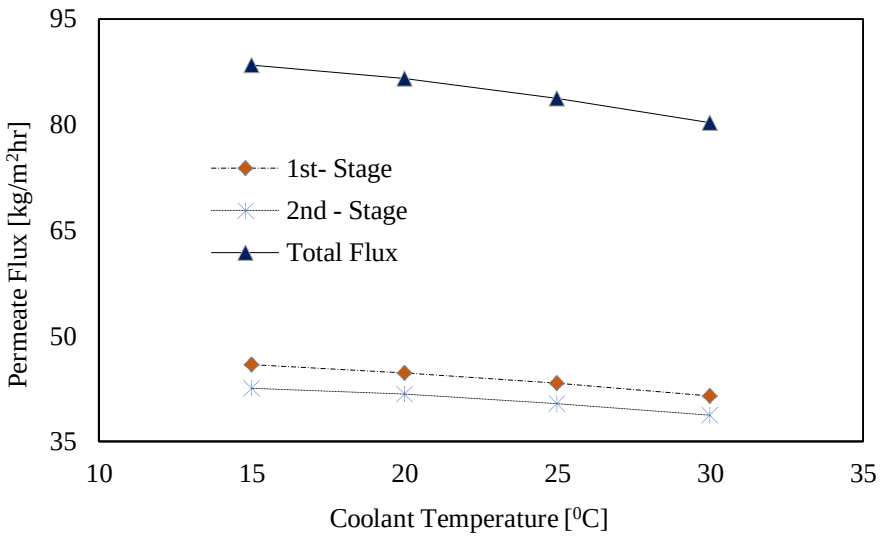

Figure 5.18 Coolant temperature as a function of permeate flux

Again, due to 2^{0}C drops in feed temperature between the inlet and exit of the first stage, the result from first stage is slightly higher than that of second stage. It must be pointed out here that the coolant temperature is fairly stable throughout the experiment because the coolant temperature rises over time in every experimental run. This may be attributed

to the fact that single cooling channel was used for double staging, which indicate faster heat exchanged between the feed solution and the cooling solution.

5.7.3 Effect of Feed flow rate on Flux

Figure 5.19 illustrates the influence of feed flow rate on permeate flux. While keeping feed inlet temperature at 70^0C, coolant temperature at 20^0C, coolant flow rate at 3 L/min, and air gap at 3mm width and feed solution at 4.06g/L, the feed flow rate was varied from 1 to 5L/min. it is obvious that higher permeate flux is obtained at higher feed flow rate. The rise in flux is due to reduction in temperature and concentration polarization effect which decreases the system production. Additionally, increasing feed flow rate encourage turbulent flow level at the feed channels and improved the heat transfer coefficient of the feed boundary layer.

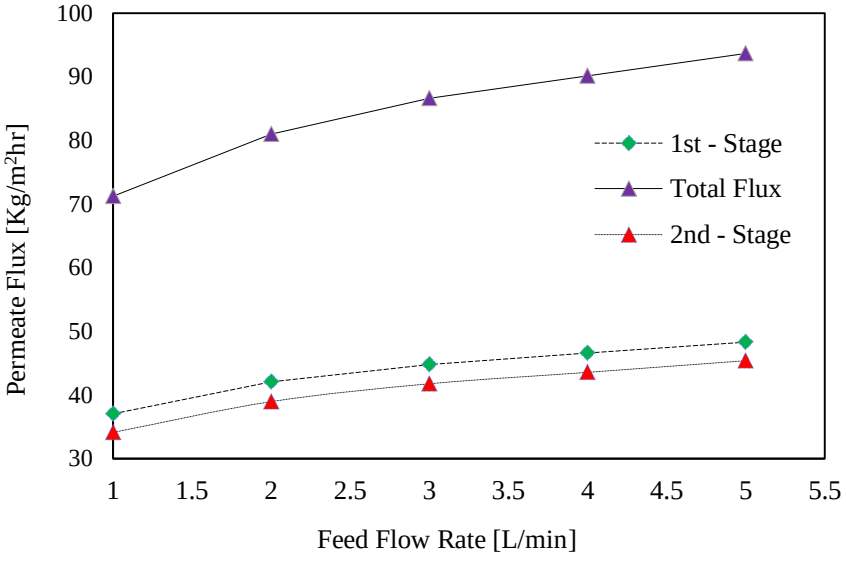

Figure 5.19 Effect of feed flow rate on permeate flux

The impact of feed flow rate on flux is more significant than that of coolant temperature. Therefore, running the system at higher feed flow rate is desirable in this context. However, precaution is advised when running the system at higher feed flow rate in order to avoid membrane pore wetting. Similar to previous observation, the result achieved for single stage unit is slightly more than half that of double stage unit.

5.7.4 Effect of Coolant flow rate on Flux

Coolant flow rate is observed to have the least effect on the permeate flux. Illustrated in figure 5.20 is the effect of increasing coolant flow rate from 1 - 3.5L/min on flux at feed temperature of 70^0C, coolant temperature of 20^0C, feed flow rate of 3 L/min, feed concentration of 4.06g/L and air gap thickness of 3mm. The essence of higher coolant flow rate is to reduce the air condensate interfacial temperature [15]. This indicates that increasing cooling water flow rate leads to higher heat transfer coefficient of the cooling surface. However, careful observation revealed that increasing coolant flow rate leads to negligible impact on the fresh water production in all cases. Increasing coolant flow rate is a waste of input energy as far as we have enough flowing water to carry away the heat transfer to the cooling surface. In fact, it has been reported [15, 85] that coolant temperature has little influence on system performance. In order to reduce cost of quality water production using AGMD, it is advisable to run the system at low flow rate (implying, less input energy demand for pumping). The total flux from double stage unit is about 96% higher than that of single stage.

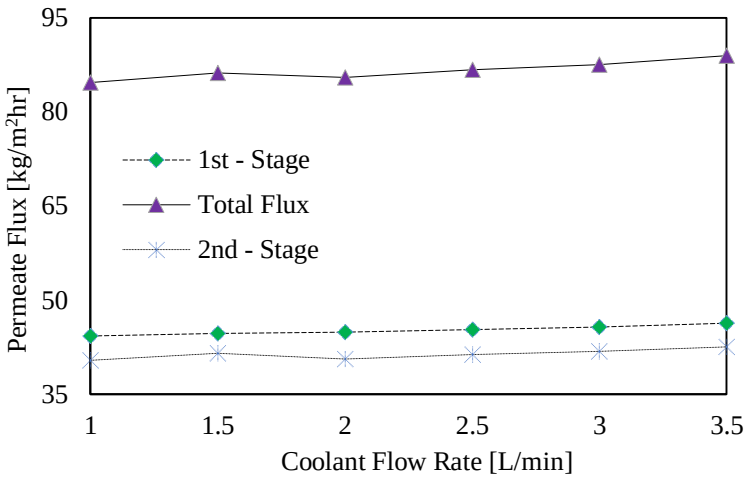

Figure 5.20 Coolant flow rate as a function of permeate flux

5.7.5 Effect of Air gap width on Flux

Due to mass transfer resistance in the air gap, air gap thickness significantly affects the production rate. To investigate the impact of air gap width on flux, the air gap thickness of 3mm, 5mm, and 7mm are considered. The investigation is conducted at feed temperature ranging from 40 to 80^{0}C.

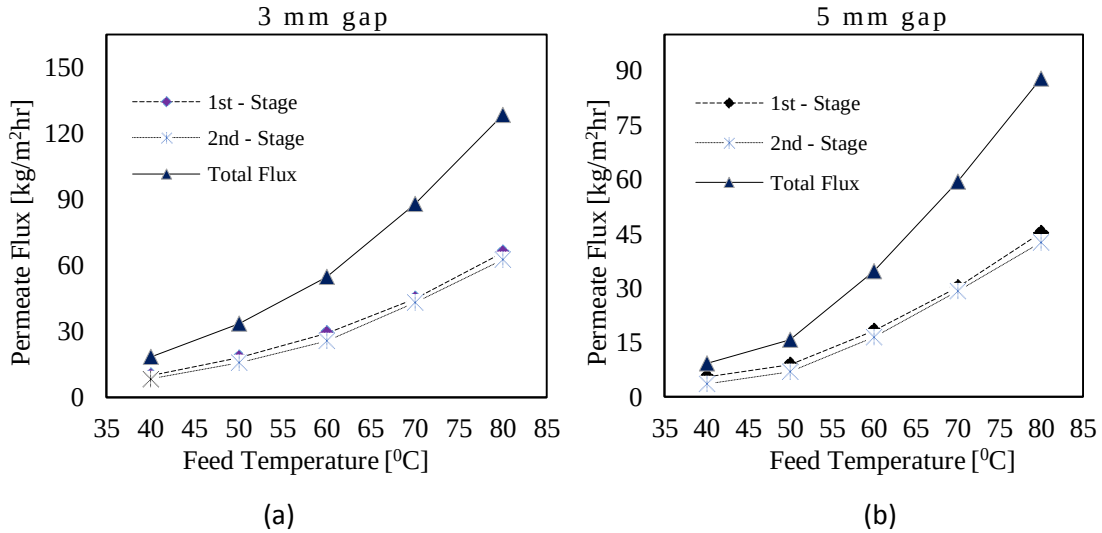

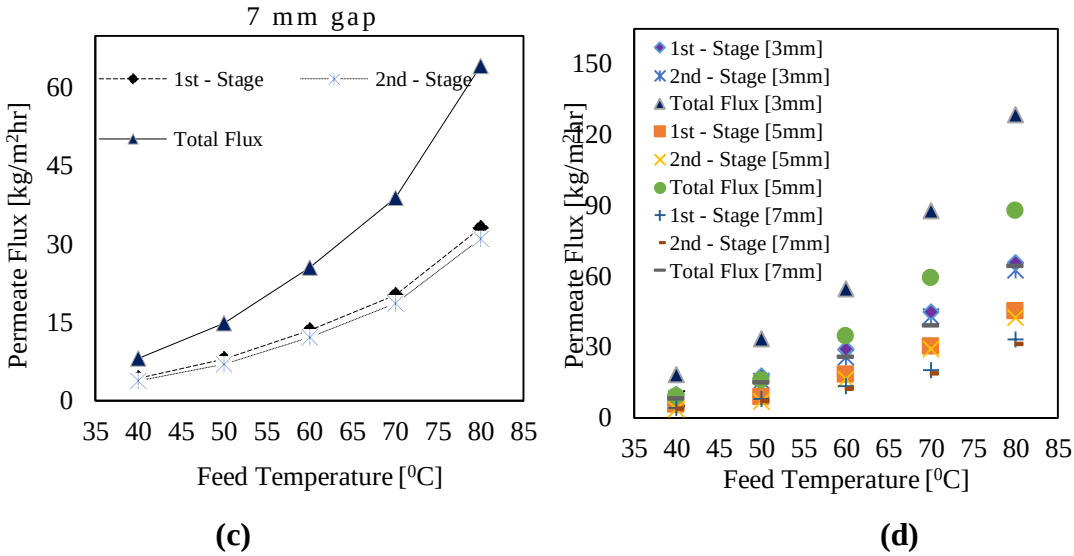

Figure 5.21 Effect of air gap thickness on permeate flux

The fixed conditions are: coolant temperature of 20^0C, feed flow rate of 3 L/min, coolant flow rate 3 L/min, and feed concentration of 4.06g/L. The results are presented in figure 5.21. It can be seen that reducing the air gap width from 7mm to 3mm at different feed inlet temperature resulted in considerable rise in distillate production especially at higher temperature. The reason for this is attributed to increment in temperature gradient within the vapour compartment as a result of declines in resistance to mass transfer. It is obvious that at every air gap position, permeate flux from double stage unit nearly double that of single stage. Since air gap width is an important factor affecting the distillate production, and then it is recommended to use minimum possible air gap width in the design in order to significantly enhance the performance of the system. Air gap width is considered to be one of the dominant factors affecting fresh water production in AGMD system

5.8 Validation of Theoretical Model

In order to validate the theoretical model presented in chapter three, comparison between the model and the experimental data were made for different AGMD operating parameters. The used membrane is PTFE 0.45µm and its properties are presented in table 4.1. The theoretical model was subsequently validated against the experimental data obtained for different membrane pore size of PTFE 0.45µm and PTFE 0.22µm membranes. Generally, results showed good agreements between the model and the experimental data which proves the validity of the used model.

5.8.1 Influence of Feed Temperature on Permeate Flux

Presented in figure 5.22 is the validation result for the influence of feed temperature on flux. The feed temperature was varied from 40 - 80^0C, while the coolant temperature was kept at 20^0C, feed flow rate at 3 L/min, coolant flow rate at 3 L/min and air gap thickness at 3mm. It can be seen that the model result is in good agreement with the experimental data since most of the model result falls within 15% of the experimental data. The maximum, minimum, and the averaged recorded percentage mismatched are 30.11%, 0.14% and 14.75% respectively. It can also be observed that the predicted flux falls below the experimental data at lower feed temperatures, but greater that the experimental data at higher feed temperature. The model was found to predict better between 60^0C and 70^0C.

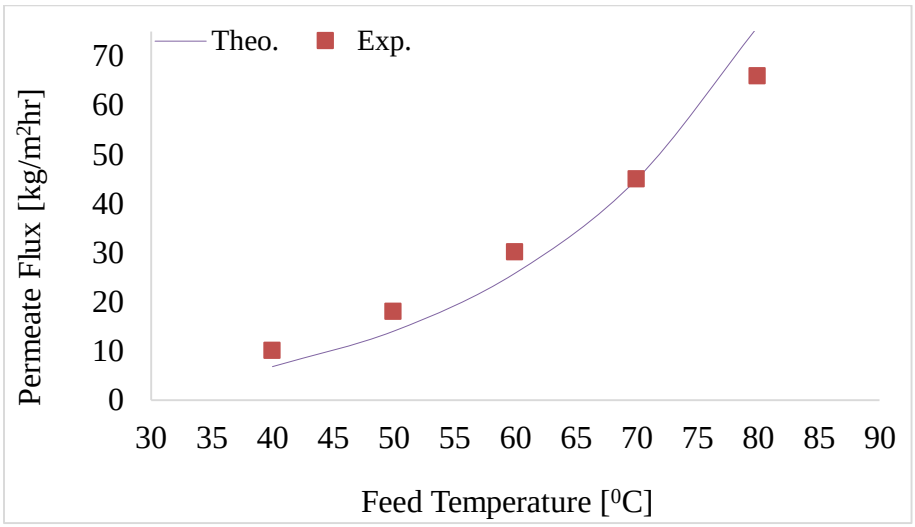

Figure 5.22 Impact of feed temperature on flux

Test Conditions: coolant temperature of 20 ^{0}C, Feed flow rate of 3 L/min, Coolant flow rate of 3 L/min and Air gap thickness of 3mm.

5.8.2 Impact of Feed Flow rate on Permeate Flux

Figure 5.23 illustrates the comparison between the theoretical model result and the experimental data for the impact of feed flow rate on flux. The feed flow rate was changed from 1 – 5 L/min, while keeping feed temperature at 70^{0}C, coolant temperature at 20^{0}C, coolant flow rate at 3 L/min and air gap thickness at 3mm. It can be noticed that both model and the experimental data are in very good agreement as most of the model result falls within 5% of the experimental data. The registered maximum and the minimum percentage error was found to be 10.06% and 0.14% while the recorded average error was found to be 4.21%. With respect to the experimental data, the model was found to over predict at lower feed flow rate and under predict at higher feed flow rate. The best model prediction is between 2-4L/min.

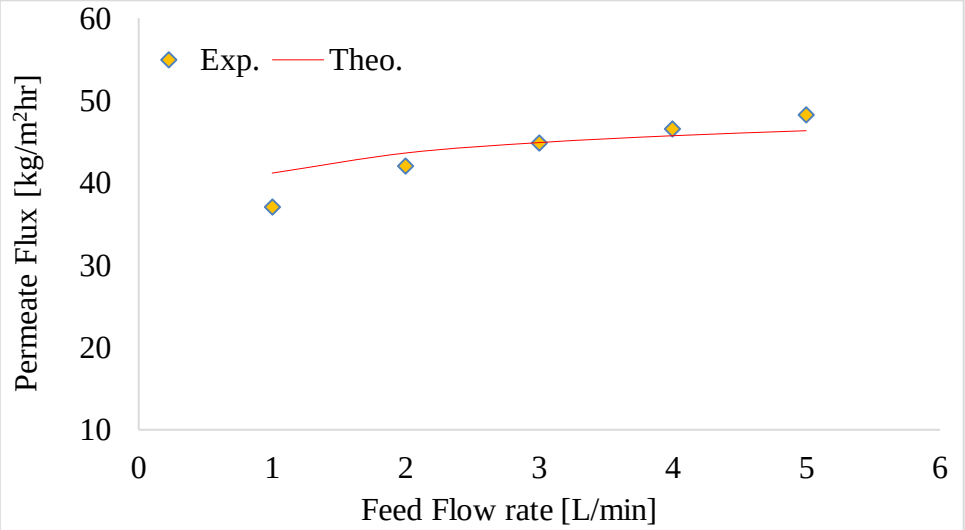

Figure 5.23 Impact of Feed flow rate on flux

Test Conditions: feed temperature of 70 ^{0}C, Coolant temperature of 20 ^{0}C, Coolant flow rate of 3 L/min and Air gap thickness of 3mm.

5.8.3 Effect of Coolant Temperature on Permeate Flux

Figure 5.24 presented the model results against the experimental data for the impact of coolant temperature on flux. The coolant temperature was varied from 15 - 30^{0}C, while the feed temperature was kept at 70^{0}C, feed flow rate at 3 L/min, coolant flow rate at 3 L/min and air gap thickness at 3mm. Good matches were observed between the model results and the experiment data as the accuracy of the model is within 5% of the experimental data. The maximum and minimum error of accuracy of 4.47% and 0.13% were recorded between the model and experimental data. It can also be noticed that the model accuracy decreases with increasing coolant temperature.

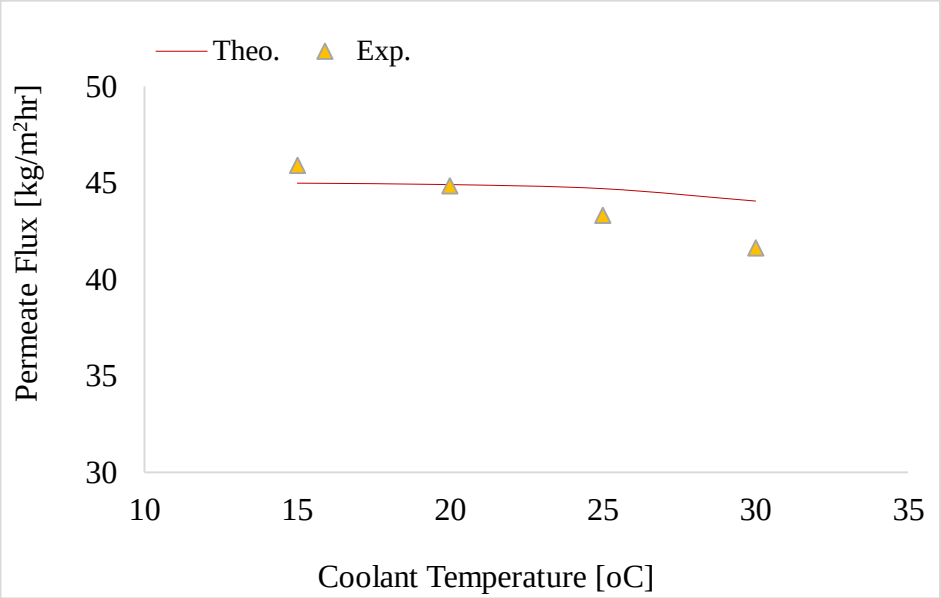

Figure 5.24 Impact of coolant temperature on flux

Test Conditions: Feed temperature of 70 ^{0}C, Feed flow rate of 3 L/min, Coolant flow rate of 3 L/min and Air gap thickness of 3mm.

5.8.4 Role of Coolant Flow rate on Permeate Flux

Presented in figure 5.25 is the validation result for the influence coolant flow rate on flux. The coolant flow rate was varied from 1 - 3.5L/min. The fixed conditions are feed temperature of 70 ^{0}C, coolant temperature of 20 ^{0}C, feed flow rate of 3 L/min and air gap thickness of 3mm. It can be noticed that the model result portrays good agreement with the experimental data. The model prediction becomes better as the coolant flow rate increases. Between the model results and the experimental data, the maximum percentage error recorded is 3.10%, while the minimum percentage error recorded is 0.12%, and the average percentage error recorded is 1.17%. This is of course a very good agreement. With respect to the experimental data, the model predicts well at all the tested coolant flow rate with the best prediction at 3L/min.

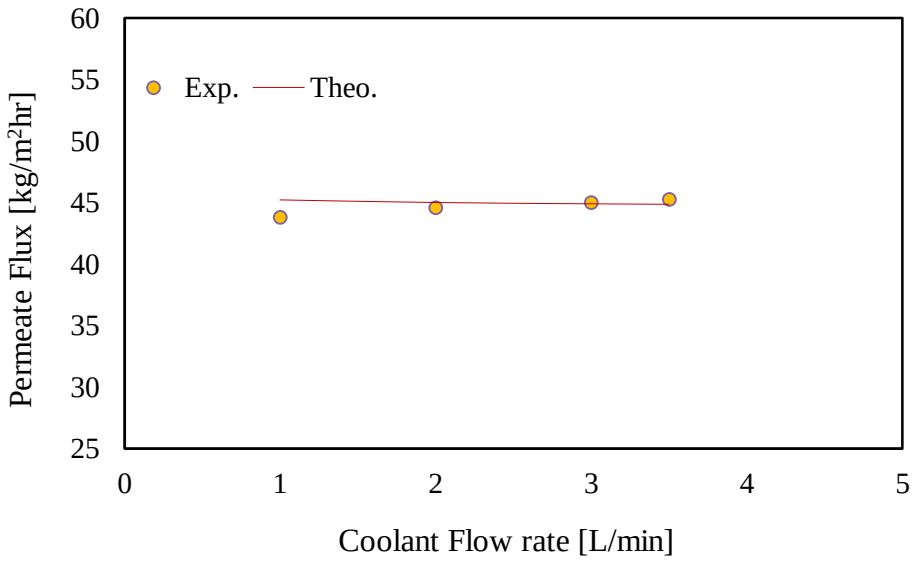

Figure 5.25 Impact of Coolant flow rate on flux

Test Conditions: feed temperature of 70 ^{0}C, Coolant temperature of 20 ^{0}C, Feed flow rate of 3 L/min and Air gap thickness of 3mm.

5.8.5 Impact of Air Gap Width on Permeate Flux

The results for the effect of air gap width on flux are presented in figures 5.26 and 5.27. Figure 5.26 illustrate the effect of air gap thickness on flux at the feed temperature of 70 ^{0}C, coolant temperature of 20 ^{0}C, feed flow rate of 3 L/min, coolant flow rate of 3 L/min and air gap thickness of 3mm. A maximum of 9.34% percentage difference was recorded between the model results and the experimental findings. The minimum and the mean percentage error of the model are 0.14% and 3.23% respectively. The results indicate that most of the model results are within 4% of the experimental data.

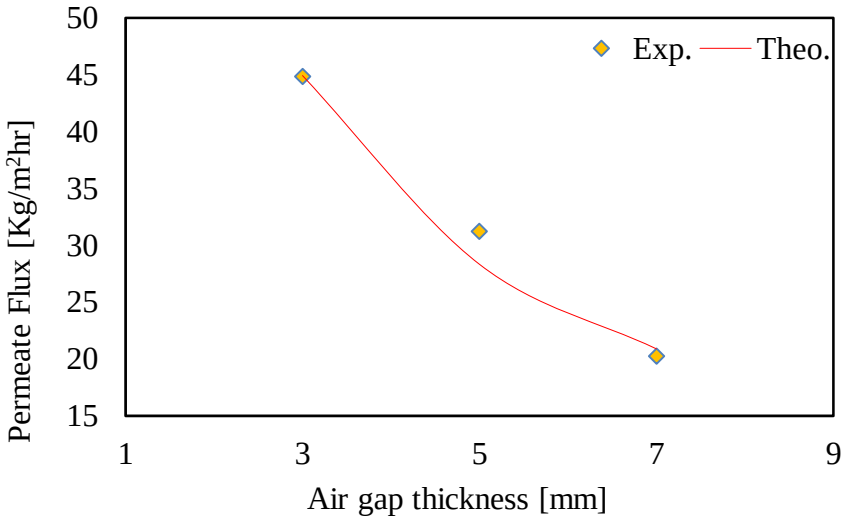

Figure 5.26 Impact of Air gap width on flux

Test Conditions: Feed temperature of 70 ^{0}C, Coolant temperature of 20 ^{0}C, Feed flow rate of 3 L/min and Coolant flow rate of 3 L/min.

Figure 5.27 displayed model results against the experimental data for the influence of air gap width on flux at different feed temperatures. The conditions are similar to that of figure 5.26 except that the feed temperature was changed in the range of 40 - 80^{0}C. In general, the model recorded fairly good matches against the experimental data since most of the model results are within 20% of the experimental data. For the case of 3mm air gap, the minimum and the maximum percentage difference between the model results and the experimental data are 30.11% and 0.14% respectively. While the maximum and the minimum percentage error of 38.72% and 4.54% between the model results and the experimental data was recorded for air gap width of 5mm respectively and the maximum and minimum error of accuracy observed between the model results and the experimental data for the case of 7mm air gap are 42.58% and 3.12% respectively. By careful analysis of the above statistics, one can concludes that the accuracy of the model decreases with increasing air gap width.

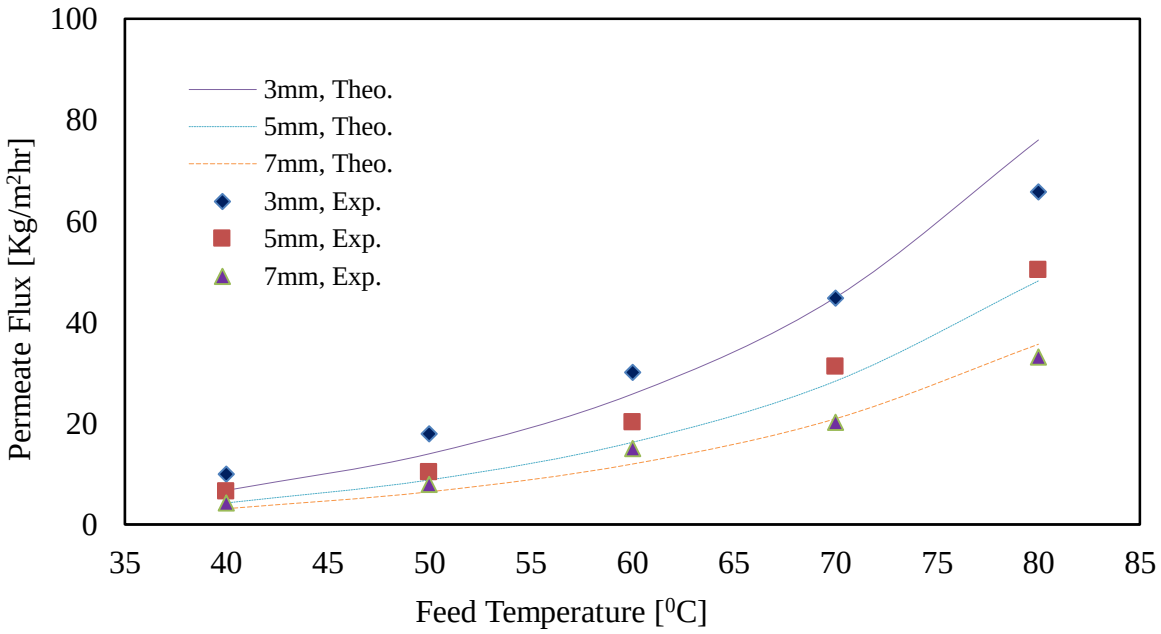

Figure 5.27 Impact of Air gap width on flux at different Feed temperature

Test Conditions: Coolant temperature of 20 ^{0}C, Feed flow rate of 3 L/min, and Coolant flow rate of 3 L/min

5.8.6 Effect of Membrane pore size on flux at different Feed Temperature

Depicted in figure 5.28 is the validation result for the influence of membrane pore size on flux at different feed temperature ranging from 40 - 80^{0}C. The coolant temperature was kept at 20 ^{0}C, while the feed flow rate was at 3L/min, the coolant flow rate at 3L/min and the air gap thickness at 3mm. Two membranes (PTFE 0.45µm and PTFE 0.22µm) are used. The recorded maximum, minimum and the average percentage error of accuracy between the model results and that experimental data for PTFE 0.22µm are 18.16%, 0.86%, and 10.59% respectively. For PTFE 0.45µm, see the discussions of figure 5.22.

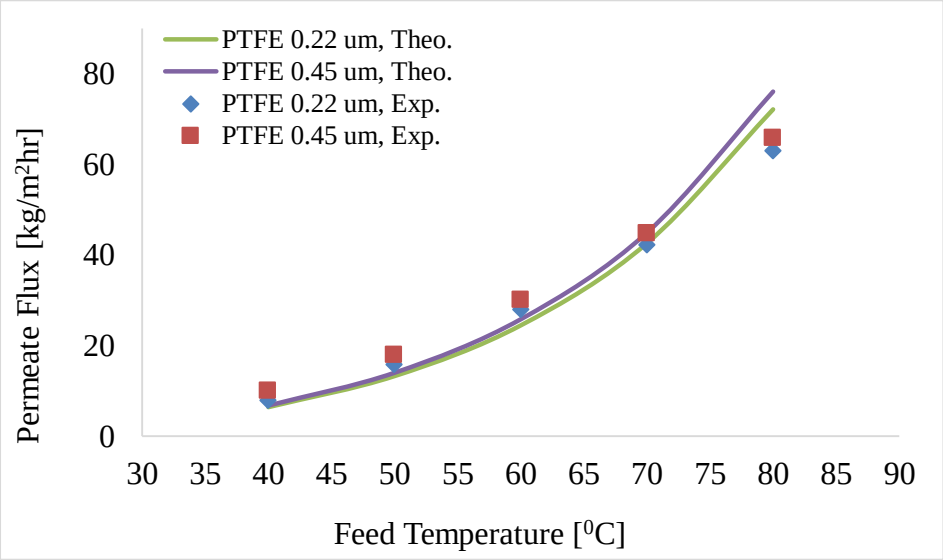

Figure 5.28 Influence of membrane pore size on flux at different feed temperature

Test Conditions: coolant temperature of 20 ^{0}C, Feed flow rate of 3 L/min, Coolant flow rate of 3 L/min and Air gap thickness of 3mm.

5.8.7 Effect of Membrane pore size on flux at different Feed Flow rate

Illustrated in figure 5.29 is theoretical and experimental data for the effect of membrane pore size on flux at different feed flow rate. The feed flow rate was varied from 1 - 5L/min, while the feed temperature was kept at 70^{0}C, and the coolant temperature at 20^{0}C, the coolant flow rate at 3L/min and air gap thickness at 3mm. The model result was noticed to be in good agreement with the experimental data. 11.50%, 0.04% and 3.21% corresponding to maximum, minimum and average percentage error are recorded for PTFE 0.22µm membrane. The statistics for PTFE 0.45µm membrane can be found with the discussion of figure 5.23. It can be observed that the model predict better at higher feed flow rate.

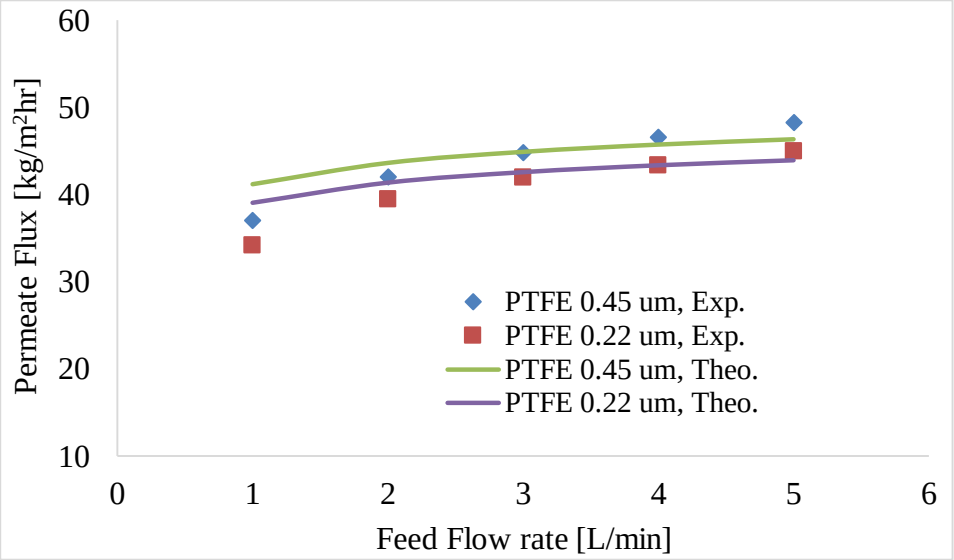

Figure 5.29 Impact of membrane pore size on flux at different Feed flow rate

Test Conditions: feed temperature of 70 ^{0}C, Coolant temperature of 20 ^{0}C, Coolant flow rate of 3 L/min and Air gap thickness of 3mm.

5.8.8 Effect of Membrane pore size at different Coolant Temperature

The theoretical and experimental data for the effect of membrane pore size on flux at different coolant temperature is presented in figure 5.30. Changing the coolant temperature from 15-30^{0}C, the feed temperature was kept at 70 ^{0}C, while feed flow rate was kept at 3L/min, the coolant flow rate at 3L/min and air gap thickness at 3mm. The model results for both used membrane material was observed to be in good agreement with the experimental data. The maximum, minimum, and the mean percentage error between the model and the experiment data for PTFE 0.22 µm are 4.42%, 1.41% and 2.13% respectively. It can be noticed that the model predict better at the lower coolant temperature.

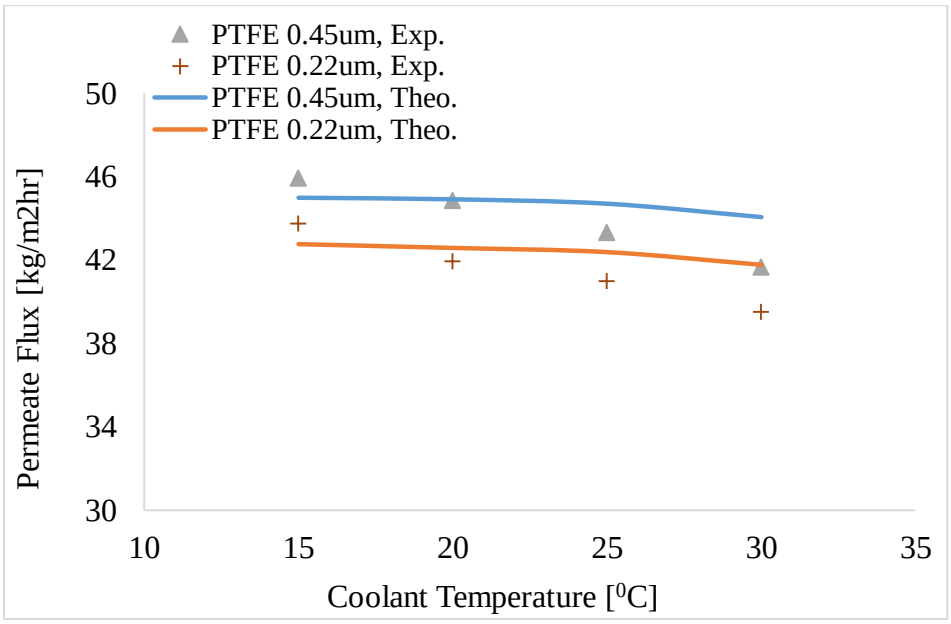

Figure 5.30 Impact of membrane pore size on flux at different coolant temperature

Test Conditions: feed temperature of 70 ^{0}C, Feed flow rate of 3 L/min, Coolant flow rate of 3 L/min and Air gap thickness of 3mm

From the foregoing analysis and discussion of the model results, it can be concluded that the model is good and is capable of predicting the permeate flux in air gap membrane distillation system with good accuracy.

5.9 Thermal Efficiency

The theoretical model was used to predict thermal efficiency and temperature polarization coefficient of the system at different values of feed temperature, coolant temperature, feed flow rate and coolant flow rate. The results obtained are presented in figures 5.31 to 5.38. Thermal efficiency is the ratio of the used energy (energy needed for heat of vaporization) to the total energy supply (total heat transfer from the feed to

permeate). The total energy supply is the sum of the useful energy and the energy lost due to conduction through membrane material. The expression for thermal efficiency is given in eq. 3.51 in chapter three. For convenience, it is provided below:

$$\eta(\%) = \frac{J_w H_w}{J_w H_w + \frac{(T_{mf} - T_{cd})}{\frac{\delta}{K_m} + \frac{b}{K_g}}} \times 100\% \qquad (3.51)$$

Where J_w is the mass flux, H_w is the heat of vapourisation associated with mass transfer, δ is the thickness of the membrane, $K_m$is the effective thermal conductivity of the membrane material and the gas filling it, K_g is the thermal conductivity of the gas filling the membrane pores and the air gap, T_{mf} is the temperature at the feed membrane surface and T_{cd} is the temperature at the condensate surface.

Reducing the temperature polarization effect and internal heat loss by conduction through the membrane as well as external heat loss to the environment leads to higher thermal efficiency. Presented in figure 5.31 is the variation of thermal efficiency with feed temperature ranging from 40 to 80^0C. The coolant temperature was kept at 20^0C, while the feed flow rate is 3L/min, and the coolant flow rate at 3L/min. The air gap thickness is 3mm. According to figure 5.31, the system thermal efficiency increases with increasing feed temperature. Thermal efficiency is low at lower feed temperature, but becomes significantly higher at higher feed temperature. This is because at higher feed temperature, conduction heat loss becomes minimal, which results in higher thermal efficiency and of course higher transmembrane permeate flux. The thermal efficiency increases from 96.81% to 99.14% when the feed temperature increases from 40 to 80^0C. This represents about 3% increment in the efficiency.

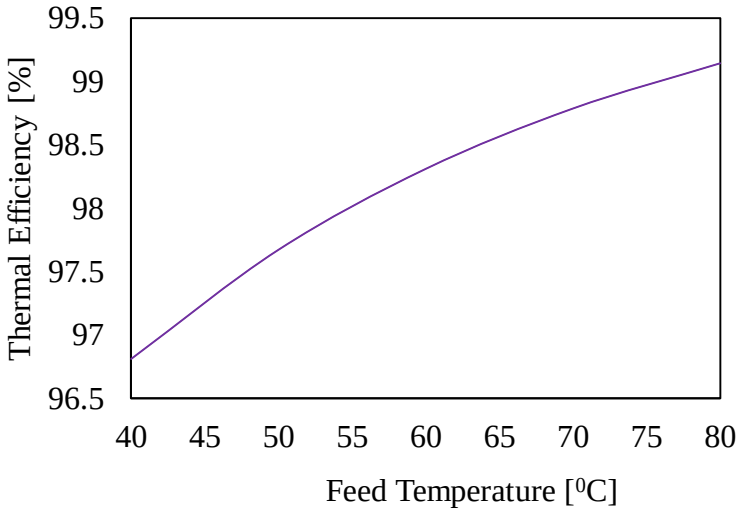

Figure 5.31 Thermal Efficiency at different feed temperature

Conditions: coolant temperature of 20^{0}C, Feed flow rate of 3 L/min, Coolant flow rate of 3 L/min and Air gap thickness of 3mm.

The system thermal efficiency was also investigated at different coolant temperature ranging from 15 to 30^{0}C. The operating conditions are feed temperature of 70^{0}C, feed flow rate of 3L/min, coolant flow rate of 3L/min and air gap width of 3mm. The obtained results are depicted in figure 5.32. Careful observation shows that the thermal efficiency tends to increase with increasing coolant temperature. The reason may be attributed to the fact that at higher coolant temperature, transmembrane temperature difference becomes less, leading to the reduction in heat lost by conduction, thereby increment in thermal efficiency. Increasing the coolant temperature from 15 to 30^{0}C leads to about 0.5% percentage rise in thermal efficiency. Thus the effect of coolant temperature on thermal efficiency is minimal compared to feed temperature effect on thermal efficiency which is about 3%.

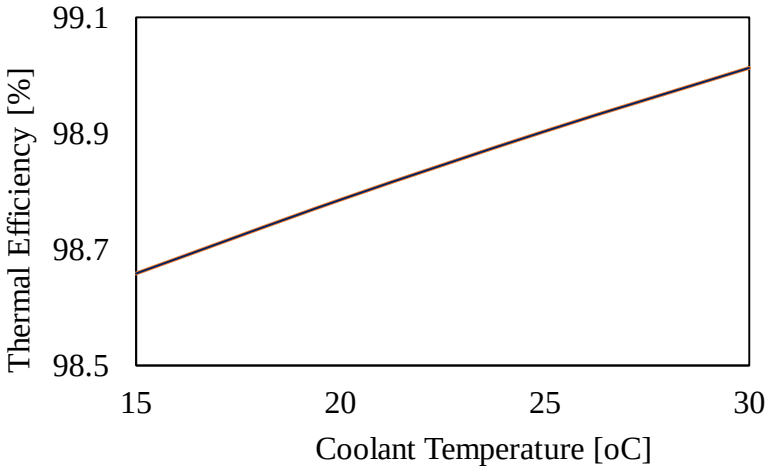

Figure 5.32 Thermal Efficiency at different Coolant temperature

Conditions: Feed temperature of 70^0C, Feed flow rate of 3 L/min, Coolant flow rate of 3 L/min and Air gap thickness of 3mm**.**

Presented in figure 5.33 is the variation of thermal efficiency with feed flow rate ranging from 1 to 5L/min. The coolant temperature was kept at 20^0C, while the feed temperature was kept at 70^0C, and the coolant flow rate at 3L/min. The air gap thickness is 3mm. The thermal efficiency increases with the increase in feed flow rate. The increase in thermal efficiency may be attributed to the fact that the temperature and concentration polarization effect become less at higher feed flow rate resulting in higher permeates flux. Although, the conduction heat loss may become high as well, but the efficiency still increases because of significant increase in flux. Increasing the feed flow rate from 1 to 5L/min leads to the increment in thermal efficiency from 98.76% to 98.8% which represent about 0.04% increment in the efficiency.

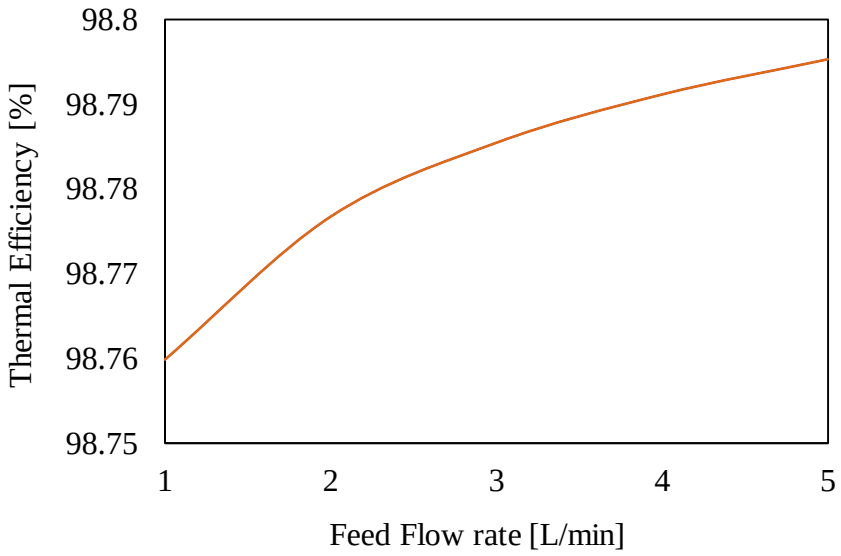

Figure 5.33 Thermal Efficiency at different feed flow rate

Conditions: Feed temperature of 70 0C, coolant temperature of 20 0C, Coolant flow rate of 3 L/min and Air gap thickness of 3mm.

The system thermal efficiency was investigated at different coolant flow rate ranging from 1 to 3.5L/min. The operating conditions are feed temperature of 70^0C, coolant temperature of 20^0C, feed flow rate of 3L/min, and air gap width of 3mm. The obtained results are depicted in figure 5.34. Increasing coolant flow rate is observed to have minimal impact on the thermal efficiency of the system. This is expected since the same operating parameter has marginal effect on permeate flux. Increasing the coolant flow from 1 to 3.5L/min marginally increases the thermal efficiency from 98.785% to 98.788%, representing about 0.003% increment in the efficiency.

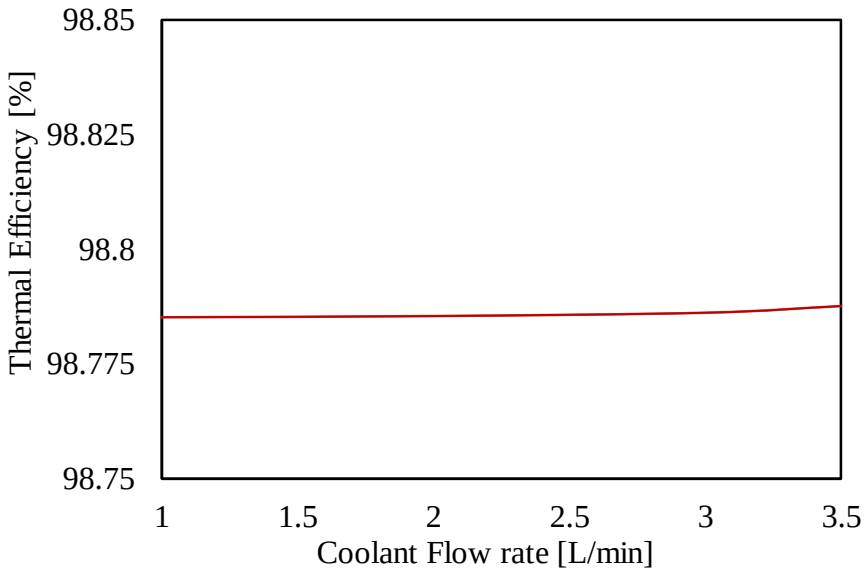

Figure 5.34 Thermal Efficiency at different Coolant flow rate

Conditions: Feed temperature of 70 0C, coolant temperature of 20 0C, Feed flow rate of 3 L/min and Air gap thickness of 3mm.

In conclusion, the system operating parameters that has the most significant effect on thermal efficiency is the feed temperature with about 45.80% increment in thermal efficiency when the feed temperature increases from 40 to 80^0C. Coolant temperature appeared to be another operation parameter that slightly impacts the system thermal efficiency. The effect of coolant and feed flow rate appears to be marginal. The maximum and the minimum recorded thermal efficiency are 99.14% and 96.81% corresponding to feed temperature of 80^0C and 40^0C respectively. Thermal efficiency appears to be influenced at higher feed temperature; therefore, it is advisable to operate the system at high feed temperature. It is worth mentioning that the thermal efficiency of AGMD system is expected to be higher than that of DCMD since the heat lost by conduction through the membrane is higher than any other MD configuration.

5.10 Temperature Polarization Coefficient

Temperature polarization is the ratio of differences in temperature between the liquid-vapour interface and the bulk temperature. θ represents the fraction of total driving force that contribute to the membrane driving force [23]. The expression for calculating temperature polarization is given in eq. 3.46. For the sake of convenient, it is repeated below:

$$\theta = \frac{T_{mf} - T_{cd}}{T_f - T_c} \tag{3.46}$$

The value of temperature polarization is expected to be one for an ideal case. However, θ is always less than one because the bulk temperatures are always greater than the difference in temperature between the interfaces of liquid-vapour. The value of temperature polarization coefficient is used to indicate if MD module is properly designed or awfully designed. MD module is poorly design if θ is less than 0.2, but MD module is considered to be well designed if θ is more than 0.6.

Figure 5.35 displayed the effect of increasing feed temperature on temperature polarization coefficient. The feed temperature was varied from 40 to 80^0C and the coolant temperature was kept at 20^0C, while the feed flow rate is 3L/min, and the coolant flow rate is 3L/min. The air gap thickness is 3mm. It can be observed that temperature polarization coefficient decrease with increasing feed temperature. This is because the higher fluxes produced by the higher vapour pressure difference result in an increase in the effective membrane heat transfer coefficient. The value of the temperature polarization coefficient decreased by about 1% only when feed temperature increased from 40^0C to 80^0C.

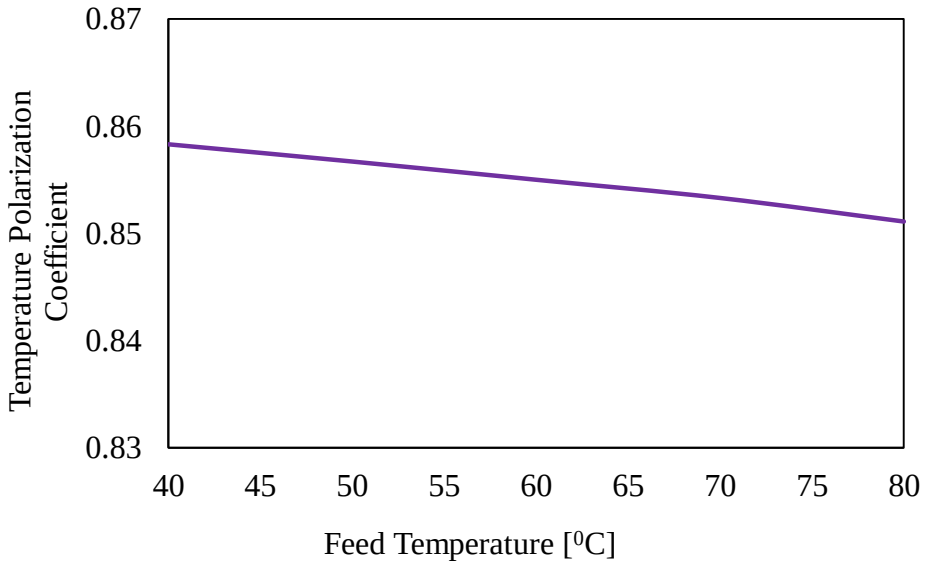

Figure 5.35 Temperature polarization coefficient at different feed temperature

Conditions: coolant temperature of 200C, Feed flow rate of 3 L/min, Coolant flow rate of 3 L/min and Air gap thickness of 3mm.

The effect of coolant temperature on temperature polarization coefficient at different coolant temperature ranging from 15 to 30^{0}C is investigated. The modelling conditions are feed temperature of 70^{0}C, feed flow rate of 3L/min, coolant flow rate of 3L/min and air gap width of 3mm. The obtained results are presented in figure 5.36. The temperature polarization coefficient tends to decrease with increasing coolant temperature. This effect is due to reduction in transmembrane vapour pressure. However, the rate of reduction in temperature polarization coefficient is small when compared to the effect of feed temperature on temperature polarization. Increasing the coolant temperature from 15^{0}C to 30^{0}C would only lead to about 0.33% percentage drop in temperature polarization coefficient.

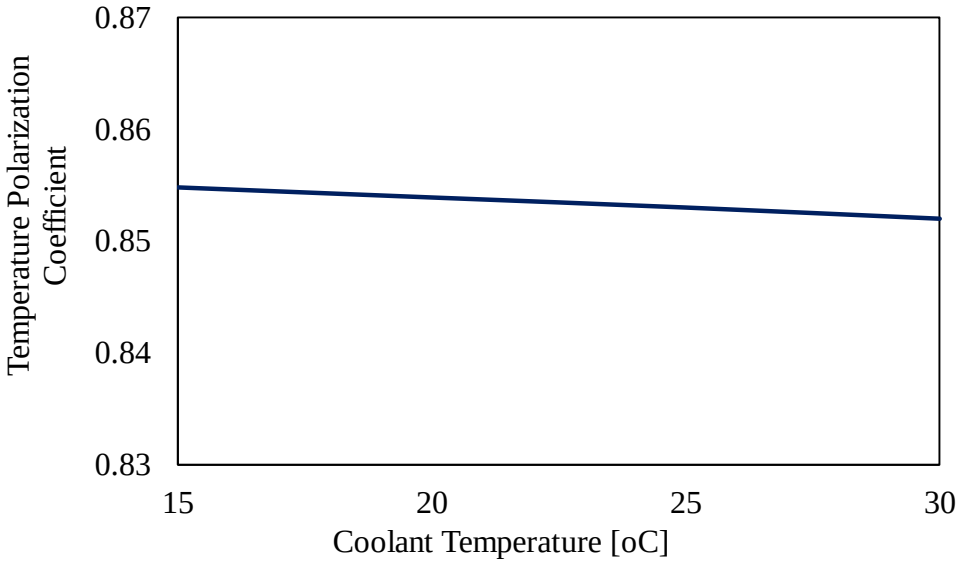

Figure 5.36 Temperature polarization coefficient at different Coolant temperature

Conditions: Feed temperature of 700C, Feed flow rate of 3 L/min, Coolant flow rate of 3 L/min and Air gap thickness of 3mm.

Presented in figure 5.37 is the variation of temperature polarization coefficient with feed flow rate ranging from 1 to 5L/min. The coolant temperature was kept at 20^0C, while the feed temperature was kept at 70^0C, and the coolant flow rate at 3L/min. The air gap thickness is 3mm. It can be noticed that the temperature polarization coefficient increases with increasing feed flow rate. The percentage increment in temperature polarization coefficient is about 10% when feed flow rate increases from 1 to 5L/min. The rise in temperature polarization coefficient may attributed to the fact that increasing feed flow rate means increasing flow turbulence level in feed channels which results in better mixing of feed solution thereby decreasing feed boundary layer resistance. As a result, the heat transfer coefficient of the feed boundary layer is improved. This leads to increment in the feed average temperature in the feed channels, resulting in the observed rise in temperature polarization coefficient.

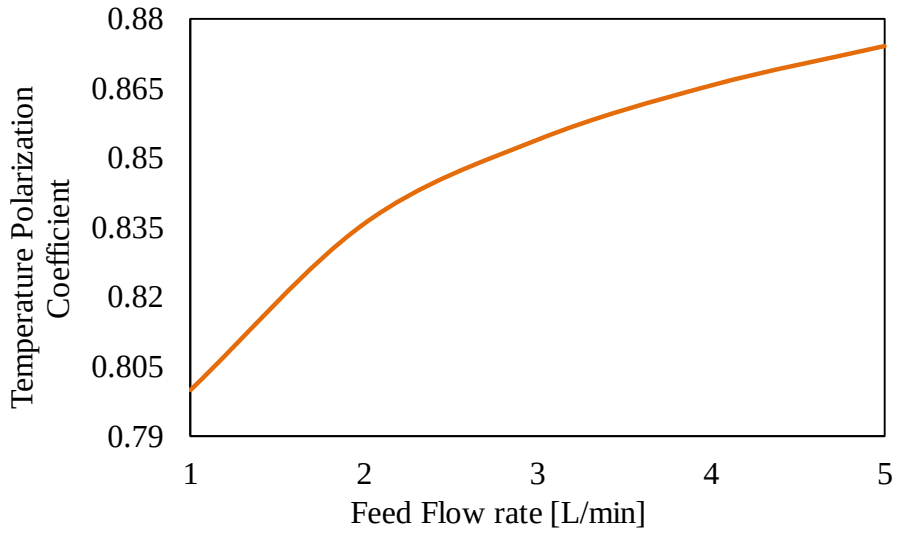

Figure 5.37 Temperature polarization coefficient at different feed flow rate

Conditions: Feed temperature of 70 0C, coolant temperature of 20 0C, Coolant flow rate of 3 L/min and Air gap thickness of 3mm.

The influence of coolant flow rate on temperature polarization coefficient was investigated. The coolant flow rate ranges from 1 to 3.5L/min. The modelling conditions are feed temperature of 70^0C, coolant temperature of 20^0C, feed flow rate of 3L/min, and air gap width of 3mm. The achieve results are presented in figure 5.38. It can be noticed that increasing the coolant flow rate led to negligible rise in temperature polarization coefficient. The reason for the little rise in temperature polarization coefficient is the the increment in the development of convective heat transfer coefficient and reduction in thermal boundary layer thickness. The percentage increment in temperature polarization coefficient recorded when the coolant flow rate increases from 1 to 3.5L/min is about 0.33%. This is considered low when compared to the effect of feed flow rate. In general, temperature polarization coefficient is better influenced by feed flow rate when compared to any other operating condition. The effect of feed temperature is next to the feed flow rate. Both effect of coolant temperature and coolant flow rate seem to be negligible.

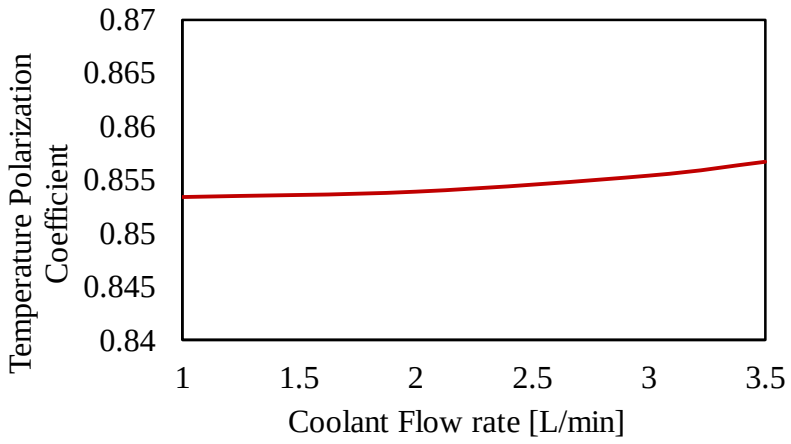

Figure 5.38 Temperature polarization coefficient at different Coolant flow rate

Conditions: Feed temperature of 70 0C, coolant temperature of 20 0C, feed flow rate of 3 L/min, and Air gap thickness of 3mm.

5.11 Gain Output Ratio

The influence of increasing feed temperature on gain output ratio is presented in figure 5.39. It can be observed that the gain output ratio increase with increasing feed temperature. The reason for this increment in gain output ratio when we increase the feed temperature may be due to the fact that decreasing the feed temperature indicates less energy consumption in the water heater. As the feed temperature increases, the partial pressure difference increases leading to higher mass flux that increases GOR. Although the calculated gain output ratio seems to be very small when compared to already establish thermal desalination system like Humidification dehumidification desalination (HDH) system. However, with the incorporation of heat recovery system in MD system, the gain output ratio is expected to increase significantly. Therefore, researchers are recommended to pay more attention to the integration of heat recovery system with MD system.

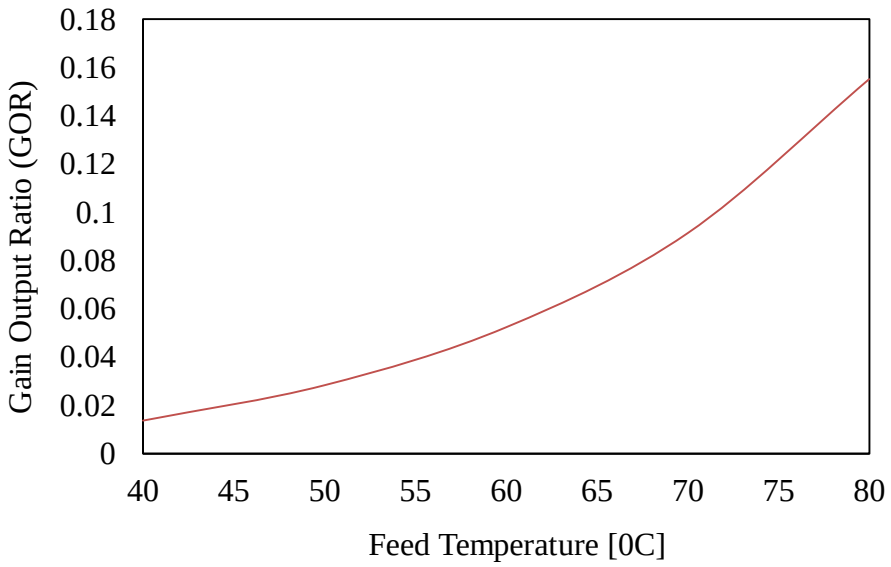

Figure 5.39 Gain output ratio at different feed temperature

Conditions: Coolant temperature of 20 0C, coolant flow rate of 3 L/min, feed flow rate of 1 L/min, and Air gap thickness of 3mm.

CHAPTER 6

OPTIMIZATION OF AGMD PERFORMANCE

In order to optimize the system performance and determine optimum variable combination that will yield the maximum system production, statistical design of experiment was employed. Design of Experiments (DOE) is a powerful statistical tool for process design and products formulation. It can be used to quantitatively identify the right input parameter to produce a high quality product or to enhance process performance. It has been successfully applied in the parametric study of AGMD.

Khayet et al. [86] applied response surface methodology to study the effect of feed temperature, coolant flow rate, feed flow rate and feed concentration in direct contact membrane distillation (DCMD). There was a good agreement between the developed model and the experimental results. Also, an algorithm was developed by exploring response surface in the valid region of operating condition using the gradient method to determine the optimal points in the region of experimentation for different membrane sheets. Optimum conditions were found to dependent on the membrane material, type and properties. Similar study has been carried out by [62, 63, 64].

In this study, experiments were conducted using air gap membrane distillation unit to determine the maximum system performance at different variables combinations. Taguchi methodology was employed to ascertain the influence of operating parameters and the optimum variables combination that will yield the maximum flux output. Feed

temperature, feed flow rate, coolant temperature, coolant flow rate and the air gap width are the considered factors.

6.1 Taguchi Techniques

Taguchi method is a structured and robust design approach for determining best combination of factors to yield product. It is used to investigate how different parameters affect the mean and variance of a system performance. The most important stage in design of experiment lies in the selection of control factors. So, many factors are included at the initial stage, while non-significant factors are identified and eliminated at this earlier stage of experimental design [87]. The DOE using Taguchi technique can economically satisfy the needs of problem solving and system design optimization, as it allows fewer experimental runs usually leading to significant reduction in time and resources requirement for experimentation. The objective of robust design is to improve product quality by minimizing the effects of variation without eliminating causes which are either too difficult or too expensive to control. The end result is a design that has minimum sensitivity to variations in uncontrollable factors. Taguchi main Philosophy are; quality should be designed into product and not inspected out of it, quality is best achieved by minimizing the deviation from the target, and the cost of quality should be measured as a function of deviation from the target system.

While Traditional Design of Experiments focuses on how different design factors affect mean results, Taguchi's DOE put emphasis on variation rather than the mean. Additionally, the former treats noise as an extraneous factor, while the latter considers it

as a central point of its analysis. Taguchi employs signal-to-noise (S/N) ratios as response variables which makes a tradeoff between setting the mean to desirable level while keeping the variance low. The S/N ratio which is always maximized in Taguchi methodology, is described under different scenario as 'Smaller is Better', 'Target is Best' and 'Larger is Better.' For Larger-is-Better situation, S/N ratio may be estimated from;

$$SN = -10log_{10}\left[\sum_i \left(\frac{1}{y_i{}^2}\right)^2 \frac{1}{n}\right] \quad (6.1)$$

Where y_i is the response at each observation and n is the number of observation.

The three levels of parameters combination is tabulated in table 6.1. Based on design of experiment, Taguchi L_{27} (3^5) orthogonal design matrix for the system optimization is tabulated in table 6.2. The table shows how each system operating parameters are combined to achieve the system performance. The used membrane material is PTFE 0.45 µm pore size.

Table 6.1 Operating parameters and their level

Factors	level 1	level 2	level 3
Feed Temperature (Tf) [^{0}C]	60	70	80
Coolant Temperature (Tc) [^{0}C]	20	25	30
Feed Flow rate (Qf) [L/min]	1	3	5
Coolant Flow rate (Qc) [L/min]	1	2	3
Air Gap Width [mm]	3	5	7

The total dissolve solute (TDS) of feed solution is 4.06 g/L. The TDS and the electric conductivity of the feed saline water and the permeate flux was measured using Omega CDH-287 conductivity meter. The solute rejection factor (R_f) or solute percentage removal may be estimated from [15, 44, 86, 87, 88, 89];

$$R_f = \left(\frac{C_f - C_p}{C_f}\right) \times 100\% \quad (6.2)$$

Where C_f and C_p are the solute concentration in the feed and in the permeate solutions respectively.

Table 6.2 Taguchi L_{27} (3^5) orthogonal design matrix for the current AGMD system

Exp. Run	Feed Temperature [^{0}C]	Coolant Temperature [^{0}C]	Feed Flow rate [L/min]	Coolant Flow rate [L/min]	Air Gap [mm]
1	60	20	1	1	3
2	60	20	1	1	5
3	60	20	1	1	7
4	60	25	3	2	3
5	60	25	3	2	5
6	60	25	3	2	7
7	60	30	5	3	3
8	60	30	5	3	5
9	60	30	5	3	7
10	70	20	3	3	3
11	70	20	3	3	5
12	70	20	3	3	7
13	70	25	5	1	3
14	70	25	5	1	5
15	70	25	5	1	7
16	70	30	1	2	3
17	70	30	1	2	5
18	70	30	1	2	7
19	80	20	5	2	3
20	80	20	5	2	5
21	80	20	5	2	7
22	80	25	1	3	3
23	80	25	1	3	5
24	80	25	1	3	7
25	80	30	3	1	3
26	80	30	3	1	5
27	80	30	3	1	7

6.2 Optimization Calculations

For performance optimization and results analysis, MINITAB 16 software was employed to design and analysed the experimental data. In total, twenty seven experimental runs were conducted with each experiment having four replicates. The Taguchi L_{27} (3^5) orthogonal arrays for the three level combination as well as the mean values of permeate flux and the signal to noise ratio are presented in table 6.3.

The main effect plots are as depicted in fig. 6.1 and fig. 6.2 which is based on average values of each experimental run. The plot is effectively used to investigate the trends and influence of each operating factor. It is obvious from fig. 6.1 that the flux production increases with increase in the feed temperature. This is due to exponential relationship between temperature and water vapour pressure [15 58, 70, 85]. The mean permeate flux also increases with increasing feed flow rate. This may be attributed to the high turbulent generated in the feed channel because of higher mixing effect. The rise in flux may also be due to increase in heat transfer coefficient in boundary layer at the feed side of membrane, leading to reduction in temperature polarization effect. It is observed that the air gap width influenced the distillate production due to mass transfer resistance in the air gap. The permeate flux is noticed to decreases with increasing air gap thickness. This is as a result of rise in temperature gradient within the vapour compartment due to reduction in resistance to mass transfer. Drops in permeate flux was observed when coolant temperature rises. The reduction in flux is caused by the decrease in driving temperature difference between the feed side and condensation surface. The mean coolant flow rate on permeate flux is obviously of no effect.

Table 6.3 Taguchi L_{27} (3^5) orthogonal design matrix and the responses

Run	Feed Temp. [^{0}C]	Coolant Temp. [^{0}C]	Feed Flow rate [L/min]	Coolant Flow rate [L/min]	Air Gap [mm]	Flux 1st Trial [kg/m^{2}h]	Flux 2nd Trial [kg/m^{2}h]	Flux 3rd Trial [kg/m^{2}h]	Flux 4th Trial [kg/m^{2}h]	Flux Average [kg/m^{2}h]	S/N Ratio [dB]
1	60	20	1	1	3	24.958	25.2013	25.1034	25.2216	25.1211	28.0005
2	60	20	1	1	5	16.2465	15.8264	16.1243	15.9987	16.049	24.1077
3	60	20	1	1	7	11.96542	12.0168	11.8973	12.1354	12.0037	21.5856
4	60	25	3	2	3	26.6991	26.82912	26.6608	26.3986	26.6469	28.5125
5	60	25	3	2	5	16.6029	16.74313	16.5296	16.6025	16.6195	24.4121
6	60	25	3	2	7	12.0269	12.16851	12.3019	11.9923	12.1224	21.6704
7	60	30	5	3	3	26.6069	26.7586	26.7026	26.77	26.7095	28.5332
8	60	30	5	3	5	16.6066	16.69917	16.5536	16.7112	16.6426	24.4242
9	60	30	5	3	7	11.8912	12.13658	12.0032	12.6631	12.1735	21.7008
10	70	20	3	3	3	52.9632	53.1124	52.8988	53.2101	53.0461	34.493
11	70	20	3	3	5	34.7985	35.056	34.986	35.124	34.9911	30.879
12	70	20	3	3	7	27.6654	27.912	28.0168	27.9513	27.8864	28.9075
13	70	25	5	1	3	58.654	58.1234	58.0134	58.2401	58.2577	35.3068
14	70	25	5	1	5	35.1245	35.1112	34.987	35.216	35.1097	30.9085
15	70	25	5	1	7	24.0012	23.3426	23.0164	23.224	23.3961	27.3797
16	70	30	1	2	3	37.9035	37.80776	37.5623	37.7893	37.7657	31.5418
17	70	30	1	2	5	23.6982	23.59387	23.463	23.5879	23.5857	27.4528
18	70	30	1	2	7	17.1106	17.14722	17.224	17.2645	17.1866	24.7036
19	80	20	5	2	3	76.526	75.89	75.512	76.255	76.0457	37.6212
20	80	20	5	2	5	48.9921	49.0135	48.9016	49.2103	49.0294	33.8091
21	80	20	5	2	7	36.0152	35.9984	36.1235	36.215	36.088	31.1472
22	80	25	1	3	3	61.5689	61.60195	61.4893	61.6687	61.5822	35.7891
23	80	25	1	3	5	38.4698	38.44252	38.1098	38.6489	38.4178	31.6903
24	80	25	1	3	7	27.895	27.9387	30.21501	27.5498	28.3996	29.0491
25	80	30	3	1	3	64.2584	64.2256	64.0246	64.2154	64.181	36.1481
26	80	30	3	1	5	38.2981	38.154	38.8965	38.5549	38.4759	31.7031
27	80	30	3	1	7	27.2654	27.3652	27.0215	27.2216	27.2184	28.697

Noise factors are uncontrollable in nature. The main purpose of noise factors is to cause performance of a system to deviate from its target value. The present of noise is expected since each experiment was repeated four times under the same conditions. The ratio of signal factors (product quality) to the noise factors (S/N ratio) should be maximized in the system because higher S/N ratio indicates better product quality. The mean S/N ratio

response for each experimental run is presented in fig. 6.2. While it increases rapidly with feed temperature, it only does so slightly with feed flow rate. With increased coolant temperature and air gap width, the noise ratio however decreases. Coolant flow rate show no effect on signal-to-noise ratio. It is obvious that the feed temperature and the air gap width have the most significant and considerable impact on the distillate production in comparison to other operating parameters.

6.3 ANOVA

The experimental data were subjected to statistical scrutiny via analysis of variance (ANOVA). ANOVA was performed to determine the significant effect of each operating parameters. The analysis was conducted at 95% confidence level (level of significant α = 0.05). The Results presented in table 6.4 shows that feed temperature and air gap width each has P-value of 0.000, coolant temperature has P-value of 0.035 and feed flow rate has P-value of 0.019. The P-value of the four controllable factors indicate that the four factors are statistically significant at confidence level of α = 0.05. As such, we reject null hypothesis and accept alternative hypothesis. However, ANOVA result also shows that coolant flow rate with P-value of 0.972 is insignificant on the system performance at 95% confident level since its P-value is greater than the target confident level. In that case, null hypothesis is accepted, while rejecting alternative hypothesis.

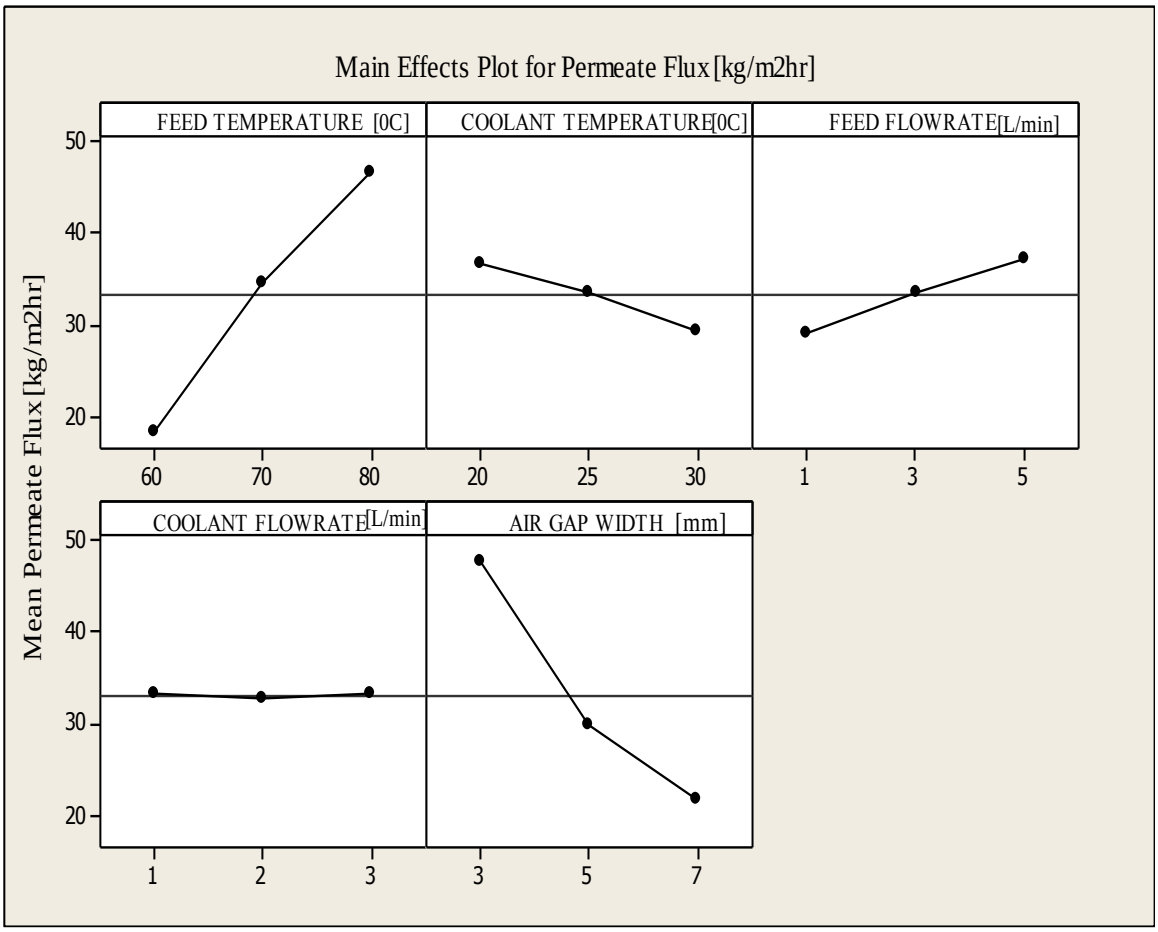

Figure 6.1 AGMD Main effect plot for mean permeate flux

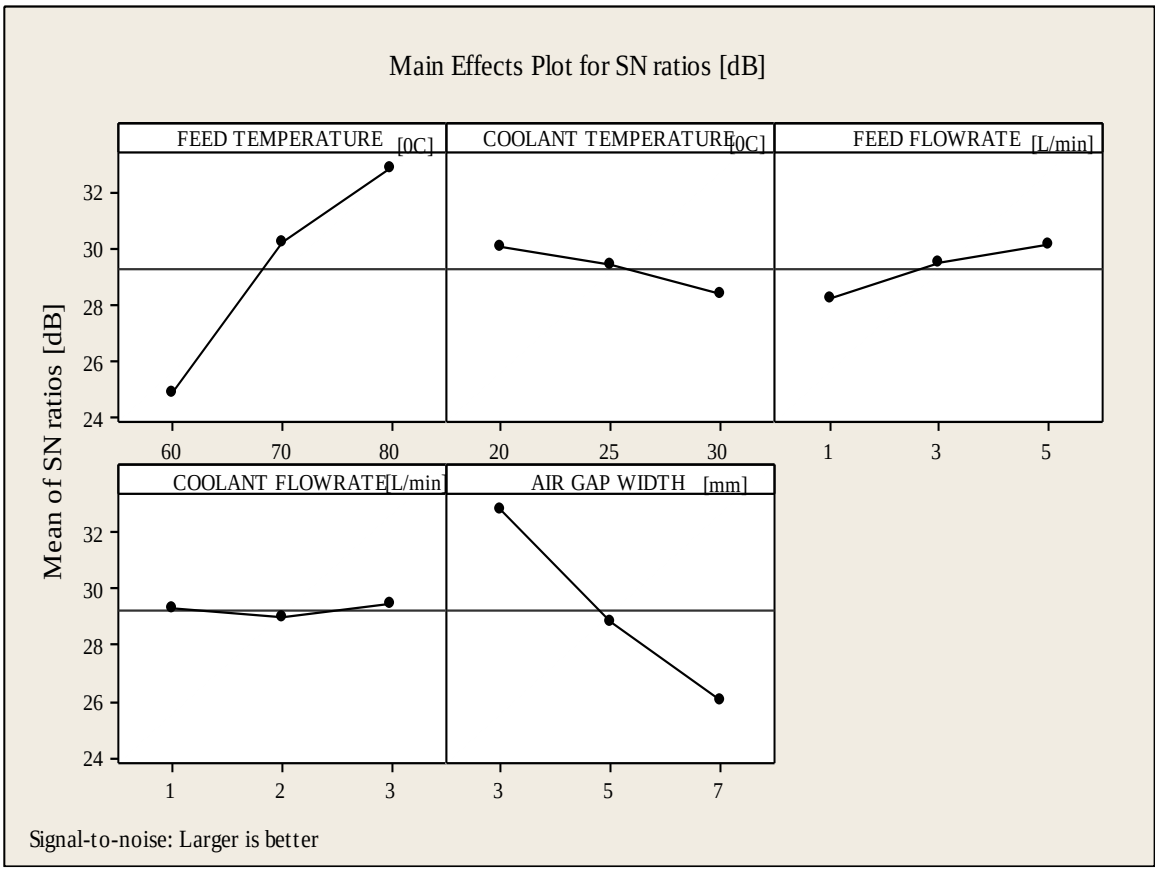

Figure 6.2 AGMD Main effect plot for mean signal to noise ratio

Table 6.4 Analysis of variance for responses, using adjusted SS for tests

Source	DF	Seq SS	Adj SS	Adj MS	F	P
Feed Temperature	2	3650.47	3650.47	1825.24	61.91	0.000
Coolant Temperature	2	245.25	245.25	122.62	4.16	0.035
Feed Flow rate	2	300.26	300.26	150.13	5.09	0.019
Coolant Flow rate	2	1.66	1.66	0.83	0.03	0.972
Air Gap Width	2	3156.36	3156.36	1578.18	53.53	0.000
Residual Error	16	471.71	471.71	29.48		
Total	26	7825.71				

S = 5.430 R-Sq = 94.0% R-Sq(adj) = 90.2%

6.4 Regression Modelling

In model generation, permeate flux was modeled as dependent variable while the feed temperature, coolant temperature feed flow rate and air gap width as independent variables. Since analysis of variance results indicates that the contribution of coolant flow rate to the flux production is insignificant, the factor is therefore ignored in the regression model generation.

Prior to model generation, the actual response surface was plotted in order to have the general idea of the suitable variables function that will enable the smooth fitting of the model to the actual response surface. Following which potential suitable models were generated, first, with feed temperature, coolant temperature feed flow rate and air gap width as variables. Thereafter, all other possible suitable combinations were generated, including quadratic terms depending on the shape of the actual response plane. Comparisons were then made and the best model to represent the property change was selected based on the adjusted correlation coefficient value (R^2 (adj)) and standard error of estimate (S) of each generated model.

Best subsets regression approach was adopted during model generation. In this approach, all possible regression equations were estimated using all possible combinations of independent variables. The best fit of the model was selected based on the highest adjusted R-square and lowest standard error estimate (S). Based on the above criteria, the best regression model for calculating flux is given by:

$$\hat{Y} = -197.79 + 5.86113\,A - 0.736906\,B + 2.03725\,C + 1.1218\,D - 0.0216244\,A^2 + 1.22207\,D^2 - 0.283021\,A*D \quad (6.3)$$

Where $\hat{Y}$ is the calculated permeate flux [kg/m^{2}h], A is the Feed temperature [^{o}C], B is the Coolant Temperature [^{o}C], C is the Feed flow rate [L/min] and D is the Air Gap Width [mm].

Table 6.5 Analysis of variance

Source	DF	Seq SS	Adj SS	Adj MS	F	P
Regression	7	7734.50	7734.50	1104.93	230.175	0.000000
A	1	3622.42	103.34	103.34	21.527	0.000179
B	1	244.36	244.36	244.36	50.905	0.000001
C	1	298.83	298.83	298.83	62.251	0.000000
D	1	3012.98	0.61	0.61	0.126	0.726263
A2	1	28.06	28.06	28.06	5.845	0.025841
D2	1	143.37	143.37	143.37	9.867	0.000028
A*D	1	384.48	384.48	384.48	80.094	0.000000
Error	19	91.21	91.21	4.80		
Total	26	7825.71				

S = 2.19098 R-Sq = 98.83% R-Sq(adj) = 98.41%

Fig. 6.3 displays normality plots of residuals. It was observed that the experimental data either passes through the mean line (fitted line) or clusters around it. This is an indication that neither normality assumption was violated nor any evidence pointing to the possible outliers. As such, we conclude that normal distribution is an approximate model for the system performance. Thus, the mean data generated is normally distributed along the fitted line. Fig. 6.4 depicts the residuals against fitted values. The tendency to have runs of positive and negative residuals indicates positive correlation which validates independence assumption. It is obvious that no recognized pattern exist in the figure which implies that constant variance assumption hold.

According to regression ANOVA (Table 6.5), the regression model is highly significant with P-Value of 0.000. However, the variable D in the ANOVA has p-value of 0.726263 which is not significant at 95% confidence level. This is due to problem of collinearity

which exist as a result of two highly correlated independent variables (see variable A*D). The generated model has R-Square of 98.83%, meaning that 98.83% of variation in permeate flux is captured by variation in feed temperature, coolant temperature and feed flow rate. With adjusted R-Sq of 998.41%, it signifies that 98.41% of variation in permeate flux is explained by variation in feed temperature, coolant temperature, feed flow rate, and air gap thickness taking into account the experimental data size and number of independent variables.

The model also has a standard error estimate (S) of 2.19098. S is the measure of variation of observed permeate flux (J) from the regression line. It is worth noting that the magnitude of S is judged based on the relative size of the system performance values in the experimental data. The general conclusion is that; the lower the S value, the better the generated model.

Analysing the terms in the regression equation (see Eq. 6.3), the highest positive main effect on the flux is contributed by feed inlet temperature (variable A). Though, the variable has negative quadratic term (A^2). Comparing the coefficient of both terms, it is obvious that the positive linear term highly overrun the negative quadratic term. Hence increasing this term (A) led to considerable increases in permeates flux. The maximum negative main effect is attributed to the cooing inlet temperature (variable B), meaning that increasing this term will result in drops in the distillate production. The other term which highly influences the flux is the air gap width (variable D). The variable is positive both in linear and quadratic form. However, its interaction with variable (A) led to a negative coefficient. Feed flow rate (variables C) also has positive main effect on

distillate production which is an indication that increasing this term will give rise to system performance.

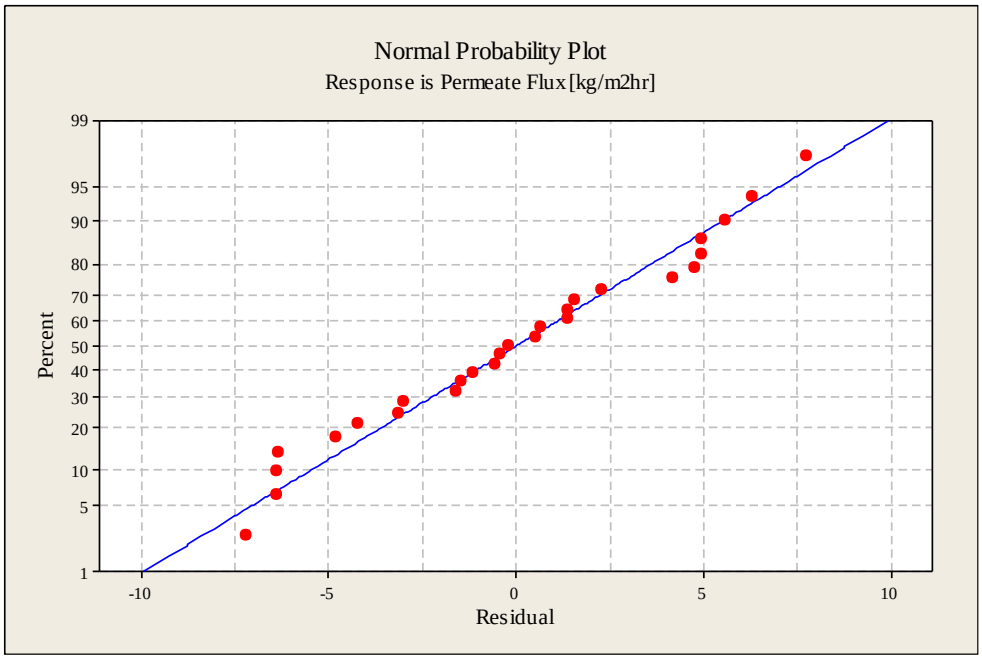

Figure 6.3 Normal probability plot

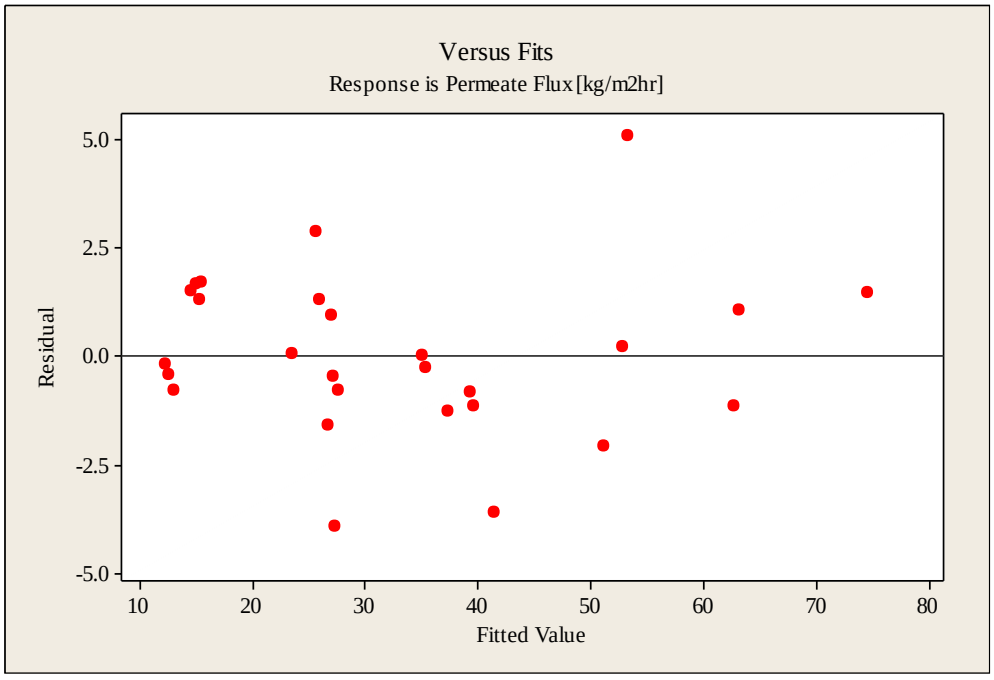

Figure 6.4 Residuals vs fits plot

6.5 Model Solutions and System Optimization

The regression model is used to calculate the flux for all the input conditions considered. The calculated values ($\hat{Y}$) together with the experimental results are tabulated in table 6.6. Comparison shows that the calculated values are in good agreement with experimental data since the model result is within 11% of the experimental data. This is an indication that the developed model is capable of calculating permeate flux. Hence, based on statistical analysis, the developed model is considered suitable for calculating AGMD system. The main aim of parameter optimization is to find a set of combined parameters that will yield optimal permeate flux. It is observed from table 6.6 that the maximum permeate flux was obtained at the nineteenth experimental run. Based on the fact that process output from Taguchi technique may not be optimal, but may only improve system output when implemented [90], MATLAB code was developed to obtain the optimum variables combination that will give the maximum distillate production.

The developed MATLAB code works in a similar way as Monte Carlo simulation work. Monte Carlo simulation evaluates a function over a factor spacing selecting the evaluated points at random. In this approach, the maximum and minimum settings of each phase shifter are used as boundaries of the initial search volume. A random number generator was used to produce random configurations and the best fraction of the resulting system performance values is selected [91].

Table 6.6 Calculated permeate flux and experimental flux with salt rejection factor

Run	Feed Temp. [^{0}C]	Coolant Temp. [^{0}C]	Feed Flow rate [L/min]	Coolant Flow rate [L/min]	Air Gap [mm]	Responses			
						Exp. Average Flux [kg/m^{2}h]	Calc. Average Flux [kg/m^{2}h] (Eq. 6.3)	Percentage difference between Exp. & Calc. [%]	Rejection Factor [%]
1	60	20	1	1	3	25.1211	26.74934	6.48166	99.986
2	60	20	1	1	5	16.049	14.58354	9.13101	99.983
3	60	20	1	1	7	12.0037	12.1943	1.58758	99.987
4	60	25	3	2	3	26.6469	27.13931	1.84789	99.978
5	60	25	3	2	5	16.6195	14.97351	9.90414	99.979
6	60	25	3	2	7	12.1224	12.58427	3.81002	99.978
7	60	30	5	3	3	26.7095	27.52928	3.06914	99.969
8	60	30	5	3	5	16.6426	15.36348	7.68604	99.975
9	60	30	5	3	7	12.1735	12.97424	6.57754	99.972
10	70	20	3	3	3	53.0461	52.83279	0.40216	99.968
11	70	20	3	3	5	34.9911	35.00657	0.04413	99.975
12	70	20	3	3	7	27.8864	26.95691	3.33304	99.977
13	70	25	5	1	3	58.2577	53.22276	8.64257	99.963
14	70	25	5	1	5	35.1097	35.39654	0.81705	99.967
15	70	25	5	1	7	23.3961	27.34688	8.64257	99.961
16	70	30	1	2	3	37.7657	41.38923	9.59471	99.980
17	70	30	1	2	5	23.5857	23.56301	0.09637	99.979
18	70	30	1	2	7	17.1866	15.51335	9.73567	99.986
19	80	20	5	2	3	76.0457	74.59136	1.91251	99.962
20	80	20	5	2	5	49.0294	51.10472	4.23286	99.971
21	80	20	5	2	7	36.088	37.39464	3.62063	99.969
22	80	25	1	3	3	61.5822	62.75783	1.90901	99.982
23	80	25	1	3	5	38.4178	39.27119	2.22145	99.984
24	80	25	1	3	7	28.3996	25.56111	9.99491	99.982
25	80	30	3	1	3	64.181	63.1478	1.60982	99.978
26	80	30	3	1	5	38.4759	39.66116	3.08059	99.972
27	80	30	3	1	7	27.2184	25.95108	4.65620	99.975

The simple algorithm for the developed codes is as follow; (a) Generate (about 6250000 point data) a linear space (distribution) of numbers between minimum and maximum values (boundary specifying the valid region). (b) Generate four dimensional arrays using distributions generated in (a). (c) Convert the generated four dimensional arrays to

column vectors. (d) Calculate the objective function (Maximum flux), minimum flux, median flux, skewness, mean flux and standard deviation. (e) Compute the optimal value of the objective function. (f) Select the values of the variables combination for which the objective function is maximum, and display output results.

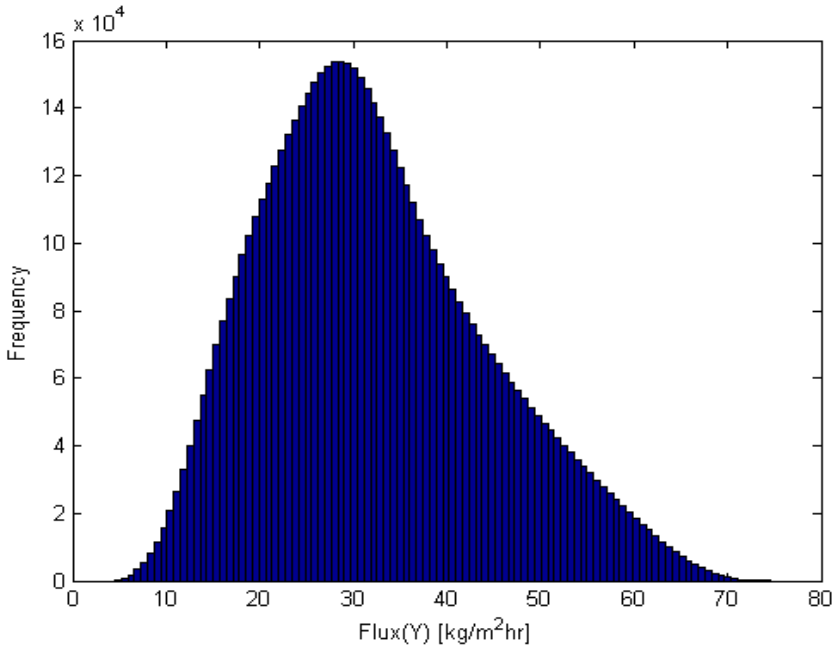

Figure 6.5 Histogram of a 6250000 sample of permeate flux

Based on above procedure, the optimum permeate flux was obtained for a number of random combinations of feed temperature, coolant temperature, feed flow rate and air gap width settings. Fig. 6.5 is a histogram representing the results of 6250000 samples calculation for a number of random combinations of operating parameters. The maximum attainable permeate flux is achieved towards the extreme right end of the plot while the minimum permeate flux can be observed at the left end of the plot. The optimum variable conditions and its corresponding AGMD system performance are summarized in table

6.7. The optimum values of all the operating parameters achieved from the Matlab codes are similar to those obtained from Taguchi results. The good agreement in the results of both approaches confirms Taguchi technique as a system optimization methodology.

Table 6.7 Optimum conditions and optimal flux

Factor	level
Feed Temperature (^oC)	80
Coolant Temperature (^oC)	20
Feed Flow rate (L/min)	5
Air Gap Width (mm)	3
Response	Flux [kg/m^2h]
Calculated Permeate flux ($\hat{Y}$)	74.5916
Experimental Permeate flux (J)	76.0457

The obtained numerical values of minimum flux, median flux, skewness, mean flux and standard deviation from the Matlab solution are 4.5068, 30.7594, 0.4993, 32.2681 and 12.0402 kg/m^2h respectively.

CHAPTER 7

CONCLUSIONS AND RECOMMENDATIONS

7.1 Conclusions

Water desalination using air gap membrane distillation had been investigated. The effect of AGMD operating parameters such as feed inlet temperature, feed flow rate, coolant temperature, coolant flow rate and air gap width on the distillate production had been investigated experimentally. The influence of membrane pore size on permeate flux was also investigated. The impact of feed solution concentration and membrane usage time on permeate flux as well as on salt rejection factor (quality of the permeated liquid) were studied and presented. A parametric study of double stage system at different AGMD operating parameters such as feed inlet temperature, coolant temperature, feed flow rate, coolant flow rate and air gap width have also been investigated. Furthermore, the optimization of the air gap membrane distillation system was investigated experimentally and statistically based on Design of Experiment (DOE) using Taguchi technique. Apart from system optimization which was based on design of experiment, other investigation were conducted in accordance with traditional (convectional) form of experiment.

Theoretical modelling had also been presented and successfully implemented using Matlab and EES codes. The effect of feed temperature, coolant temperature, feed flow rate, coolant flow rate and air gap width on permeate flux was investigated analytically. The role of membrane pore size on permeate flux was also investigated and presented.

The AGMD thermal efficiency as well as temperature polarization coefficient was thoroughly investigated theoretically at different system operating parameters such as feed temperature, feed flow rate, coolant temperature and coolant flow rate.

The following ranges of data were considered during the investigation:

- Feed temperature: 40^0C to 80^0C
- Coolant temperature: 15^0C to 30^0C
- Feed flow rate: 1L/min to 5L/min
- Coolant flow rate: 1L/min to 3.5L/min
- Air gap width: 3mm, 5mm and 7mm.

The used membranes material is polytetrafluoroethylene (PTFE) having two different pore sizes of 0.45 µm and 0.22 µm. The tested feed solutions are distilled water, laboratory prepared salt water solution and row seawater. The tested feed water solutions concentration are: 0.075g/L, 4g/L, 10g/L, 20g/L, 30g/L, 40g/L, 50g/L and 60g/L.

In view of above, the following conclusions can be drawn from the investigation:

- **Effect of operating parameters on flux**

Permeate flux increases with increasing feed temperature and feed flow rate. However, it decreases with increasing air gap width and coolant temperature. Increasing the coolant flow rate tends to marginally increase the system performance. Feed temperature recorded the maximum of 732.05% increment in flux when it was varied from 40^0C to 80^0C. The next operating parameter with a considerable impact on flux after feed temperature is the air gap width claiming a maximum of 131.23% rise in flux when it was decreased from 7mm to 3mm. The average percentage increment in flux for feed flow

rate is 31.97% when the feed flow rate increases from 1 to 5L/min and, while that of coolant temperature is 25.89% when the coolant temperature decreases from 30 to 15^0C. The maximum percentage increment in flux recorded when the coolant flow rate was increased from 1 to 3.5L/min is just 1.72% when. Based on the aforementioned fact, the system performance is essentially dominated by the effect of both feed temperature and air gap width. Feed flow rate and coolant temperature have relative considerable effect on flux. While the effect of coolant flow rate on system performance is marginal or negligible.

- **Effect of membrane pore size**

The PTFE membrane having 0.45µm pore size recorded about 10.97% rise in permeate flux over PTFE 0.22µm pore size membrane when the feed temperature increases from 40 to 80^0C, while about 6.51% was recorded when feed flow rate increases 1 to 5L/min and about 5.98% recorded when the coolant temperature increases from 15 to 30^0C. This is indications that permeate flux increases with membrane pore size. There was no clear difference in the quality of permeate flux produced using the two membrane material. Therefore, the conclusion is flux increases with increasing in membrane pore size.

- **Effect of feed concentration and membrane degradation**

The effect of feed concentration on permeate flux is relatively low when compared to other desalination technology like RO. Increasing the feed solutions concentration from 0.075g/L to 60g/L could lead to an average of about 5% reduction in the measured flux at different feed temperature, and an average of about 6% at different feed flow rate. Thus, AGMD system can be used for desalting seawater without the necessity for pre-treatment. For long time experiment and membrane degradation, it had been observed

that continuous usage of membrane for the period of 38 hour leads to an average reduction of about 9% in flux as a result of membrane fouling and degradation. For the period of 38 hours of membrane continuous usage, the measured salt rejection factor was found to be above 99.94%.

- **Theoretical modelling**

The theoretical model was validated against experimental data. In the case of each operating parameter, good agreement was generally realised as most of the theoretical data are within a maximum of 15% of the experimental data. For the case of membrane pore size, the deviation between the model results and the experimental data are within 4% of the experimental data.

The system thermal efficiency increases significantly with increasing feed temperature because the conduction heat loss becomes minimal at higher feed temperature, higher evaporation rate, and higher vapour pressure, leading to a higher system thermal efficiency. Thermal efficiency also increases with increasing coolant temperature and feed flow rate. However, it remains constant in the case of increasing coolant flow rate. The rise in thermal efficiency as a result of increasing feed flow rate is attributed to improved heat and mass transfer coefficients at higher Reynolds number. The maximum recorded thermal efficiency which is obtained at feed temperature of 80^0C was 99.14%.

The temperature polarization coefficient decreases with increasing feed and coolant temperature. However, it increases with increasing feed and coolant flow rates. The percentage increment in temperature polarization coefficient is 9.62% when feed flow rate was increased from 1L/min to 5L/min. This is attributed to higher turbulence level in

flow that is generated at the feed channels, leading to better mixing of feed solution, thereby decreasing feed boundary layer resistance to heat transfer. As such heat transfer coefficient of the feed boundary layer is improved and increased the feed average temperature in the feed channels, hence the observed rise in temperature polarization coefficient. Generally, the obtained temperature polarization coefficient is within 0.7 to 0.9. This is also an indication that the used module is well designed.

- **Multi-Staging**

The maximum attainable permeate flux from the double stage and single stage system was found to be 128.46kg/m^2hr and 65.81 kg/m^2hr respectively at the feed temperature of 80^0C, coolant temperature of 20^0C, feed flow rate of 3L/min, coolant flow rate of 3L/min, feed solution concentration of 4.06g/L and air gap width of 3mm. In every experimental data, the flux obtained from double stage module almost doubles that of single stage. With the above fact, we concludes that the performance of double stage system double that of single stage system.

- **System optimization**

Taguchi method and applied regression were employed to model and optimized the performance of an AGMD unit for water desalination. Effects of feed temperature, feed flow rate, coolant temperature coolant flow rate and air gap width were investigated. The influence of coolant flow rate was found to be marginal on system flux, so it was not included in regression model generation.

The regression model calculations are in good agreement with the experimental data. The solutions from the regression model for the system flux are within 10% of the

experimental data (table 6.6). Hence, the developed regression model is adequate for the calculation of permeate flux within the range of experimental limit. The optimum system performance from the experiment and the generated model were found to be 76.0457 kg/m^2h and 74.5916 kg/m^2h respectively. The optimum value of the combined operating parameters are 80^oC feed temperature, 5 L/min feed flow rate, air gap width of 3mm and 20^oC coolant temperature. The deviation at the optimum conditions between model calculation and the experimental result is 1.95%.

7.2 Recommendations

The following points are recommended for future work:

- Incorporate power meter to measure the specific and total energy consumption to the system.
- The module and the piping system should be properly insulated to minimized heat loss to the environment.
- Though Plexiglas material used in our module manufacturing prove to be good, but better material that can provide minimal loss to the surrounding and resistance to breakage (cracking) is a welcome development.
- Wider and thinner air gap width should be investigated in order to study and include the effect of natural convection in the theoretical analysis.
- Improve module design in order to investigate the effect of module channel dimensions such as module depth, length, spacers, etc.

- More detailed study on multi-staging module should be done to improved system performance and minimized the input energy consumption by the system
- Used internal heat recovery to enhanced the system thermal efficiency
- MD is an energy intensive technology, so direct use of alternative sources of energy such as solar energy as the primary source of energy is a welcome development.
- Further development of new membrane material specifically for membrane distillation is essential

The implementation of the aforementioned points will help improved the overall performance of the MD system and help in large scale and industrial realization of the membrane distillation applications in water desalination.

APPENDICES

Appendix A: Matlab code for flux prediction

```
clc
close all
cpg = 4182;       %    specific heat capacity in the gas phase
ky = 645e-3;      %    thermal conductivuty of gas phase
kf = 656e-3;      %    feed water thermal conductivity
dhf = 0.011;      %    feed channel hydraulic diameter
rhof = 982.3;     %    feed water density
cpf = 4186;       %    feed water specific heat capacity
Af = 3.96e-4;     %    feed channel area
Lf = 66e-3;       %    feed channel length
kc = 598e-3;      %    cold water thermal conductivity
dhc = 0.011;      %    cold channel hydraulic diameter
rhoc = 999;       %    cold water density
cpc = 4184;       %    cold water specific heat capacity
Lc = 66e-3;       %    cold channel area
Ac = 3.96e-4;     %    cold channel area
g = 9.81;         %    acceleration due to gravity
rhod = 998;       %    density of condensate
miu = 959e-6;     %    viscosity of condensate
kd = 606e-3;      %    thermal conductivity of condensate
Ld = 66e-3;       %    height of the plate
kcd = 109;        %    thermal conductivity of the plate
l = 1.5e-3;       %    thickness of the plate
del = 154e-6;     %    Membrane thickness
r = 0.22e-6;      %    membrane pore radius
E = 0.8;          %    membrane porosity
R = 8.314;        %    gas constant
MW = 0.0180152;   %    molecular weight of water
bp= del*tau +   b; %     air gap width
miuf = 453e-6;    %    feed water viscosity
miuc = 1080e-6;   %    coolant water viscosity
tau = ((2-E)^2)/E; %    membrane tortuosity
% tau = 1/E;
Mg  = 1.065;      %    Salt concentration (g/L)
Mo = Mg/58.44;    %    mole solute concentration
Ds=24e-6;         %    air-water mass diffusivity as standard condition
hy = ky/b;
kgas=0.029;  %  Thermal conductivity of the gas filling the membrane pore
kmater=0.27;      %    thermal conductivity of the membrane material


%    operating parameters
% Tb = 313:2:353;
b = 3e-3;         %    Air gap width
Tb = 343;         %    Feed solution temperature
```

```
Tc = 293;          %    Coolant solution temperature
Qf = 8.33333e-5;   %    Feed solution flow rate
Qc = 5e-5;         %    coolant solution flow rate


% Correlations and model equations start here
n = length(Tb);
Tmf = 320*ones(1,n); Tpg = 300*ones(1,n); %guessed value
J = ones(1,n);

error = 1;
while error > 0.0001
   error = 0;
   for i = 1:n
      Tm(i) = (Tmf(i) + Tpg(i))/2; %   mean temperature
      delh(i) = (1.7535*Tm(i) + 2024.3); % heat of vaporization of water

% correlation for diffusion coefficient of water vapour at the average temperature in the air gap
      D   =  Ds*(Tm(i)/298)^2.334;

%  Total pressure in the cell
      P(i) = (1.895e-5*Tm(i)^2.072)/D;

% vapour pressure at the feed membrane side
      Ppff(i)  = (exp(23.238 - 3841/(Tmf(i) - 45)));
% vapour pressure at the air gap width
      Ppgg(i)  = (exp(23.238 - 3841/(Tpg(i) - 45)));

% vapour pressure at the feed membrane side with feed concentration
Pf(i)    = (1-Mo)*Ppff(i);

% Mean total pressure in the module
      pm(i)=(Ppgg(i)+Pf(i))/2;

      % air pressure in the module
      P_air = P(i)-pm(i);

%   estimation of permeate flux
      J(i)     = (E*P(i)*D*(Pf(i) - Ppgg(i)))/(bp*R*Tm(i)*P_air);

   % correlation for heat transfer coefficient
      hf = (1.86*kf*(rhof*Qf*cpf*dhf^2/(Af*kf*Lf))^(1/3))/dhf;
      hhf(i)    = hf + cpf*J(i);
      hc = (1.86*kc*(rhoc*Qc*cpc*dhc^2/(Ac*kc*Lc))^(1/3))/dhc;
      hd(i) = 0.943*(g*rhod*delh(i)*kd^3/(Ld*miu*(Tpg(i) - Tc)))^(1/4);
      Missing commands……..
      hp(i) = (1/hd(i) + l/kc + 1/hc)^(-1);
      H(i) = (1/hhf(i) + 1/hs(i) + 1/hp(i))^(-1);

% temperature at the feed membrane side and at the condensate vapour side
      Tmfn(i) = Tb(i) - H(i)*(Tb(i) - Tc + J(i)*delh(i)/hs(i))/hf;
      Tpgn(i) = Tc + H(i)*(Tb(i) - Tc + J(i)*delh(i)/hs(i))/hf;
      err = max(abs(Tmfn(i)-Tmf(i)), abs(Tpgn(i)-Tpg(i)));
      JJ=3600*J(i);

%calculation of thermal efficiency and temperature polarization coefficient
```

```
        Qvap=J(i)*delh(i)*1000;
        Qcond=(km/del)*(Tmf(i)-Tpg(i));
        efficiency=(Qvap/(Qvap+Qcond))*100;
        polar=(Tmf(i)-Tpg(i))/(Tb-Tc);

%isostress model
        km=((E/kgas)+(1-E)/kmater)^(-1);

        if err > error
           error = err;
        end
        error;
    end
    Tmf = Tmfn;
    Tpg = Tpgn;
end
plot(Tb-273,J*3600,'-*')
xlabel('Tb')
ylabel ('Permeate flux (kg/(m^2/s))')
```

Appendix B: EES code for flux prediction

```
C_bf=72e-3[g/L]                    {Bulk feed concentration}
D_s=24e-6[m^2/s]                   "D_s is the air-water diffusion coefficient at standard
 condition"
d_hf=1.1e-2[m]                   {hydraulic diameter of the feed side}
A_f=3.96e-4[m^2]                   {area of the feed side}
L_f=66e-3[m]                       {characteristic length of the feed side}
d_hc=1.1e-2[m]                   {hydraulic diameter of the coolant side}
A_c=3.96e-4[m^2]                   {area of the coolant side}
L_c=66e-3[m]                       {characteristic lengirth of the coolant side}
g=9.81[m/s^2]                    { acceleration due to gravity}
L_d=66e-3[m]                       {heigth of the plate}
K_p=109[W/mK]                    { thermal conductivity of the plate}
epsilon=0.8                      {membrane porocity}
R=8.314[J/Kmole]                 {gas constant}
M_w=0.018[kg/mole]               {molecular weigth of water}
r_p=0.225e-6[m]                  {membrane pore radius}
delta=154e-6[m]                  { membrane thicness}
l_p=1.5e-3[m]                      { thickness of the plate}

{The operating parameters are}
b=3e-3[m]                          {air gap width}
T_f=343[K]                       { feed temperature}
T_c=293[k]                       {coolant temperature}
Q_c=5e-5[m^3/s]                {feed flow rate}
Q_f=5e-5[m^3/s]                  { coolant flow rate}

"below are the specific heat capacity, thermal conductivity and density at the feed side respectively"
c_f=Cp(Water,T=343,P=101325)
k_f=Conductivity(Water,T=343[K],P=101325[Pa])
rho_f=Density(Water,T=343,P=101325)

"below are the specific heat capacity, thermal conductivity and density at the coolant side respectively"
c_c=Cp(Water,T=291,P=101325)
k_c=Conductivity(Water,T=291,P=101325)
rho_c=Density(Water,T=291,P=101325)
b`=tau*delta+b

"specific heat capacity in the gas phase"
c_pg=Cp(Steam,T=315,P=101325)

"thermal conductivuty of gas phase"
k_y=Conductivity(Steam,T=315,P=101325)

"below are the thermal conductivuty, density and viscosity of condensate respectively"
k_d=Conductivity(Water,T=300,P=101325)
rho_d=Density(Water,T=300,P=101325)
mu_d=Viscosity(Water,T=300,P=101325)

"Correlations and model equations start here"
h_f=1.86*(k_f/d_hf)*((rho_f*Q_f*c_f*d_hf^2)/(A_f*k_f*L_f))^(1/3)
h_c=1.86*(k_c/d_hc)*((rho_c*Q_c*c_c*d_hc^2)/(A_c*k_c*L_c))^(1/3)
```

```
h_d1=abs(g*(rho_d^2)*DELTAH*k_d^3)^(1/4)
h_d2=(L_d*mu_d*(abs(T_pg-T_c)))^(1/4)
h_d=0.943*(h_d1/h_d2)

h_y=k_y/b
h_p=((1/h_d)+(l_p/K_p)+(1/h_c))^(-1)
h11=J1 * c_pg
h22=1-exp(-1*abs(J1 * c_pg))/h_y
h12=h11/h22
H=((1/h_f)+(1/h12)+(1/h_p))^(-1)

"tau=((2-epsilon)^2)/epsilon  " "This relation may be replaced by the one below"
tau = 1/epsilon
T_m=(T_pg+T_mf)/2
DELTAH=1.7535*T_m+2024.3 [kJ/kg]

{"The diffusion coefficient is related to temperature   "see Banet  thesis Eq. 4.18""}
D  = D_s*(T_m/298)^2.334   "where D_s is the diffusion coefficient at standard condition"
P_air=(P-P_pg)
P=((0.00001895)*abs(T_m)^2.072)/D


"calculate the feed side membrane temperature, condesate temperature at the plate and the mean
 temperature"
T_pg=T_c+(H/h_p)*(T_f-T_c+(J1*DELTAH/h12))
T_mf=T_f-(H/h_f)*(T_f-T_c+(J1*DELTAH/h12))

"Using Antoine Equation, water vapour pressure can be estimated by"
P_pg = exp(23.1964 - 3816.44/(T_pg - 46.13))
P_pf  =  exp(23.1964 - 3816.44/(T_mf - 46.13))


"Now introducing the effect of salinity through the following equation"
P_pf_1 = (1-x_s)*P_pf

"where x_s is the molar concentration and it is given as "
x_s = C_bf/58.44

"the next equation applies the model for molecular diffusion and then flux"
C11=epsilon*P*D
C22=(R*T_m*(b`)*P_air)
C1=C11/C22
Missing commands ……...……..
Flux= J1*3600

"the thermal efficiency can be calculated as"
Efficiency=(Q_v/(Q_v+Q_cond))*100

"where Q_v and Q_cond are the heat of vaporization and conduction heat transfer accross the
 membrane respectively and they are calculated as below"

Q_v=DELTAH*J1*1000
Q_cond=(k_m/delta)*(T_mf-T_pg)

"where k_m is the thermal conductivity of membrane and the gas filling it and its can be estimated from
 "
```

```
k_m=(epsilon/k_gas+(1-epsilon)/k_mate)^(-1)

"where  k_mate is the thermal conductivity of membrane material and  k_gas is the thermal
 conductivity of the gas filling it"
k_gas=0.029
k_mate=0.259

"the temperature polarization coefficient is given as"
Polarization=(T_mf-T_pg)/(T_f-T_c)
```

Appendix C: Matlab code for flux optimization

```
clear all
close all
clc
% Assign minimum and maximum limit to each variable (define the domain)
z1min=60; z1max=80; z2min=20; z2max=30; z3min=1;z3max=5;z4min=3; z4max=7;

% Each the number of distribution for each variable will be 50 (meanining 6250000 number of
distribution)
Ngrid = 50;
Z1 = linspace(z1min, z1max, Ngrid);
Z2 = linspace(z2min, z2max, Ngrid);
Z3 = linspace(z3min, z3max, Ngrid);
Z4 = linspace(z4min, z4max, Ngrid);
M  = Ngrid^4;
z1 = zeros(M,1);
z2 = zeros(M,1);
z3 = zeros(M,1);
z4 = zeros(M,1);
for i = 1:Ngrid
   for j = 1:Ngrid
      for h = 1:Ngrid
         Missing commands……
            m = k + (h -1)*Ngrid + (j -1)*Ngrid^2 + (i - 1)*Ngrid^3;
            z1(m) = Z1(k);
            z2(m) = Z2(h);
            z3(m) = Z3(j);
            z4(m) = Z4(i);
         end
      end
   end
end
% the onjective function
Y = -197.79 + 5.86113*z1 - 0.736906*z2 + 2.03725*z3 + 1.1218*z4 - 0.0216244*z1.^2 +
1.22207*z4.^2 - 0.28302*z1.*z4;

y = max(Y);         % give the maximum value of the objective function
z1opt = z1(Y == y);
z2opt = z2(Y == y);
z3opt = z3(Y == y);
z4opt = z4(Y == y);
x = [z1opt,z2opt,z3opt,z4opt,y];   % give the optimum value of each variable that gave the objective
function

% to plot the histogram
hist(Y,100)
xlabel('Flux(Y) [kg/m^2hr]')
ylabel ('Frequency')

% specify the value of the following
ymin = min(Y)        % minimum value of the distribution
ymax = max(Y)        % maximum value of the distribution
ymed = median(Y)     % midium value of the distribution
```

```
k    = kurtosis(Y)   % kurtosis of the distribution
S    = skewness(Y)   % skewness of the distribution
ymean = mean(Y)      % mean of the distribution
ystd  = std(Y)       % standard deviation of the distribution
```

REFERENCES

[1] H. T. El- Dessouky, and H. M. Ettouney, ‘‘fundamentals of salt water desalination,’’ Elsevier, 2002.

[2] "Water Scarcity: International Decade for Action 'Water for Life 2005-2015". Retrieve 20, October 2013.

(http://www.un.org/waterforlifedecade/scarcity.shtml).

[3] Human Development Report 2006. UNDP, 2006, coping with water scarcity-Challenge of the twenty-first century. UN-Water, FAO, 2007.

(http://www.fao.org/nr/water/docs/escarcity.pdf).

[4] M. A. Dawoud, “The role of desalination in augmentation of water supply in GCC countries,” Desalination, 186, pp. 187-198, 2005.

[5] Fresh water and sea water properties, International towing tank conference, 2011. (http://ittc.sname.org/CD%202011/pdf%20Procedures%202011/7.5-02-01-03.pdf).

[6] D. T. Jamieson, “Experimental methods for the determination of the Properties of saline water,” desalination, 59, pp. 219-240, 1986.

[7] International energy agency, water for energy.

(http://www.worldenergyoutlook.org/resources/water-energynexus/).

[8] http://www.wabag.com/performance-range/processes-and-technologies/msf-multi-stage-flash/

[9] http://www.wabag.com/performance-range/processes-and-technologies/me-tvc-multi-effect-with-thermal-vapour-compression/

[10] D. E. Reisner, and T. Pradeep, “Aqua nano technology: Global Prospects,” CRC Press, Taylor and Francis Group pp. 541, 2014.

[11] Desalination by reverse osmosis

(https://www.oas.org/dsd/publications/Unit/oea59e/ch20.htm)

[12] http://en.wikipedia.org/wiki/Forward_osmosis

[13] Fact sheet, Desalination processes around the world, Water Education Corporation.
http://www.watercorporation.com.au//media/files/teachers/lessons%20and%20teaching%20resources/lesson%20plans/activity%20sheets%20and%20fact%20sheets/desal-around-the-world-fact-sheet.pdf

[14] J. R. Beckman, "Dewvaporation Desalination 5,000-Gallon-Per-Day Pilot Plant," U.S. Department of the Interior, Bureau of Reclamation, Technical Service Center, Water and Environmental Services Division, Water Treatment Engineering Research Team, 2008.

[15] M. Khayet, and T. Matsuura, "Membrane distillation principles and applications," Elsevier, B.V., Ch. 1, 2, 6, 8, 10-13, 2011.

[16] http://en.wikipedia.org/wiki/Low-temperature_thermal_desalination

[17] S. Porada, L. Weinstein, R. Dash, A. van der Wal, M. Bryjak, Y. Gogotsi, and P. M. Biesheuvel, "Water Desalination Using Capacitive Deionization with Microporous Carbon Electrodes," ACS Applied Materials and Interfaces, 4, PP. 1194-1199, 2012.

[18] http://en.wikipedia.org/wiki/Solar_desalination

[19] V. G. Gude, N. Nirmalakhandan, and S. Den, "Renewable and sustainable approaches for desalination," Renewable and Sustainable Energy Reviews, 14, pp. 2641-2654, 2010.

[20] R. Govind, and R. Foster, "Systems, Apparatus, and Methods for Separating Salts from Water," application number: US 14/310,388, filing date Jun 20, (2014), publication Number US20140299529 A1, and publication date Oct 9, 2014.

[21]. A. S. Jonsson, R. Wimmerstedt, and A. C. Harrysson, "Membrane distillation-A theoretical study of evaporation through microporous membranes," Desalination, 56, pp. 237-249, 1985.

[22] A. Alklaibi, and N. Lior, "Transport analysis of air-gap membrane distillation," Journal of membrane science, 255(1), pp. 239-253, 2005.

[23] R.W. Schofield, A.G. Fane, and C. J. D. Fell, "Gas and vapour transport through micro porous membranes. I. Knudsen–Poiseuille transition," Journal of Membrane Science, 53 (1-2), pp. 159-171, 1990.

[24] M. Khayet, "Membrane process-Vol.1 Desalination by Membrane Distillation,"

[25] A. Kullab, "Desalination Using Membrane Distillation, Experimental and Numerical Study," Doctoral Thesis, ISBN 978-91-7501-133-2, 2011.

[26] P. Onsekizoglu, "Membrane Distillation: Principle, Advances, Limitations and Future Prospects in Food Industry," In Tech Open, DOI: 10.5772/37625, 2012.

[27] A. Alkhudhiri, N. Darwish, and N. Hilal, "Membrane distillation: A comprehensive review," Desalination, 287, pp. 2-18, 2012.

[28] J. H. Zhang, N. Dow, M. Duke, E. Ostarcevic, J. D. Li, and S. Gray, "Identification of material and physical features of membrane distillation membranes for high performance desalination," Journal of Membrane Science, 349, pp. 295-303, 2010.

[29] L. M. Camacho, L. Dumee, J. Zhang, J. li, M. Duke, J. Gomez and S. Gray. "Advances in Membrane Distillation for Water Desalination and Purification Applications," Water, 5, pp. 94-196, 2013.

[30] F. He, J. Gilron, H. Lee; L. Song; K.K. Sirkar, "Potential for scaling by sparingly soluble salts in crossflow DCMD," Journal of Membrane Science, 311, pp. 68-80, 2008.

[31] F. Lagana, G. Barbieri, and E. Drioli, "Direct contact membrane distillation: modelling and concentration experiments," Journal of Membrane Science, 166, pp. 1-11, 2000.

[32] A. Alkhudhiri, N. Darwish, and N. Hilal, "Treatment of high salinity solutions: Application of air gap membrane distillation," Desalination, 287, 55–60, 2012.

[33] M. Khayet, and T. Matsuura, "Preparation and characterization of polyvinylidene fluoride membranes for membrane distillation," Ind. Eng. Chem. Res., 40 (24), 5710-5718, 2001.

[34] M. Khayet, K. C. Khulbe, and T. Matsuura, "Characterization of membranes for membrane distillation by atomic force microscopy and estimation of their water vapour transfer coefficients in vacuum membrane distillation process," Journal of Membrane Science, 238, pp. 199-211, 2004a.

[35] S. Srisurichan, R. Jiraratananon, and A.G. Fane, "Mass transfer mechanisms and transport resistances in direct contact membrane distillation process," Journal of Membrane Science, 277 (1-2), pp. 186-194, 2006.

[36] M. Khayet, T. Matsuura, J. I. Mengual, and M. Qtaishat, "Design of novel direct contact membrane distillation membranes," Desalination, 192, pp. 105-111, 2006.

[37] C. A. Smolders and A.C.M. Franken, "Terminology for membrane distillation," Desalination, 72, pp. 249-262, 1989.

[38] K. W. Lawson, and D. R. Lloyd, "Membrane distillation," Journal of membrane Science,124(1), pp.1-25, 1997.

[39] D. U. Lawal, A. E. Khalifa, "Flux Prediction in Direct Contact Membrane Distillation," International Journal of Materials, Mechanics and Manufacturing, Vol. 2, No. 4, 2014.

[40]. M. C. De Andres, J. Doria, M. Khayet, L. Pena, and J. I. Mengua, "Coupling of a membrane distillation module to a multi-effect distiller for pure water production," Desalination, 115(1), pp. 71-81, 1998.

[41] C. Feng, K.C. Khulbe, T. Matsuura, R. Gopal, S. Kaur, S. Ramakrishna, and M. Khayet, "Production of drinking water from saline water by air-gap membrane distillation using polyvinylidene fluoride nanofiber membrane," Journal of Membrane Science, 311, pp. 1-6, 2008.

[42] G.W. Meindersmaa, C. M. Guijtb, and A. B. de Haana, "Desalination and water recycling by air gap membrane distillation," Desalination, 187, pp. 291-301, 2006.

[43] M. Matheswaran, T. O. Kwon, J. W. Kim, and L. S. Moon, "Factors Affecting Flux and Water Separation Performance in Air Gap Membrane Distillation," J. Ind. Eng. Chem., Vol. 13, No. 6, pp. 965-970, 2007.

[44]. B. L. Pangarkar, and M. Sane, "Performance of air gap membrane distillation for desalination of ground water and seawater," Word Academy of Science, Engineering and Technology, 75, pp. 973-977, 2011.

[45]. D. Singh, and K. K. Sirkar, "Desalination by air gap membrane distillation using a two hollow-fiber-set membrane module," Journal of Membrane Science, 421-422, pp. 172-179, 2012.

[46] R. Tian, H. Gao, X.H. Yang, S.Y. Yan, and S. Li, "A new enhancement technique on air gap membrane distillation," Desalination, 332, pp. 52-59, 2014.

[47] A.E. Khalifa, "Water and Air Gap Membrane Distillation for Water Desalination-An Experimental Comparative Study," Separation and Purification Technology, Accepted, 2014.

[48]. R. W. Schofield, A.G. Fane, and C. J. D. Fell, "Heat and mass transfer in membrane distillation," Journal of Membrane Science, 33(3), pp. 299-313, 1987.

[49]. M. Gryta, and M. Tomaszewska, "Heat transport in the membrane distillation process," Journal of membrane science, 144(1), pp. 211-222, 1998.

[50]. G. L. Liu, C. Zhu, C. S. Cheung, and C. W. Leung, "Theoretical and experimental studies on air gap membrane distillation," Heat and mass transfer, 34(4), pp. 329-335, 1998.

[51]. L. Martínez-Díez, and M. I. Vázquez-González, "Temperature and concentration polarization in membrane distillation of aqueous salt solutions," Journal of Membrane Science, 156(2), pp. 265-273, 1999.

[52]. M. Khayet, P. Godino, and J. I. Mengual, "Theory and experiments on sweeping gas membrane distillation," Journal of membrane Science, 165(2), pp. 261-272, 2000.

[53]. M. Khayet, M. P. Godino, and J. I. Mengual, "Theoretical and experimental studies on desalination using the sweeping gas membrane distillation method," Desalination, 157(1-3), pp. 297-305, 2003.

[54] U. Dehesa-Carrasco, C.A. Pérez-Rábago, and C. A. Arancibia-Bulnes, "Experimental evaluation and modeling of internal temperatures in an air gap membrane distillation unit," Desalination, 326, pp. 47-54, 2013.

[55] A. S. Alsaadi, N. Ghaffour, J. D. Li, S. Gray, L. Francis, H. Maab, and G. L. Amy, "Modeling of air-gap membrane distillation process: A theoretical and experimental study," Desalination, Journal of Membrane Science, 445, pp. 53-65, 2013.

[56] C. M. Guijta, G. W. Meindersmab, T. Reithb, and A. B. de Haanb, "Air gap membrane distillation 1. Modelling and mass transport properties for hollow fibre membranes," Separation and Purification Technology, 43, pp. 233-244, 2005.

[57] C. M. Guijta, G. W. Meindersmab, T. Reithb, and A. B. de Haanb, "Air gap membrane distillation 2. Model validation and hollow fibre module performance analysis," Separation and Purification Technology, 43, pp. 245-255, 2005.

[58] M. A. I. Gil, M. C. G. Payo1, and C. F. Pineda, "Air gap membrane distillation of sucrose aqueous solutions," Journal of Membrane Science, 155, pp. 291-307, 1999.

[59] M. C. G. Payo, M. A. I. Gil, and C. F. Pineda, "Air gap membrane distillation of aqueous alcohol solutions," Journal of Membrane Science, 169, pp. 61-80, 2000.

[60] H. Geng, H.Wu, Pingli Li, and Q. He, "Study on a new air-gap membrane distillation module for desalination," Desalination, 334, pp. 29-38, 2014.

[61] A. E. Khalifa, D. U. Lawal, and M. A. Antar. "Performance of Air Gap Membrane Distillation Unit for Water Desalination," (Accepted, ASME-IMECE conference Montreal, Canada, 2014.)

[62] M. Toraj, and M. A. Safavi, "Application of Taguchi method in optimization of desalination by vacuum membrane distillation," Desalination, 249, pp. 83-89, 2009.

[63] M. Khayet, and C. Cojoucaru, "Air gap membrane distillation: Desalination, modeling and optimization," Desalination, 287, pp. 138-145, 2012.

[64] D. U. Lawal, and A. E. Khalifa, "Theoretical and Statistical Models for Predicting Flux in Direct Contact Membrane Distillation," International Journal of Engineering Research and Applications, Vol. 4, Issue 8 (5), pp. 124-135, 2014.

[65] F. A. Banat, and J. Simandl, "Desalination by membrane distillation: a parametric study," Sep. Sci. Technol., 33 (2), pp. 201-226, 1998.

[66] R. B. Bird, W.E. Stewart, and E.N. Lightfoot, "Transport Phenomena," second ed., Wiley, New York, 2002.

[67] J. Phattaranawik, R. Jiraratananon, and A.G. Fane, "Effect of pore size distribution and air flux on mass transport in direct contact membrane distillation," Journal of Membrane Science, 215, pp. 75-85, 2003.

[68] Y. Yun, R. Ma, W. Zhang, A. G. Fane, and J. Li, "Direct contact membrane distillation mechanism for high concentration NaCl solutions," Desalination, 188, pp. 251-262, 2005.

[69] F. A. Banat, "Membrane Distillation for Desalination and Removal of Volatile Organic Compounds from Water," PhD Thesis, McGill University, Montreal, Canada, 1994.

[70] M. N. A. Hawlader, R. Bahar, K. C. Ng, and L. J. W. Stanley. "Transport analysis of an air gap membrane distillation (AGMD) process," Desalination & Water Treatment, 42, pp. 333-346, 2012.

[71] S. Kimura, and S. Nakao, "Transport phenomena in membrane distillation," Journal of Membrane Science, 33, pp. 285-298, 1987.

[72] J. Phattaranawik, R. Jiraratananon, and A.G. Fane, "Heat transport and membrane distillation coefficients in direct contact membrane distillation," Journal of Membrane Science, 212 (1-2), pp. 177-193, 2003.

[73] M. Khayet, A. Velázquez, and J. I. Mengual, "Modelling mass transport through a porous partition: effect of pore size distribution," J. Non-Equilib. Thermodyn., 29 (3), pp. 279-299, 2004.

[74] J. Phattaranawik, R. Jiraratananon and A.G. Fane, "Effect of pore size distribution and air flux on mass transport in direct contact membrane distillation," Journal of Membrane Science, 215, pp. 75-85, 2003.

[75] P. Termpiyakul, R. Jiraratananon, and S. Srisurichan, "Heat and mass transfer characteristics of a direct contact membrane distillation process for desalination," Desalination, 177 (1-3), pp. 133-141, 2005.

[76] M. Tomaszewska, M. Gryta, and A.W. Morawski, "A study of separation by the direct contact membrane distillation process," Sep. Technol., 4 (4), pp. 244-248, 1994.

[77] C. M. Tun, A. G. Fane, J. T. Matheickal, and R. Sheikholeslami, "Membrane distillation crystallization of concentrated salts-flux and crystal formation," Journal of Membrane Science, 257 (1-2), pp. 144-155, 2005.

[78] M.A. Izquierdo-Gil, C. Fernández-Pineda, and M. G. Lorenz, "Flow rate influence on direct contact membrane distillation experiments: different empirical correlations for Nusselt number," Journal of Membrane Science, 321 (2), pp. 356-363, 2008.

[79] M. Gryta, M. Tomaszewska, and A.W. Morawski, "Membrane distillation with laminar flow," Sep. Purif. Technol., 11 (2), pp. 93-101, 1997.

[80] E. Curcio, and E. Drioli, "Membrane distillation and related operations - A review," Separation and Purification Reviews, 34, pp. 35-86, 2005.

[81] G. C. Sarti, C. Gostoli, and S. Matulli, "Low energy cost desalination processes using hydrophobic membranes," Desalination, 56, pp. 277-286, 1985.

[82] https://ujdigispace.uj.ac.za/bitstream/handle/10210/2158/EPropertiesofwater.pdf?sequence=6

[83] http://webserver.dmt.upm.es/~isidoro/dat1/Mass%20diffusivity%20data.pdf

[84] L. Martinez, and J. M. R. Maroto, "On transport resistances in direct contact membrane distillation," Journal of Membrane Sciences, 295, pp. 28-39, 2007.

[85] F. A. Banat, and J. Simandl, "Membrane distillation for dilute ethanol: Separation from aqueous streams," Journal of Membrane Science, 163, pp. 333-348, 1999.

[86] M. Khayet, C. Cojocaru, and C. P. Garcıa, "Application of Response Surface Methodology and Experimental Design in Direct Contact Membrane Distillation," Ind. Eng. Chem. Res., 46, pp. 5673-5685, 2007.

[87] S. S. Madaeni, and S. Koocheki, "Application of Taguchi method in the optimization of wastewater treatment using spiral-wound reverse osmosis element," Chemical Engineering Journal, 119, pp. 37-44, 2006.

[88] M. Khayet, and J. I. Mengual, "Effect of salt type on mass transfer in reverse osmosis thin film composite membranes," Desalination, 168, pp. 383-390, 2004.

[89] M. Khayet, C. Cojocaru, and M. Essalhi, "Artificial neural network modeling and response surface methodology of desalination by reverse osmosis," Membrane Science, 368, pp. 202-214, 2011.

[90] C. N. Carmita, "Optimization of cutting parameters for minimizing energy consumption in turning of AISI 6061 T6 using Taguchi methodology," Clean Energy Production, 53, pp. 195-203, 2013.

[91] J. Verboomen, D. Van Hertem D, P. H. Schavemaker, F. J. C. M. Spaan, J. M. Delince, R. Belmans, and W. L. Kling, "Monte Carlo Simulation Techniques for Optimisation of Phase Shifter Settings," Euro. Trans. Electr. Power, 17, pp. 285-296, 2007.

VITAE

Name	:	Dahiru Umar Lawal
Nationality	:	Nigeria
Date of Birth	:	08-Oct-1984
Email	:	L.dahiru@.yahoo.com
Address	:	21 Unity Road, Fagge, Kano, Nigeria.
Academic background:		Master of Science (M.S.), November, 2014. Mechanical Engineering Department, King Fahd University of Petroleum & Minerals, Dhahran, Saudi Arabia.
		Bachelors of Engineering (B.Eng.), `June, 2010. Mechanical Engineering Department, Bayero University, Kano, Kano, Nigeria.

Publications : Performance and Variables Optimization of Air Gap Membrane Distillation System for Water Desalination (Under review "Arabian Journal for Science and Engineering", Dec. 2014).

Experimental Investigation of Double-Stage Air Gap Membrane Distillation Unit (Under review "Desalination and Water Treatment", Oct. 2014).

D. U. Lawal, and A. E. Khalifa, "Flux Prediction in Direct Contact Membrane Distillation" International Journal of Materials, Mechanics and Manufacturing, Vol. 2, No. 4, 2014.

D. U. Lawal, and A. E. Khalifa, "Theoretical and Statistical Models for Predicting Flux in Direct Contact Membrane Distillation" International Journal of Engineering Research and Applications, ISSN: 2248-9622, Vol. 4, Issue 8 (1), 2014.

A. E. Khalifa, D. U. Lawal, and M. A. Antar. "Performance of Air Gap Membrane Distillation Unit for Water Desalination" (Accepted for publication, ASME-IMECE conference Montreal, Canada) 2014.

"Fundamental Study on Desalination Using Air Gap Membrane Distillation: An Experimental Investigation" (Under review).